CHARLES UNIVERSITY IN PRAGUE
FACULTY OF MATHEMATICS AND PHYSICS

DOCTORAL THESIS

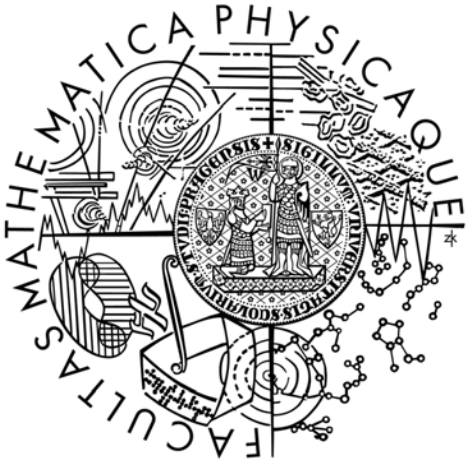

Jan Labuta

Study of interactions in macromolecular and supramolecular systems

Department of Macromolecular Physics

Supervisor: RNDr. Lenka Hanyková, Dr.

Prague 2008

Acknowledgements

The work presented in this thesis has been carried out under the supervision of RNDr. Lenka Hanyková, Dr. at the Department of Macromolecular Physics, Faculty of Mathematics and Physics, Charles University in Prague, Czech Republic.

I would like to thank my supervisor RNDr. Lenka Hanyková, Dr. for her kind leadership, continuous interest, advises and help in accomplishing the experiments and writing thesis. My warmest thanks also go to Dr. Jonathan P. Hill and Dr. Katsuhiko Ariga for their guidance and valuable discussions during the work in Supermolecules Group in National Institute for Materials Science at Tsukuba, Japan.

Finally, very special thanks are addressed to my parents, sister and brother. They were supportive and always encouraged me to follow through.

Support of this work by Ministry of Education, Youth and Sports of the Czech Republic (project MSM0021620835), Grant Agency of the Charles University (Grant 294/2004/B) and Ministry of Education, Culture, Sports, Science and Technology of Japan (Grant-in-Aid for Science Research in a Priority Area: ”Super-Hierarchical Structures”) is also gratefully acknowledged.

In Prague; August 7, 2008

RNDr. Jan Labuta

Contents

Preface **3**

1 Introduction I **4**

1.1 Introduction to stimuli-responsive systems 4

1.2 Phase separation 6

1.2.1 Liquid-liquid phase separation 6

1.2.2 Phase separation in polymer solutions 7

1.2.3 Theoretical approach to coil-globule transition 9

1.3 Overview of PVME studies 11

1.4 Objectives of the doctoral thesis (macromolecular part) 14

2 Experimental I **16**

2.1 Samples 16

2.2 NMR measurement 17

2.2.1 Experimental setup for ^{1}H, ^{13}C NMR spectra and ^{1}H, ^{13}C NMR relaxation times measurement 17

2.2.2 Experimental setup for partially relaxed ^{1}H NMR spectra measurement 18

2.3 DSC measurements 18

2.4 Optical microscopy measurement 19

2.5 Digital image processing 19

2.6 DLS measurement 19

3 Resultes and discussion I **21**

3.1 Temperature dependences of ^{1}H NMR spectra 21

3.1.1 Phase separated fraction – FID sequence 21

3.1.2 Phase separated fraction – FID vs. spin echo sequence 25

3.1.3 ^{1}H NMR spectra – broad peak subtraction (spin-spin relax. time) . 28

3.2 ^{1}H NMR spectra and ^{1}H spin-spin relaxation times T_2 of EtOH 29

3.3 ^{13}C NMR spectra and ^{13}C spin-spin (T_2) and spin-lattice (T_1) relaxation times of EtOH 37

3.4 DSC measurements 43

3.4.1 Narrow temperature range DSC measurement 43

3.4.2 Wide temperature range DSC measurement 47

3.5 Optical microscopy measurement . . . 49
3.6 Digital image processing – size distribution of globules . . . 57
3.7 DLS measurement – size distribution of globules . . . 58
3.8 Comparison of OM and DLS globule size distributions . . . 60
4 Conclusions I . . . 64
5 Introduction II . . . 68
5.1 Introduction to porphyrins . . . 68
5.2 Anion binding . . . 71
5.3 Objectives of the doctoral thesis (supramolecular part) . . . 72
6 Experimental II . . . 74
6.1 Samples . . . 74
6.2 Characterization . . . 75
6.2.1 Used spectrophotometers and spectrometers . . . 75
6.2.2 X-ray crystallography . . . 76
6.3 Synthesis . . . 76
7 Resultes and discussion II . . . 78
7.1 Solvatochromism . . . 78
7.2 UV/Vis Spectrophotometry of anion binding . . . 82
7.3 ^{1}H NMR spectroscopy . . . 87
7.4 Anion selectivity by a combination of anion binding and solvatochromic effects . . . 91
8 Conclusions II . . . 97
9 References . . . 99
10 List of publications . . . 105

Preface

The thesis deals with study of interactions in macromolecular (part I) and supramolecular (part II) systems. In macromolecular section the properties of poly(vinyl methyl ether) as a representative of thermoresponsive polymers is investigated from different points of view. In the second, supramolecular, section the solvatochromism and anion binding abilities of two porphyrin derivatives are studied. Each part has its own introduction, experimental, results and discussion and conclusions. In the end of the thesis there are references followed by list of publications.

1 Introduction I

1.1 Introduction to stimuli-responsive systems

The investigation of physical properties of so-called “smart” polymer systems has attracted a great deal of attention both theoretical and experimental. It is now well established that such stimuli-responsive systems, especially water swollen networks – hydrogels [1], undergo a volume phase transition (collapse) induced by a small change in external parameters like temperature, solvent composition, pH, etc. This phenomenon was experimentally discovered for polyacrylamide gels (collapse induced by a change in solvent composition) almost 30 years ago [2]. At the collapse, the gel volume can decrease 10-1000 times. Collapse was usually interpreted as a first-order phase transition [3] but there are also studies claiming that this is rather a second-order transition [4].

It is also well known that some synthetic polymers, such as poly(vinyl methyl ether) (PVME), with amphiphilic character in aqueous solutions exhibit a lower critical solution temperature (LCST) behaviour. They are soluble at low temperatures but heating above the LCST results in phase separation which is especially at polymer concentrations $c \geq 1$ wt% macroscopically manifested by milk-white turbidity of the solution [5,6]. On the molecular level, both temperature-induced phase separation in solutions and similar volume phase transition (collapse) in crosslinked hydrogels are assumed to be a macroscopic manifestation of a coil-globule transition.

W. Stockmayer [7] was the first who predicted, in 1959, that if the attraction between monomers becomes stronger than attraction between monomers and solvent molecules, the polymer undergo a phase transition of the same sort as the transition from gas to liquid. Segments of the polymer "condense on to themselves" and instead of a loose coil the system ends up with a "dense drops" - a polymer globule [8].

Terms "polymer globules" and "coil-globules transition" came into polymer field from molecular biophysics. Some of the most important biological polymers – protein enzymes – usually appear in living cells in globular form. If something happens to the solvent surrounding the proteins (it gets overheated, or the contents are disturbed), the proteins may be denatured. In other words, they lose all their biochemical activity. Denaturation of proteins usually implies a dramatic change in shape and it is accompanied by a strong absorption of heat. The first scientists who worked on coil-globule transition were inspired by the thought that it might shed some light on the denaturation of proteins. It seemed quite plausible that when denaturation occurred, the dense globular structure would be destroyed and the protein would take on the shape of a coil. Only later did it turn out that there is no straightforward analogy between coil-globule transition and protein denaturation. However, the coil-globule transition was quite extraordinary and exciting in its own right. The studies have expanded, covering all kinds of polymers. A globular state has been discovered for many other systems. Not only proteins, but also DNA molecules and macroscopic polymer networks, for example, can have a globular structure.

The phase transition is probably associated with the changed balance between various types of interactions, mainly hydrogen bonds and hydrophobic interactions [6]. Their thermosensitivity, or generally their ability to react on the change in various external stimuli, makes these systems interesting for possible biomedical and technological applications such as actuators, sensors, valves, switching device etc [1,9,10]. The fact that the LCST of some polymers is near to human body temperature makes them viable as drug release systems [11-13].

1.2 Phase separation

1.2.1 Liquid-liquid phase separation

It is well known that the system consisting of two partially miscible liquids (i.e. liquids that do not mix in all proportions and at all temperatures) can exhibit critical solution temperature behaviour. Suppose that a liquid *B* is gradually added to another liquid *A* at a certain temperature *T** (Figure 1). The molar ratio x_B of the liquid *B* is gradually rising. When a small amount (up to x_{B1}) of the liquid *B* is added, it dissolves completely, and the binary system remains a single-phase. When more *B* is added, there comes a state (at x_{B1}) when *B* is no longer dissolved. The sample now consists of two phases being in equilibrium with each other. Further addition of *B* (the molar ratio between x_{B1} and x_{B2}) results in a slight dissolving of *A* in *B* (the amount of one phase increases at the extent of another). And finally, the system reverts again into the single phase (over x_{B2}) when as much of *B* is present so that it dissolves all the *A* [14,15].

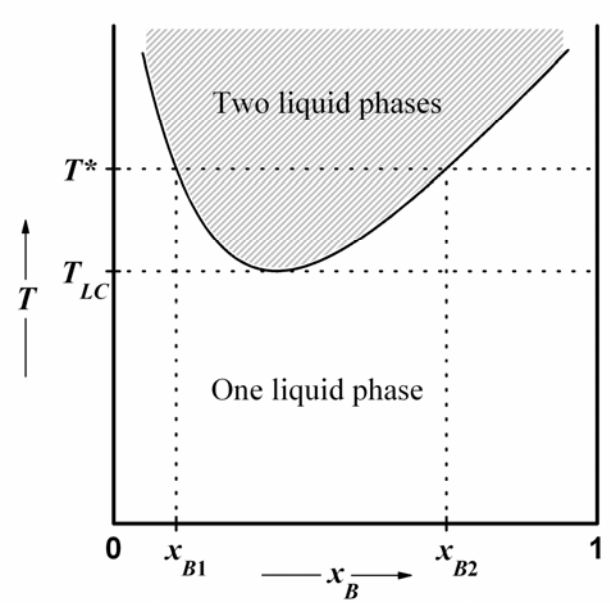

Figure 1. Temperature-composition phase diagram for liquid mixture with LCST behaviour.

Whether the system consists of one or two phases could be also influenced by temperature (Figure 1). There are two types of critical liquid mixtures behaviour:

lower (LCST) and upper (UCST) critical solution temperature behaviour. The UCST is the highest temperature at which phase separation occurs. Above UCST the two components are fully miscible. This temperature exists because the greater thermal motion overcomes any potential energy advantage in molecules of one type being close together.

Our attention, in this thesis, will be focused precisely on the lower critical solution temperature (LCST) behaviour of poly(vinyl methyl ether) (PVME). LCST behaviour is reflected so that two components are fully miscible below critical temperature (T_{LC}) while above they form two phases (Figure 1). In this case, at low temperatures the two components are miscible since they form a weak complex (e.g. stabilized by amphiphilic interactions, hydrogen bonding, van der Waals interactions) while at higher temperatures the complexes break up and the components are separated.

1.2.2 Phase separation in polymer solutions

An analysis of a classical Flory-Huggins equation of swelling equilibrium of polymer networks led to results that under suitable conditions in a network two polymeric phases may coexist. These phases have different conformation of chains and concentration of segments. A small change in the polymer-solvent interactions, which may be given by a change in the external parameters, for example, by temperature or composition of solvent, then leads to a pronounced change in the degree of swelling of the gel. This phenomenon (collapse) shows the character of the first-order phase transition [16-18]. Later, it was experimentally discovered by Tanaka [19]. He used networks of polyacrylamide diluted in a mixture of acetone and water. In these experiments, the temperature was not varied. The interactions between polymer and solvent are changing if some extra acetone was poured into the solution since acetone, in contrast to water, is a bad solvent for polyacrylamide. It was found that at 42 vol% of acetone, the network collapses suddenly and its volume drops by a factor of nearly 20 (Figure 2). Later experiments showed that for the occurrence of the collapse, the presence of charges on the chains seems to be necessary [20].

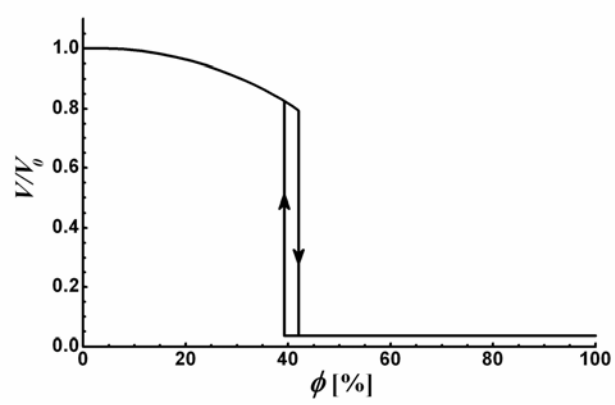

Figure 2. The volume of a polyacrylamide network in a mixture of acetone and water, as a function of the volume percentage of acetone. V_0 is the volume that the network had when prepared. (The figure is taken from Ref. [19].)

The connection between collapse in hydrogels and phase transition in polymer solutions originates from the same phenomenon – coil-globule transition. The idea of coil-globule transition on molecular level is that above LCST, polymer chains undergo an intramolecular phase transition from expanded coil state to the compact globular structure. During the crossing of critical temperature there is a change in interactions between polymer and solvent characterized as shift from good-solvent behaviour to poor-solvent behaviour. Good-solvent behaviour occurs when polymer segment-solvent contacts are more favoured than segment-segment contacts. If the attraction between the segments becomes sufficiently large the polymer will separate to a globule whose density is close to that of dry polymer [21]. The temperature at which this occurs is close to the θ temperature - the temperature at which the attractive forces just balance the excluded volume forces. A more precise definition of the θ temperature is the temperature at which the second virial coefficient of the osmotic pressure vanishes [22]. It is commonly supposed that at the θ point the polymer has its random coil dimensions. For a given solution above its θ temperature, where the attractive forces between polymer segments predominate, polymer-polymer contacts can increase by two different mechanisms: the contraction of the individual chains (intramolecular condensation) or the interpenetration of different chains (intermolecular condensation). If only one chain is present in the solution, it would separate to a globule; in a solution of finite concentration of polymer, chain contraction and aggregation will be competitive processes and phase

separation could occur either by coalescence of globules or the aggregates made up of interpenetrating chains. The phase separation has been proven to be rather close to the point of intermolecular condensation at which the polymer aggregates. Fundamentally, two different approaches have been developed [23]: the simplest Flory-type models [22,24] and the more rigorous Lifshitz-type model [25]. These models will be discussed in following subsection.

Since we focus in this work on PVME in D_2O/ethanol mixtures, the segment-segment and segment-solvent interactions should be specified closely at this point. The LCST of PVME in water is about 35 °C [6,26-28]. PVME structure contains the hydrophilic (ether oxygen) and hydrophobic part (mainly methyl group), which play an important role in interactions with the solvent (cf. Figure 3 in subsection 2.1). The segment-solvent interaction is manifested as a hydrogen bond between ether oxygen and hydroxyl hydrogen of water or ethanol while segment-segment interaction has its origin in hydrophobic effect (the tendency of nonpolar groups to associate in aqueous solutions). The hydrogen bonds are very sensitive to temperature changes. Therefore, the fragile stability between hydrophilic and hydrophobic interaction can be easily break by heating above 35 °C. The hydrophobic interactions start to predominate and the globules are formed.

1.2.3 Theoretical approach to coil-globule transition

As it was mentioned above, there are two approaches for theoretical study of coil-globule transition. In following text, the construction based on Flory's approximate arguments is presented and some remarks, regarding the Lifshitz consistent approach, are mentioned in the end.

The collapse from coil to globule of a single polymer chain was treated as a transition from the regime where attractive interactions between solvent molecules and monomeric units are dominant to the regime where attractive interactions between monomers are dominant [22,24]. The Gibbs free energy of a swollen coil consists of the sum of two terms:

$$G(\alpha) = G_{el}(\alpha) + G_{int}(\alpha), \qquad (1)$$

where α is a scalar order parameter of the macromolecule, so-called collapse ratio, and reflects size of the chain. The parameter α satisfies inequality $0 < \alpha \leq 1$. The first term $G_{el}(\alpha)$ is the elastic entropy contribution to the free energy associated with stretching the coil by the factor α, $G_{el}(\alpha) = -TS(\alpha)$. Ptitsyn et al [24] estimated this term under the assumption that Gaussian statistics is valid for both coil and globular states and obtained:

$$G_{el}(\alpha) = \frac{3}{2} RT\left(\alpha^2 - \ln \alpha^2\right). \tag{2}$$

The second term $G_{int}(\alpha)$ in equation (1) is the energy of the monomer interaction in the coil. It includes both monomer-monomer and monomer-solvent interactions. When the bonding of monomer in the chain is neglected, the approximate relation similar to the van der Waals equation for real gases was proposed [24]:

$$G_{int}(\alpha) = -\frac{N^2 \upsilon z U}{2V} - NRT \ln\left(1 - \frac{N\upsilon}{2V}\right), \tag{3}$$

where N is the number of statistical segments in the chain, υ is the volume excluded by each statistical segment to other segments, U is an energy gain that each statistical segment gives with respect to the contacts between statistical segments and solvent molecules, z is the coordination number, $V = \alpha^3 V_0$, where V_0 is the volume of the macromolecule at the θ temperature when the segment-segment and segment-solvent interactions are equal and the chain has unperturbed dimensions.

Since the two terms were expressed the minimization of the total Gibbs free energy $G(\alpha)$ as a function of α should be next step. The condition for a minimum, $\partial G(\alpha) / \partial \alpha = 0$, leads us to the equilibrium value of α. After substituting for the derivative, we have the equation

$$\alpha^5 - \alpha^3 = q + \rho \alpha^{-3}, \tag{4}$$

where q is a measure of the interaction between two statistical segments, while ρ is a measure of the interaction between three statistical segments. The equation determines the size of a coil, $R = \alpha N^{1/2} l$, where l is Kuhn length, as a function of two characteristic parameters, q and ρ. The analysis of this problem also shows that the parameters q and ρ correspond to particular system characteristics. Parameter q can be related to the temperature (the range $q < 0$ corresponds to the temperature $T < \theta$,

and $q > 0$ corresponds to $T > \theta$). Parameter ρ depends on the osmotic third virial coefficient, and the study of this coefficient for different types of monomer has shown that ρ parameter, basically, describes the rigidity of the polymer chain. Generally it can be concluded that the collapse ratio α is a function of temperature, solvent quality and polymer chain rigidity. The fact that in the thermodynamic limit, the coil-globule transition may be either of the first- or of the second-order, essentially depends on whether the thickness-to-length ratio of a statistical segment (rigidity) of polymer is below or above some limiting value.

Lifshitz and co-workers [25], by solving a nonlinear Schrödinger-type equation, were able to calculate the density distribution of monomers inside a spherically symmetric globule showing that the distribution depends only on $[(T - \theta) / \theta] N^{1/2}$. For rigid and semi-rigid polymer chains the Gibbs energy exhibits two minima near the transition point θ, as expected for a first-order transition. They also showed that at the transition point, the temperature derivative of the Gibbs energy has a jump proportional to $N^{1/2}$. This jump corresponds to the latent heat associated with ordinary first-order phase transitions. For flexible polymer chains the transition is smooth and looks like a second-order phase transition. In such a way both Flory-type and Lifshitz-type approaches lead to the similar conclusions about the nature of the coil-globule transition in macromolecular system.

1.3 PVME studies overview

A study of phase separation in polymer solutions using various methods is widespread. The overview of PVME studies is presented in following text.

Interaction of water (H_2O) with PVME solutions of different concentration was studied by H. Maeda [29] by near-infrared spectroscopy. The changes in water band were characterized by the change in its wavelength of maximum absorbance. From the concentration dependence of water peak wavelength three different regions of water behavior were found. Region-III (at highest polymer concentrations) is characterized by a cooperative polymer-water complex, involving hydrogen bonding of water to oxygen atoms of the polymer. The region-II (intermediate concentrations) also appears to be formed a hydrogen-bonded water clusters around hydrophobic

groups. Free water appears only in region-I at the lowest polymer concentrations. This can be interpreted as a cooperative collapse of the hydrogen-bonded water structure to free water, resulting in the aggregation of the polymer chains due to the exposure of their hydrophobic groups at the cloud point.

Horne et al [27] investigated the effect of different types of alcohols on the cloud point temperature of PVME. Concentration of some alcohol in water/alcohol mixtures shifts significantly the cloud point temperature. It was found that propanol has little effect on cloud point whereas lower molecular weight alcohols (methanol, ethanol) stabilize the hydrogen bonds and shift slightly the cloud point towards higher temperature. Higher molecular weight alcohol, n-buthanol, destabilize the interactions in system and decreases strongly the cloud point temperature.

In IR spectroscopic study of PVME aqueous solution done by Y. Maeda [30] it was found that below LCST, the hydrophilic ether oxygens on the polymer makes hydrogen bonds with water molecules, which overcomes the unfavorable decrease in entropy of water due to a formation of an iceberg structure around the hydrophobic moiety and stabilizes the solution. With increasing temperature, the hydrogen bonds of the ether oxygens are broken and apolar groups are concomitanly dehydrated in the transition region from ca. 33 to 40 °C. Above the temperature region, the hydrophobic interaction between apolar moieties becomes dominant and induces separation of polymer chains from solvent (water). PVME concentration dependence of the position of IR bands shows that the methyl groups are more dehydrated than the ether oxygen at higher water/monomer ratios.

Aseyev et al [31] were investigating the PVME in dilute aqueous solutions below 0.25 g/l above LCST using several methods such as dynamic, DLS, and static, SLS, light scattering and high sensitivity differential scanning calorimetry (HS DSC). They found that particles (globules) are spherical and have very narrow size distribution. The size of formed particles depends on the initial concentration and the heating rate of the solution and it is not significantly affected by the molar mass of individual macromolecules. Once being formed, the particles neither precipitate nor disintegrate upon dilution. The size of globules did not change at least for several weeks, showing the absence of any significant association of globules. In the thermodynamically poor solvent, individual macromolecules associate decreasing the

overall entropy of the solution. Aggregation stops when the entropy loss balances the potential energy of a new meta-stable state at elevated temperature. Narrow size distribution of the globules also suggests entropic origin of the intermolecular association. The stability of the dispersion upon dilution at 50 °C and zero value of the osmotic second virial coefficient indicate that the surface of the particles at temperatures above the LCST may possess a hydrophilic character. The macromolecules self organize and build up particles with the polar groups turned towards the surrounding aqueous phase.

Modulated-temperature scanning calorimetry (MT DSC), DSC and IR spectroscopy measurements on PVME/water systems [32-34] revealed the following. A larger nonreversing heat flow contribution is found upon cooling, indicating a slower undergoing transition upon cooling than upon heating. Solutions with high PVME concentration (> 60 wt%) do not show crystallization and melting of water. This abrupt change in crystallization and melting behaviour is related to the vicinity of the glass transition temperature (ca. -25 °C) generating a dramatic slowing down of the nucleation rate. This effect at higher polymer concentration has nothing to do with the formation on molecular complexes between PVME and water. Below -20 °C, in solution with 30 wt% of PVME, two types of ice was found. One is formed by free water and the other is formed by frozen bound water. IR data show that there are no hydrogen bonds between water molecules and polymer groups.

Micro-Raman spectroscopic investigation [35] of PVME/water/alcohol ternary mixtures showed that transition temperature monotonically increase with increasing fraction of alcohol (methanol and ethanol). Because acceptor number for hydrogen bonding of MeOH is the highest among the alcohols examined (methanol, ethanol, 2-propanol, t-butanol) in their work, it can form the strongest hydrogen bond with the oxygen atom of PVME. The obtained results also suggest that association between the alcohols and PVME is mainly driven by hydrophobic interaction. More hydrophobic alcohols associate with PVME easier, raise the hydrophobicity of PVME, and finally reduce the transition temperature to a larger extent.

Recently, ^{1}H NMR spectroscopy was employed for study of temperature-induced phase separation in PVME/D_2O solutions and gels [36]. A similar behaviour was found for linear and crosslinked systems, indicating the formation of rather

compact globular-like structures during the phase transition, which are colloidally stable in solution. ^{1}H NMR relaxation measurements revealed that a certain portion of water molecules are bound at elevated temperatures in PVME globules in semidilute and concentrated solutions (c = 2-10 wt%) [37-39]. With time this bound water is slowly released from globular-like structures, the releasing process takes ~24 hrs. This finding implies that most existing studies of the phase separation in semidilute or concentrated PVME aqueous solutions deal in fact with metastable state where globular-like structures still contain bound water. On the contrary, dehydration of PVME chains is rapid in dilute solutions [39]. A slow exchange and relatively weak hydrogen bonding were found from the position of the separate NMR signal for bound HDO in highly concentrated PVME/D_2O solutions (polymer concentrations c = 20-60 wt%) [40]. At the same time, the molar ratio [PVME monomeric unit]/[bound D_2O] ≅ 2.7 is constant in the range of concentrations c = 20-60 wt%, i.e., the polymer concentration in the polymer-rich phase (globules) is 89 wt%, in accord with the phase diagram published in Ref. [32]. Spin-spin relaxation times as obtained for the separate signal of bound HDO (~40 ms) are two orders of magnitude shorter in comparison with free HDO; nevertheless, a rather small spatial restriction of the motion of HDO can be responsible for this difference. Direct connection of the fraction of bound water with the conformational structure of PVME has been suggested [40].

1.4 Objectives of the doctoral thesis (macromolecular part)

Until recently the application of NMR spectroscopy in investigations of the phase separation in solutions of thermoresponsive polymers was rather seldom as well as study on PVME itself. Therefore, NMR and some other methods such as differential scanning calorimetry (DSC), optical microscopy (OM) and dynamic light scattering (DLS) were employed for investigation of PVME in D_2O/ethanol mixtures (PVME/D_2O/EtOH). These methods provide mutual support for enlightment of PVME properties.

In the text following below, the experimental methods and obtained results will be discussed. The main aims of this study can be concisely described as:

1) Study of the influence of PVME concentration and EtOH content in D_2O/EtOH mixtures on occurrence and extent of the phase separation using NMR spectroscopy.
2) Measurement of influence of phase separation on dynamic of solvent molecules (D_2O and EtOH) in PVME/D_2O/EtOH solutions using NMR relaxation experiments.
3) Investigation of phase separation for different PVME concentrations and different EtOH contents in D_2O/EtOH mixtures using DSC, OM and DLS methods.
4) Detailed microscopic morphology study of phase separation in PVME/D_2O/EtOH solutions.
5) Determination of globule size distribution and comparison of OM and DLS results.

2 Experimental I

2.1 Samples

PVME (Figure 3) was purchased from Aldrich (supplied as 50 wt% solution in water, molecular weight determined by GPC in THF: average molecular weight M_w = 60 500, polydispersity index $M_w/M_n \cong 3$). After drying, solutions with appropriate PVME, D_2O (99.9 % of deuterium) and EtOH concentration were prepared. In general, seven different PVME concentrations c = 0.1, 0.6, 1, 6, 10, 20 and 30 wt% in four D_2O/EtOH mixtures with volume fraction of EtOH c_{EtOH} = 1, 5, 10 and 20 vol% were used (no apparent milk-white opalescence was observed at elevated temperatures for solutions with EtOH content higher than 20 vol% in water/EtOH mixture). Methods of the sample preparation and solution concentrations used for each measurement will be discussed in detail below.

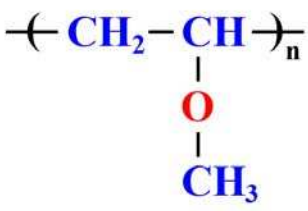

Figure 3. Structure of poly(vinyl methyl ether) (PVME). Hydrophilic (red) and hydrophobic (blue) parts are specified in the structure.

2.2 NMR measurement

All samples of PVME/D_2O/EtOH solutions in 5-mm NMR tubes were degassed and sealed under argon.

The measurement procedures are specified in two following subsections. Each subsection corresponds to the experimental setup for appropriate part of NMR results in section 3 (Results and discussion).

2.2.1 Experimental setup for ^{1}H, ^{13}C NMR spectra and ^{1}H, ^{13}C NMR relaxation times measurement

High-resolution ^{1}H NMR spectra were recorded with a Bruker Avance 500 spectrometer operating at 500.1 MHz. Typical measurements conditions were as follows: 90° pulse width 14.25 μs, relaxation delay 10 s, spectral width 5 kHz, aquisition time 1.64 s, 16 scans. ^{13}C spectra were accumulated usually with 100 scans with relaxation delay 80 s and spectral width 12.5 kHz under full proton decoupling. A ^{13}C pulse duration of 7 μs was applied for the single 90° pulse used for each scan. The integrated intensities were determined with the spectrometer integration software with an accuracy of ±1 % and ±3 % for ^{1}H and ^{13}C NMR spectra, respectively. The temperature was maintained constant within ± 0.2 °C using BVT 3000 temperature unit.

The ^{1}H spin-spin relaxation times T_2 on the merged EtOH/HDO OH signal and on EtOH CH_2 and CH_3 signals were measured using the Carr-Purcell-Meiboom-Gill (CPMG) [41] pulse sequence $90°_x$–$(t_d$–$180°_y$–$t_d)_n$–acquisition, with t_d = 5 ms; the total time of T_2 relaxation was an array of 12 values. In T_2 measurements at temperatures above the LCST we also used t_d = 0.5 ms and the total time of T_2 relaxation was an array of 32 values. Every experiment was done with 8 or 16 scans and relaxation delay between scans was 80 s. The ^{13}C T_2 relaxation times of ethanol groups were measured using CPMG sequence with ^{1}H 180° pulse added to remove cross-correlation between chemical shift anisotropy and dipole-dipole interactions [42]. The interval t_d = 5 or 0.5 ms and relaxation delay 80 s were used in ^{13}C T_2 measurements (the relaxation delay was adequately long to allow a complete

recovery of ^{13}C magnetization). The ^{13}C spin-lattice relaxation times T_1 of ethanol were measured using an inversion recovery pulse sequence 180°–τ_d–90° with 8 scans separated by a relaxation delay of 80 s. All obtained ^1H and ^{13}C T_2 and T_1 relaxation curves had the monoexponential character and fitting process always enabled us to determine the single value of the respective relaxation time.

2.2.2 Experimental setup for partially relaxed ^1H NMR spectra measurement

^1H NMR spectra were also obtained using a JEOL AL300BX spectrometer operating at 300.4 MHz equipped with appropriate JEOL temperature control unit (temperature fluctuation ±0.3 K). Instead of using only previous approach (first paragraph in subsection 2.2.1) of recording ^1H NMR spectra based on a simple excitation-acquisition pulse sequence $90°_x$–acquisition (FID), the block of transversal relaxation was incorporated. The resulting sequence (spin-echo pulse sequence) is $90°_x$–t_d–$180°_y$–t_d–acquisition with echo time $2t_d$ = 8 ms (16 scans).

Most of NMR measurements were carried out under the conditions described in subsection 2.2.1. The measurements which were done using description here are presented in subsections 3.1.2 and 3.1.3.

2.3 DSC measurement

DSC measurements were carried out using an EXSTAR 6000 instrument (SEIKO Electronics Inc.). Calibration was performed routinely using high purity standards (water, mercury and indium) under a constant nitrogen flux. Samples of approximately 15 mg mass were encapsulated in aluminium pans. All DSC measurements were performed at a heating/cooling rate of 2 °C/min. Two procedures for the different temperature ranges and multiplicity of heating-cooling cycles were employed. These procedures are specified below in the corresponding subsections.

All DSC thermograms were plotted as dependencies of specific heat capacity c_p [J/g°C] on temperature T [°C]. For the coil-globule transition of PVME, c_p is given recalculated per unit mass of PVME, whereas for discussion of solvent properties (D_2O/EtOH), c_p was recalculated per unit mass of solution. The characteristic

transition temperature was determined from DSC thermograms as the onset temperature T_{on}. Further characterization of transition was performed using calculation of the enthalpy increment per unit mass of PVME ΔH by means of integration of the experimental DSC thermograms.

2.4 Optical microscopy measurement

Optical microscopy (OM) measurements were carried out under nitrogen atmosphere using an Olympus BX51 microscope equipped with Olympus MP5Mc/OL digital camera and Linkam THMS600 hot stage and Linkam TMS94 controller/LNP94 cooling system. The morphology development was observed for a thin sample layer placed between a support glass slide and a cover slip inserted in the hot stage. Scale bars and measurement temperatures are inserted in each image layer.

2.5 Digital image processing

Detailed evaluation of globule size distribution was performed using the ImageJ software (Image Processing and Analysis in Java).

2.6 DLS measurement

Globule size distributions were determined using an SALD-7100 (Shimadzu Co. Ltd.) analyzer equipped with 375 nm UV laser diode. The globule size was obtained from the autocorrelation function of the intensity fluctuation of the scattered light. These measurements yielded the diffusion coefficient D which was subsequently used to calculate the globule hydrodynamic radius R_H using the Stokes-Einstein equation, $D = kT / 6\pi\eta R_H$, where k is the Boltzmann constant, T is the absolute temperature, and η is dynamic viscosity (calculated using the viscosity of components forming the solvent). The sample was heated to 40 °C and data were collected at ~20 s intervals during spontaneous cooling to ambient temperature. Since the reproducibility of measurements on samples of relatively high PVME

concentration was poor, data obtained from a sample with PVME concentration c = 0.6 wt% and EtOH concentration c_{EtOH} = 1 vol% was used.

3 Results and discussion I

3.1 Temperature dependences of ^{1}H NMR spectra

3.1.1 Phase separated fraction – FID sequence

All studied solutions were cloudy at temperatures above the LCST and no precipitation (sedimentation) was observed even after long time (~ days). An example of high-resolution ^{1}H NMR spectra of PVME/D_2O/EtOH solution (c = 6 wt%, c_{EtOH} = 5 vol%) measured at two slightly different temperatures (37 °C and 40 °C) is shown in Figure 4. The assignment of resonances to various types of protons of PVME and ethanol is shown directly in a spectrum measured at 37 °C; the strong line on the left is a merged signal of ethanol/HDO OH protons. The splitting of CH, CH_3 and CH_2 resonances of PVME is due to tacticity [36]. The most important effect observed in the spectrum measured at a higher temperature (40 °C) is a marked decrease in the integrated intensity of all PVME lines. This is due to the fact that at temperatures above the LCST the mobility of most PVME units is reduced to such an extent that corresponding lines become too broad to be detected in high-resolution spectra. A narrow component with unrestricted mobility (with much smaller integrated intensity) that is directly detected in high-resolution NMR spectra corresponds to PVME units in the dilute (polymer-pure) phase; from former results it follows that it corresponds mainly to low-molecular-weight fraction of PVME where the chains are too short to exhibit a cooperative coil-globule transition [39]. The depicted changes of the NMR spectra have been previously observed for D_2O

solutions of PVME [36-40,43] and acrylamide-based polymers ([43] and references therein). They confirm that reaching LCST results in marked line broadening of a major part of PVME units, evidently due to the phase separation and formation of rather compact globules. No reduction of integrated intensities at temperatures above LCST was observed for EtOH signals. The integrated intensities of EtOH monotonously decrease with absolute temperature, as expected, so confirming that all EtOH molecules are directly detected in ^{1}H NMR spectra in the whole range of temperatures.

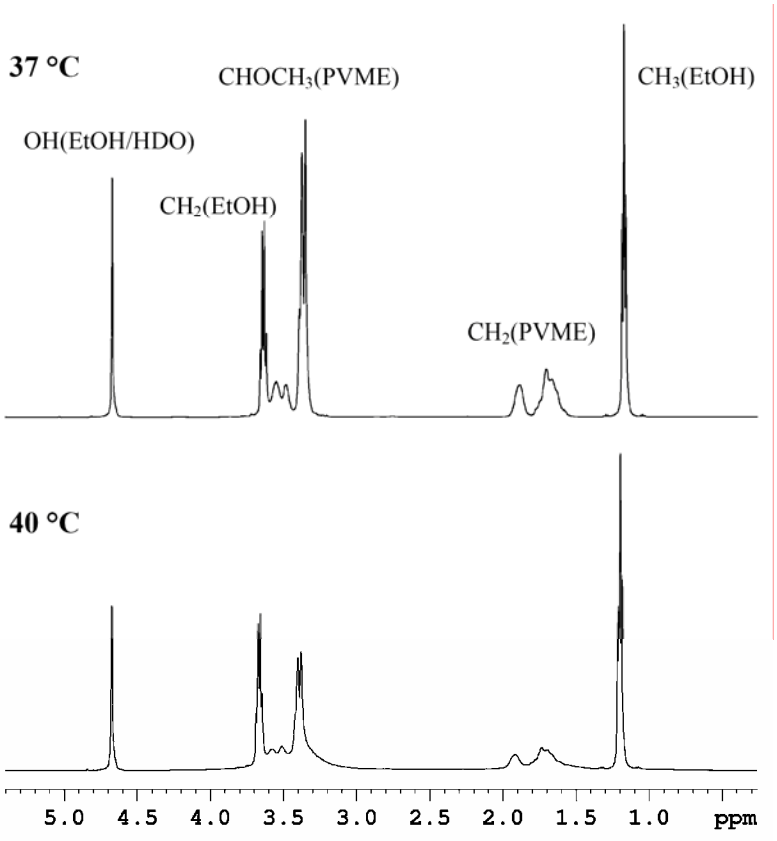

Figure 4. ^{1}H NMR spectra of PVME/D_2O/EtOH solution (c = 6 wt%, c_{EtOH} = 5 vol%) measured at 37 °C and 40 °C.

For further analysis, in accord with procedure published in Ref. [36-40,43], we shall define the phase-separated PVME fraction as fraction of PVME units in concentrated, polymer-rich phase; the mobility of these PVME units is significantly lower in comparison with that at temperatures below the LCST transition. We have

determined the values of fraction p of phase-separated PVME units (units in globules) from relation

$$p = 1 - \frac{I}{I_0}, \qquad (5)$$

where I is the integrated intensity of the given polymer line in a partly phase-separated system and I_0 is the integrated intensity of this line if no phase separation occurs [36,37,43]. For I_0 we took values based on integrated intensities below the phase transition, using the fact that integrated intensities should decrease with absolute temperature as $1/T$. It originates from integration of Bloch's equations solution which gives the relation for integrated intensities of the NMR bands as $I = K\,N\,(1+\gamma B_1 T_1 T_2)^{-1/2}\,(1/T)$, where K is a constant, N is the number of protons per unit volume contributing to the given band, T is the absolute temperature, γ is the gyromagnetic ratio, B_1 is the intensity of the radio frequency magnetic field, and T_1 and T_2 are spin-lattice and spin-spin relaxation times of corresponding band [44,45]. The expression $s = (1+\gamma B_1 T_1 T_2)^{-1/2}$ is the saturation factor which is usually close to unity. The integrated intensities were measured ~ 20 min after the corresponding temperature was reached (by heating).

In the analysis of the phase transition behaviour, first, the influence of the polymer concentration c on the transition region was investigated. Temperature dependences of the fraction p of PVME, as obtained from integrated intensities of $CHOCH_3$ protons of PVME, are shown for EtOH content in D_2O/EtOH mixture, c_{EtOH} = 10 vol%, and various polymer concentrations in Figure 5. From this figure it follows that the transtion in more concentrated solutions (c = 6 and 20 wt%) sets in at a temperature lower by ≈ 5 °C in comparison with the dilute solution (c = 0.1 wt%). This shift of the transition is probably a consequence of the preferred polymer-polymer contacts at higher concentrations, allowing hydrophobic interactions to predominate at lower temperatures. Lower polymer concentrations show more gradual character of the transition and at the same time, the fraction at temperatures above the transition is only $p \approx 0.5$; thus approximately 50 % of polymer units have unrestricted mobility even at temperatures above the transition.

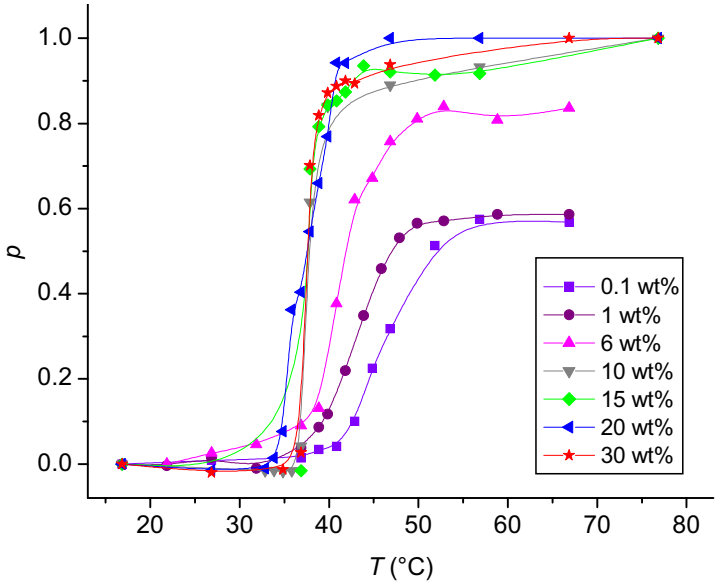

Figure 5. Temperature dependences of phase-separated fraction p as determined from integrated intensities of $CHOCH_3$ band in ^1H NMR spectra of PVME/D_2O/EtOH solutions with c_{EtOH} = 10 vol% and various polymer concentrations.

The effect of ethanol content in D_2O/EtOH mixture on the phase transition in PVME solutions is demonstrated in Figure 6 where temperature dependences of the fraction p corresponding to solutions with polymer concetration c = 1 wt% and various EtOH content are plotted. To complete these plots, the temperature dependence of the fraction p for PVME/D_2O solution (without ethanol) [36] is also included in Figure 6. This figure shows clearly that the phase transition shape depends on the ethanol content. The transition region is shifted towards higher temperatures with the increasing amount of EtOH in D_2O/EtOH mixture, and at the same time the transition extent (fraction p) markedly decreases. For example, the transition of the solution with the highest EtOH content (c_{EtOH} = 20 vol%) sets in at temperature higher by 15 °C in comparison with that of PVME in D_2O. Simultaneously, for this sample the width of the transition region is approximately 30 °C and the value of the phase-separated fraction p above the transition is roughly 0.5. The shift of the transition temperature with increasing ethanol content in PVME/D_2O/EtOH solutions is in accord with previous measurements of the cloud points in PVME/water/alcohol solutions [27,35]. The assumption of the positive role of ethanol (which is a better solvent) in stabilization of polymer-solvent interactions is supported by the found decrease of the fraction p above the transition with

increasing ethanol content (Figure 6). The ethanol molecules probably prevent hydrophobic polymer-polymer interactions and therefore the transition is shifted towards higher temperatures and becomes less "perfect" (the transition is broader and phase-separated fraction *p* above the transition is smaller).

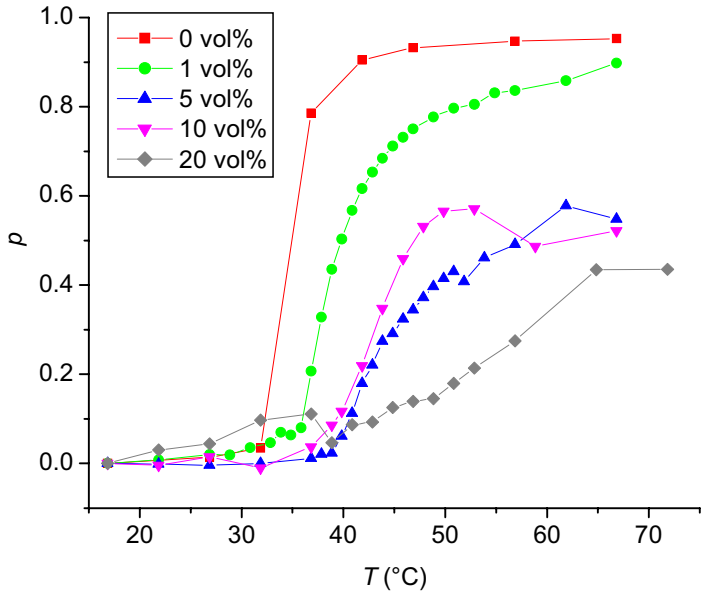

Figure 6. Temperature dependences of phase-separated fraction *p* as determined from integrated intensities of $CHOCH_3$ band in ^1H NMR spectra of PVME/D_2O/EtOH solutions with c = 1 wt% and various content of EtOH in D_2O/EtOH mixtures.

3.1.2 Phase separated fraction – FID vs. spin-echo sequence

A different approach for determination of fraction of phase-separated PVME units was used. This technique is based on the spin-echo pulse sequence as described in experimental section (2.2.2). The spin-echo pulse sequence (with echo time $2t_d$ = 8 ms) avoids the appearance of resonances due to phase-separated units of PVME which overlap the peaks corresponding to the non-separated fraction of PVME. Echo time $2t_d$ was set according to previous ^1H spin-spin relaxation measurements. The time $2t_d$ should be long enough to remove resonance of phase-separated units of PVME from spectrum and short enough to not decrease significantly other resonances. Thus, we can observe only the resonances due to PVME non-separated fraction.

Examples of high-resolution ^{1}H NMR spectra of PVME/D_2O/EtOH solution (c = 20 wt%, c_{EtOH} = 1 vol%) measured at two different temperatures (below LCST 32 °C and above LCST 40 °C) and by two different pulse sequence (FID and spin-echo) are shown in Figure 7. Assignment of peaks corresponding to protons of PVME and EtOH is also shown. From a comparison of the spectra in Figure 7a and 7c it is evident that the spin-echo pulse sequence suppresses all PVME resonances except that due to $CHOCH_3$. This resonance remains intense and is suitable for further processing. In Figure 7d (as compared with 7b) the CH and CH_2 resonances of PVME as well as the broad peak are suppressed and the spectrum reveals information only about the non-separated units represented by the PVME $CHOCH_3$ resonance (Figure 7d, at 3.3 ppm). The latter resonance seems to consist mainly from CH_3 resonance above LCST (at 40 °C).

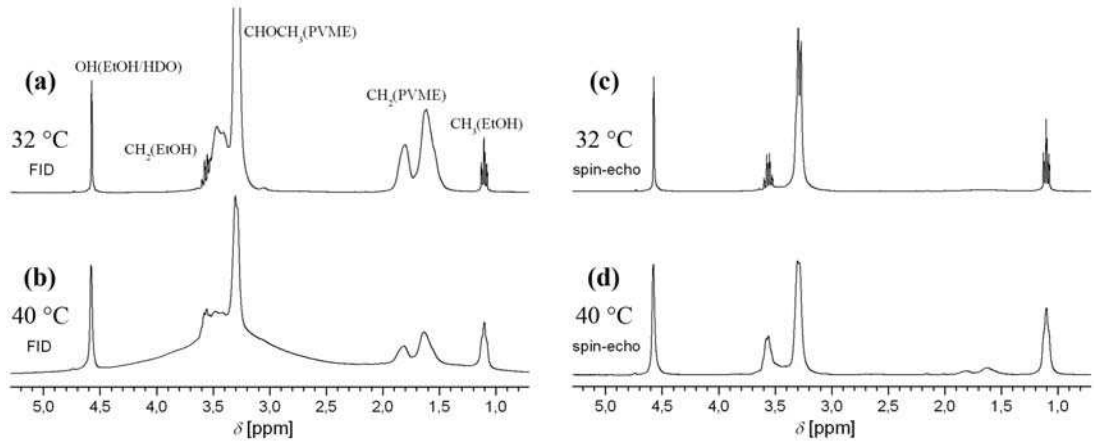

Figure 7. ^{1}H NMR spectra of PVME/D_2O/EtOH solutions (c = 20 wt%, c_{EtOH} = 1 vol%) measured at 32 °C (a,c) and 40 °C (b,d) using FID (a,b) and spin-echo (c,d) pulse sequences.

Temperature dependencies of the fraction p of PVME, as obtained from the integrated intensities of $CHOCH_3$ protons of PVME, are plotted in Figure 8. In Figure 8a, a comparison between the FID pulse sequence and spin-echo approach is shown. Spectral deconvolution was inaccurate in the FID sequence approach of p determination because of multiple overlaps of three peaks (CH_2 of EtOH, CH and CH_3 of PVME). Moreover, above the LCST, broad peaks due to the separated fraction become more intense. These features make deconvolution inconvenient. The spin-echo sequence circumvents the overlap problem although the resonances may

be now influenced by their own relaxation time T_2. This effect can be neglected since we are interested in the PVME resonances over the narrow (10 °C) temperature interval during which the phase separation occurs. In this case, the spin-echo sequence leads to much improved spectral resolution.

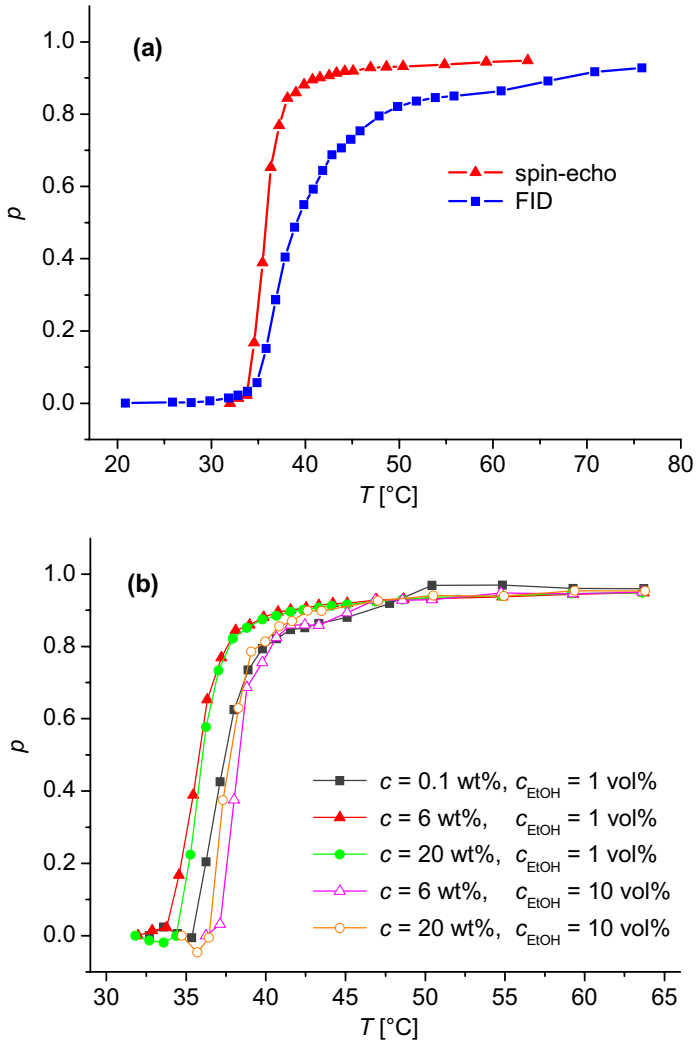

Figure 8. Temperature dependencies of phase-separated fraction p as determined from integrated intensities of the non-separated fraction of the $CHOCH_3$ peak in ^1H NMR spectra (Figure 7). (a) Comparison of fraction p as obtained using FID and spin-echo pulse sequence for PVME/D_2O/EtOH solution (c = 6 wt%, c_{EtOH} = 1 vol%). (b) Phase-separated fraction p as obtained from spin-echo pulse sequence for samples with various PVME concentrations c at two different EtOH concentrations c_{EtOH}.

The FID pulse sequence approach indicates a more gradual transition (Figure 8a-■) while the spin-echo pulse sequence approach gives a much sharper one (Figure 8a-▲). Similarly, a sharp transition of the fraction p could be found in systems where

the polymer resonances are well-resolved [46]. Figure 8b shows data collected for solutions with various polymer and ethanol concentrations measured using the spin-echo pulse sequence.

When one compares Figures 5 and 8b it is seen that spin-echo pulse sequence gives higher value of fraction p above phase separation (above LCST) that FID sequence.

3.1.3 ^{1}H NMR spectra – broad peak subtraction (spin-spin relaxation time)

Measurements of FID and spin-echo pulse sequence at the same temperature also give us information about the mobility of PVME phase-separated units. First, the spectrum measured by using the spin-echo pulse sequence was subtracted from the spectrum measured using the FID sequence. The resulting spectrum was fitted by using a mixture of Gauss and Lorentz curves (Gauss-Lorentz). The ratio of these two peak shapes was not a fixed parameter although in most cases it was 100% Lorentz curve. There were two cases where the ratio was around 75% Lorentz and 25% Gauss shape. The fit accuracy was dependent on the region used for fitting. Final error was estimated by varying the width of the fitted region (approximately from 1 ppm to 2.5 ppm). Spectral subtraction permitted use of a wider fitting region and reduced the final estimated error. The half-width $\Delta\nu$ of the Gauss-Lorentz curve for various temperatures above the LCST for the sample with concentrations c = 6 wt% and c_{EtOH} = 1 vol% is plotted in Figure 9a.

The half-width $\Delta\nu$ is related to the spin-spin relaxation time T_2 by the following formula:

$$\Delta\nu = \frac{1}{\pi T_2}. \qquad (6)$$

The corresponding spin-spin relaxation times T_2 were determined using formula (6) and plotted in Figure 9b. This method for T_2 determination is relatively fast (compared with use of the CPMG sequence) but it results in smaller T_2 values since they are influenced by inhomogenous line broadening. According to this assumption, the values contained in Figure 9b are somewhat smaller than relaxation times T_2 obtained by using the CPMG sequence in reference [39] (0.91 ms for PVME/D_2O

solution with the same polymer concentration at 36.4 °C). Increase in T_2 (Figure 9b) values upon increasing temperature seems to be rather general character of spin-spin relaxation time.

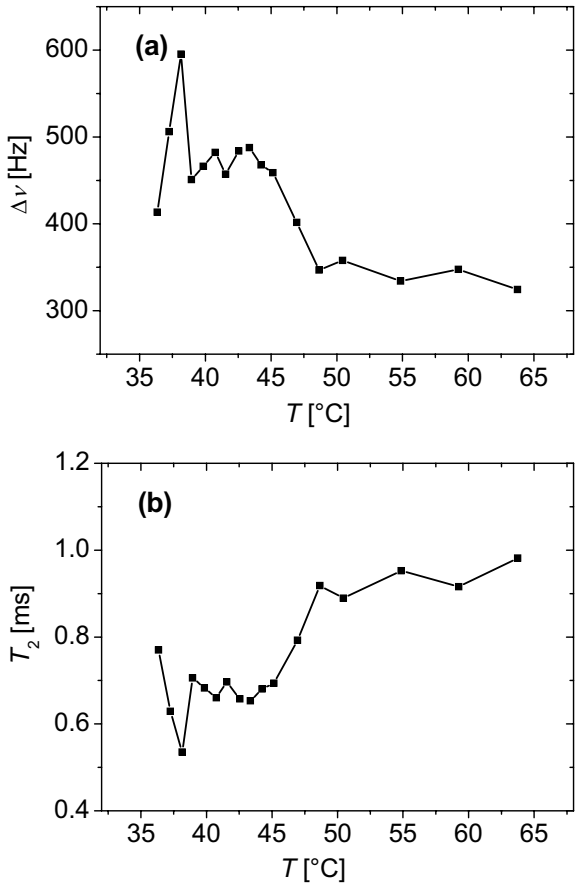

Figure 9. (a) Temperature dependencies of half-width Δv of Gauss-Lorentz curve obtained from spectra of PVME/D_2O/EtOH solution (c = 6 wt%, c_{EtOH} = 1 vol%) (b) Temperature dependencies of spin-spin relaxation time T_2 calculated using formula (6). Estimated error is ±15%.

3.2 ^{1}H NMR spectra and ^{1}H spin-spin relaxation times T_2 of EtOH

In ^{1}H NMR spectra of the studied PVME solutions in D_2O/EtOH mixtures (containing 1-20 vol%, i.e., 0.3-7.2 mole% of EtOH) there is a merged single line of EtOH and HDO OH protons (cf. Figure 4). In this respect the situation is the same as in water/EtOH mixtures of the same composition [47]. Taking into account the fact that the used D_2O contains 99.9 % of deuterium then it follows that while for the

mixture EtOH/D_2O containing 1 vol% of EtOH, the molar ratio EtOH/HDO = 3/2 and the contribution of both species to the merged OH peak is roughly comparable, for mixtures EtOH/D_2O containing 5, 10 and 20 vol% of EtOH the respective molar ratios are EtOH/HDO = 8/1, 24/1 and 36/1. This means that especially for PVME solutions in EtOH/D_2O mixtures containing 10 or 20 vol% of EtOH the OH protons of EtOH predominantly contribute to the merged EtOH/HDO peak and contribution from HDO to this peak can be neglected. This is confirmed by integrated intensities of EtOH signals. Thus, e.g., for PVME solution (c = 20 wt%) in D_2O/EtOH mixture containing 20 vol% of EtOH, the ratio of integrated intensities of OH, CH_2 and CH_3 signals of EtOH related to 1 proton is 1:0.95:0.94. We have found that slight departure from the expected ratio 1:0.97:0.97 is due to the presence of small amount (1 mole%) of H_2O in the used EtOH. Therefore for D_2O/EtOH mixtures contaning 20 vol% of EtOH, the contribution of EtOH, H_2O and D_2O (HDO) to the merged OH peak is in the ratio EtOH/H_2O/D_2O = 32/0.6/1; we took here into account the fact that while EtOH and D_2O (i.e., HDO) contribute to the merged OH signal by 1 proton, H_2O contributes to this signal by 2 protons. For D_2O/EtOH mixtures containing 10 vol% of EtOH, we have found from integrated intensities of EtOH signals that this ratio is EtOH/H_2O/D_2O = 22/0.4/1.

Measurements of ^{1}H spin-spin relaxation times T_2 of EtOH molecules in PVME/D_2O/EtOH systems should provide us an information about their mobility, and consequently about contacts between EtOH molecules and polymer chains. A comparison of the T_2 relaxation behaviour of EtOH with that previously found for HDO in PVME/D_2O solutions [38-40,43] should enable us to compare the behaviour of both types of small molecules during temperature-induced phase transition. To observe the effect of the polymer concentration on dynamic behaviour of EtOH we have chosen three samples with EtOH content in EtOH/D_2O mixture, c_{EtOH} = 10 vol%, and polymer concentrations c = 0.1, 6 and 20 wt%. Table 1 shows the values of ^{1}H spin-spin relaxation times T_2 of EtOH as obtained for these samples at temperatures 37 °C (below the transition) and 52 °C (above the transition).

As it follows from Table 1, for dilute solution (c = 0.1 wt%) T_2 values of all proton types of EtOH do not change as the solution undergoes the phase transition. This result is in accord with behaviour of water (HDO) as it was previously found

from T_2 measurements in PVME/D_2O solution of the same polymer concentration [38-40].

Table 1. ^1H spin-spin relaxation times T_2 of EtOH for PVME solutions in D_2O/EtOH mixtures with c_{EtOH} = 10 vol%.

c [wt%]	T_2 [s][a]					
	OH[b]		CH_2		CH_3	
	37 °C	52 °C	37 °C	52 °C	37 °C	52 °C
0.1	0.9	0.9	6.7	6.7	5.6	5.5
6	2.5	0.16	4.2	0.06	4.3	0.12
20	0.8	2.2[c], 0.02[d]	3.2	6.4	5.0	7.8

[a] Estimated experimental error ±5 %.
[b] Contribution of HDO to merged EtOH/HDO OH peak is negligible.
[c] Free EtOH, peak at 4.65 ppm (cf. Figure 11).
[d] Bound EtOH, peak at 4.4 ppm (cf. Figure 11).

The behaviour found for T_2 values of EtOH in the solution with c = 6 wt% is quite different (cf. Table 1). At elevated temperature above the transition (52 °C) the relaxation times T_2 of all EtOH groups are 1-2 orders of magnitude shorter than those at 37 °C. This behaviour that again for HDO has been previously observed for PVME/D_2O solutions with c = 2-10 wt% [38-40] shows that in PVME/D_2O/EtOH solutions with c = 6 wt% at temperature above the transition there is a portion of EtOH molecules bound in globules. The exponential character of T_2 relaxation curves and the fact that there is always a single line of the respective proton group in the NMR spectrum indicate for EtOH molecules a fast exchange between bound and free sites regarding T_2 values (the residence time of the bound states is ≤ 0.01 s, i.e., at least one order of magnitude shorter than the observed T_2; cf. Table 1 and Ref. [39]). In order to distinguish between two different dynamic states of solvent molecules (D_2O and EtOH) we introduce term “free” for solvent molecules in bulk without interaction with polymer and term “bound” for solvent molecules interacting with polymer.

There are two most important possible sources of the short T_2 values of EtOH observed for PVME solution (c = 6 wt%) in D_2O/EtOH mixture at temperature above the LCST transition:

(i) a lower, spatially restricted mobility, similarly to the phase-separated PVME;

(ii) chemical exchange.

The dependence of measured T_2 values on the time interval t_d in CPMG pulse sequence is often used for characterization of microsecond-millisecond chemical exchange [48,49]. Figure 10 shows such dependence as obtained for OH protons of EtOH for PVME solution (c = 6 wt%) in D_2O/EtOH mixture with c_{EtOH} = 10 vol%.

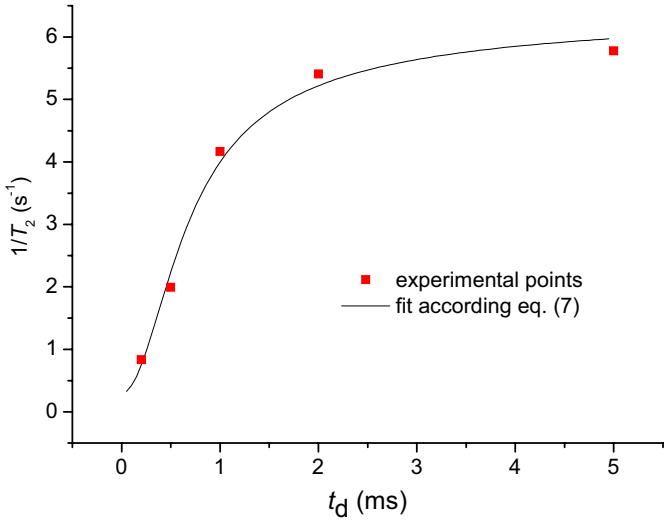

Figure 10. Dependence of spin-spin relaxation rate $(T_2)^{-1}$ on the interval t_d in CPMG sequence as obtained for EtOH OH protons in PVME/D_2O/EtOH solution (c = 6 wt%, 10 vol% of EtOH in D_2O/EtOH mixture) kept at 52 °C. Solid curve is a fit according equation (7) with k_{ex} = 2500 s^{-1} and $(R_2)^0$ = 0.296 s^{-1}.

From this figure it follows that contribution of chemical exchange to the spin-spin relaxation rate $(T_2)^{-1}$ is important. Solid curve in Figure 10 shows the best fit as obtained using the equation [49]

$$(T_2)^{-1} = \frac{p_A p_B \Delta^2 \omega^2}{k_{ex}} \left(1 - \frac{\tanh(k_{ex} t_d)}{k_{ex} t_d} \right) + (R_2)^0, \qquad (7)$$

with k_{ex} = 2500 s^{-1} and $(R_2)^0$ = 0.296 s^{-1}. Here k_{ex} is the rate constant for exchange process, $(R_2)^0$ is the spin-spin relaxation rate in the absence of the exchange assumed to be the same in states A and B, p_A and p_B are populations of the states, Δ is the chemical shift difference between the states and ω is resonance frequency. In equation (7) we assumed that the exchange is fast and that the exchange time τ_{ex} is

much slower than the motional correlation time τ_c causing other relaxation mechanisms. Since the exchange time τ_{ex} satisfies the formula $\tau_{ex} = 1/ k_{ex}$, we obtained $\tau_{ex} = 0.4$ ms.

While for PVME/D_2O/EtOH solutions with $c \leq 10$ wt% there was only one merged signal of the EtOH/HDO OH protons, for higher concentrations $c \geq 20$ wt% and temperatures above the LCST transition a new signal of EtOH/HDO OH protons was detected with ~0.25 ppm smaller chemical shift in comparison with the main EtOH/HDO OH peak. In Figure 11, where the ^{1}H NMR spectrum of the PVME/D_2O/EtOH solution with c = 20 wt% and c_{EtOH} = 20 vol% is shown, a new EtOH OH signal (we neglect the contribution of HDO to this signal) is marked by asterisk.

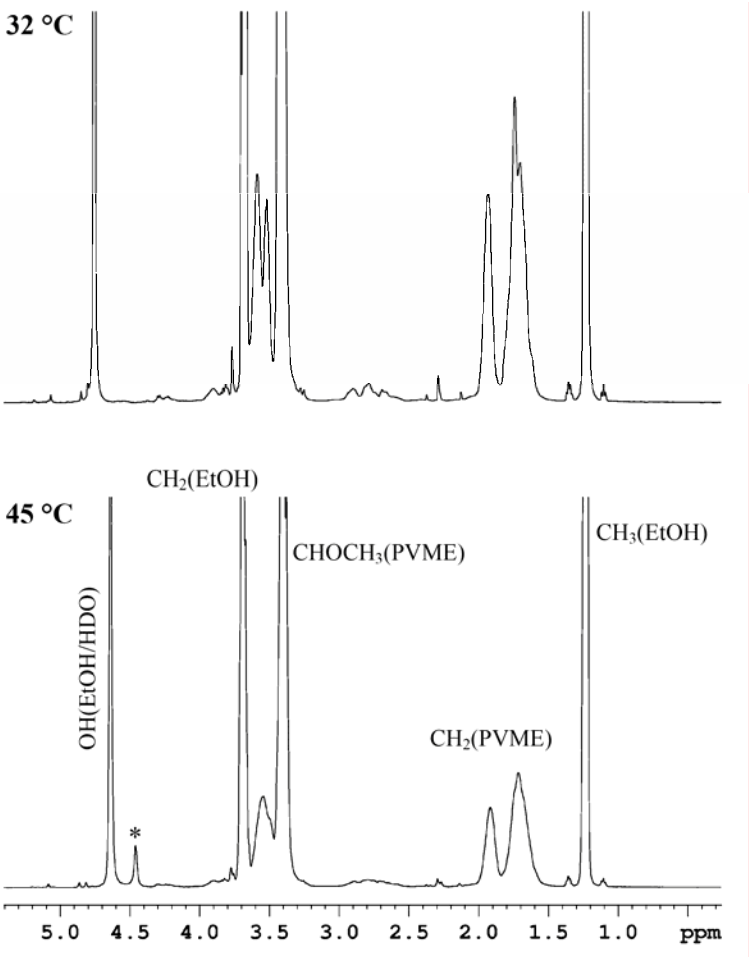

Figure 11. ^{1}H NMR spectra of PVME/D_2O/EtOH solution (c = 20 wt%, c_{EtOH} = 20 vol%) measured at 32 °C and 45 °C. OH line of the bound EtOH is marked by asterix.

This new EtOH OH signal appears only at temperatures above the phase transition and evidently corresponds to EtOH molecules bound in globular-like structures. For EtOH in highly concentrated PVME/D_2O/EtOH solutions, therefore, there is a slow exchange between bound and free sites. Similarly results were found for bound and free water in highly concentrated PVME/D_2O solutions [40]. Here the term "slow exchange" includes also the situation that there is no exchange at all (the residence time is infinity). From the condition $1/\tau << \Delta\nu$ [50], where τ is the residence time and $\Delta\nu$ is the difference of the respective chemical shifts in hertz, it follows that for the residence time of bound EtOH molecules it holds $\tau >>$ 8 ms. From integrated intensities of lines corresponding to OH protons in free and bound EtOH/HDO (cf. Figure 11), the relative amount of EtOH/HDO molecules bound in PVME globules can be determined (Table 2).

Table 2. Fraction of bound EtOH/(HDO) and chemical shift of bound EtOH/(HDO) OH protons in PVME/D_2O/EtOH solutions (c = 20 wt%) at 42 °C.

Content of EtOH in D_2O/EtOH mixture c_{EtOH} [vol%]	Fraction of bound EtOH/(HDO)[a] [%]	Chemical shift of OH protons in bound EtOH/(HDO)[a] [ppm]
1	10	4.26
5	8	4.30
10	8	4.41
20	8	4.56

[a] For contents of $c_{EtOH} \geq 5$ vol% a contribution of HDO to the merged EtOH/HDO OH signal is negligible.

From Table 2 it follows that the relative amount of bound EtOH/HDO as a function of EtOH fraction in D_2O/EtOH mixture is virtually constant. Table 2 also contains chemical shifts of the OH line of bound EtOH/HDO. It is well known that hydrogen bonding leads to larger chemical shifts in ^{1}H NMR spectra [50,51]. The fact that the chemical shift of the bound EtOH/HDO OH protons is always smaller in comparison with the main OH signal of free EtOH/HDO indicates that for the EtOH/HDO (with predominant contribution of EtOH for D_2O/EtOH mixtures with $c_{EtOH} \geq 5$ vol%)

bound in globular-like structures the hydrogen bonding is somewhat weaker in comparison with that existing in neat D_2O/EtOH mixtures. Increasing amount of EtOH in D_2O/EtOH mixture results in higher values of the chemical shift of OH protons of bound EtOH/HDO (cf. Table 2) as a consequence of the strengthening of the hydrogen-bonding structure. The same trend was found also in neat water/EtOH mixtures with EtOH fraction ≤ 20 vol% where the presence of small quantity of EtOH promotes the formation of new water-ethanol hydrogen bonds and/or incremented water-water association [47].

The assignment of two separated OH lines in concentrated PVME/D_2O/EtOH solutions to free and bound EtOH (or EtOH/HDO for solutions with small EtOH fraction in D_2O/EtOH mixture) is corroborated by measurements of spin-spin relaxation times T_2 on both signals (cf. Table 1, c = 20 wt%). Significantly longer T_2 values as obtained at 52 °C for the signal of the free EtOH in comparison with the value measured at 37 °C are evidently due to the fact that at higher temperature the respective EtOH molecules do not interact with PVME, and therefore they are really free while at temperature 37 °C a significant part of EtOH molecules interact with polymer forming, e.g., hydrogen bonds and their motions are consequently somewhat restricted; a contribution from the chemical exchange can be also important in the latter case. On the other hand, due to spatially restricted mobility, T_2 value of OH protons of EtOH bound in globular-like structures is two orders of magnitude shorter in comparison with free EtOH (cf. Table 1). Also for CH_2 and CH_3 protons of EtOH, T_2 values at 52 °C were significantly longer in comparison with those at 37 °C, indicating that also for these proton types the separate lines of free and bound EtOH can exist for concentrated PVME/D_2O/EtOH solutions (cf. Table 1). However, for CH_2 and CH_3 EtOH groups the lines of the bound EtOH were not detected; they might be overlapped by signals of $CHOCH_3$ and CH_2 protons of PVME segments in the dilute phase (cf. Figure 11).

We were interested in knowing whether the amount of EtOH bound in PVME globules formed in concentrated aqueous solutions is changing with time or not. Sample was kept at temperature above the phase transition (52 °C in our case) and time dependence of the spin-spin relaxation time T_2 of EtOH OH protons was measured to this purpose. As it follows from Figure 12 where such time dependence

is shown for PVME/D_2O/EtOH solution with c = 6 wt% and c_{EtOH} = 10 vol%, T_2 values do not change during 17 hrs. However, after 40 hrs the T_2 significantly increased and then remains constant; the respective T_2 is even larger than the value observed at temperature below the transition (cf. Table 1).

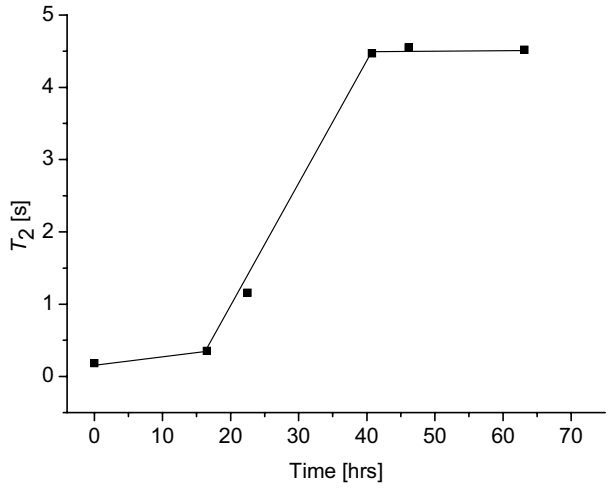

Figure 12. Time dependence of spin-spin relaxation time T_2 of EtOH OH protons in PVME/D_2O/EtOH solution (c = 6 wt%, c_{EtOH} = 10 vol%) kept at 52 °C.

This result shows that EtOH molecules originally bound in globular-like structures are with time very slowly released from these structures. The same process was previously found for bound water (HDO) in semidilute or concentrated PVME/D_2O solutions but releasing of EtOH as demonstrated in Figure 12 is slower as compared with the dehydration process in PVME/D_2O solution of the same polymer concentration [39]. We also followed the relative intensity of the separate OH resonance of bound EtOH in PVME/D_2O/EtOH solution (c = 20 wt%, c_{EtOH} = 10 vol%) and we have found that after 4 hrs at 52 °C the relative intensity of this line decreased to one half. From the same experiment at 42 °C it follows that the relative intensity of the separate OH resonance of bound EtOH decreased after 4 hrs to one fifth, i.e., the fraction of bound EtOH dropped from original 8 % to 1.6 %. These results show that at these conditions the releasing process is much faster.

3.3 ^{13}C NMR spectra and ^{13}C spin-spin (T_2) and spin-lattice (T_1) relaxation times of EtOH

^{13}C NMR spectra of PVME/D_2O/EtOH solution with polymer concentration c = 6 wt% and EtOH content in D_2O/EtOH mixture c_{EtOH} = 10 vol%, measured at 37 and 47 °C, i.e., below and above the LCST transition, respectively, are shown in Figure 13. The assignment of observed resonances to PVME and EtOH carbon types is marked in the spectrum measured at 37 °C. The pronounced reduction of intensities of polymer bands can be observed at 47 °C due to the formation of rather compact globules, similarly as in ^{1}H NMR spectra (cf. Figure 4). The intensities of EtOH signals are virtually unaffected by the transition; therefore we applied ^{13}C NMR relaxation measurements on these signals to study dynamics of EtOH molecules during the transition process.

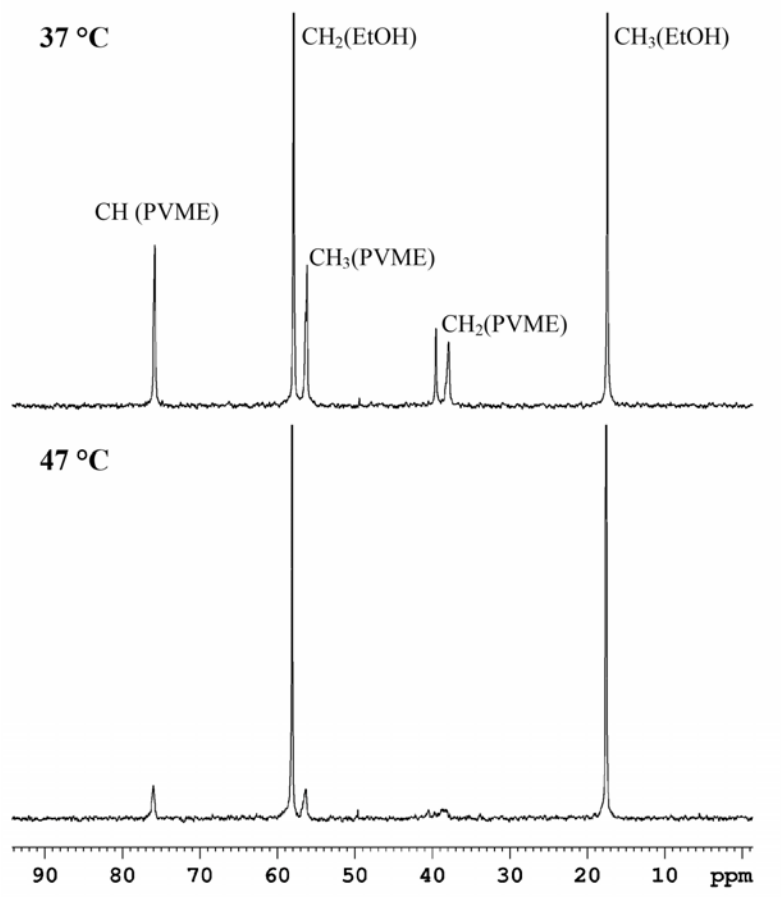

Figure 13. ^{13}C NMR spectra of PVME/D_2O/EtOH solution (c = 6 wt%, c_{EtOH} = 10 vol%) measured at 37 °C and 47 °C.

Tables 3 and 4 summarize ^{13}C spin-spin relaxation times T_2 and spin-lattice relaxation times T_1 as obtained for CH_2 and CH_3 ethanol carbons in PVME/D_2O/EtOH solutions with c = 0.1 and 6 wt% and ethanol fraction in D_2O/EtOH mixture c_{EtOH} = 10 vol%. In all cases the relaxation curves were single exponential. One can see that even at temperature below the phase transition (37 °C), T_2 values are somewhat shorter than the respective T_1 values; we assume that this rather unusual behaviour for small molecules is due to small spatial anisotropy in their motion as consequence of their interactions (by hydrogen bonding) with PVME segments (cf. ref. [40] and further text below).

Table 3. ^{13}C spin-spin relaxation times T_2 of EtOH for PVME solutions in D_2O/EtOH mixture with c_{EtOH} = 10 vol%.

c [wt%]	T_2 [s]			
	CH_2		CH_3	
	37 °C	52 °C	37 °C	52 °C
0.1	4.3	6.6	9.0	10.2
6	8.5	3.0	7.0	1.2

Table 4. ^{13}C spin-lattice relaxation times T_1 of EtOH for PVME solutions in D_2O/EtOH mixture with c_{EtOH} = 10 vol%.

c [wt%]	T_1 [s]			
	CH_2		CH_3	
	37 °C	52 °C	37 °C	52 °C
0.1	13.3	17.0	9.0	12.4
6	12.6	15.4	9.0	11.8

In accord with results of ^1H T_2 measurements shown in previous paragraph, completely different behaviour of EtOH can be seen for these two polymer concentrations from Table 3. While for the c = 0.1 wt%, ethanol T_2 values at 52 °C are somewhat longer than those at 37 °C, as expected for higher temperature, for c = 6 wt% a marked reduction of T_2 values was found for the phase separated system. This confirms that in 6 wt% solution a certain portion of EtOH molecules is bound in

globular-like structures with fast exchange between bound and free sites. Detailed relaxation study on PVME/D_2O [39] proposed that the globules have a complex internal structure and our results obtained by OM (see subsection 3.5) confirmed this suggestion.

From Table 4 it follows that T_1 values are insensitive to the phase transition, even for c = 6 wt% the values at 52 °C are always somewhat longer than those at 37 °C. Situation is here similar as it was previously found for HDO molecules in PVME/D_2O solution of the same polymer concentration where also a different sensitivity of T_1 and T_2 relaxation times to the LCST transition was established and interpreted in such a way that while the rates of the motion of bound and free HDO molecules are virtually the same, the motion of bound HDO is spatially restricted and anisotropic. The internuclear vector cannot reach all orientations and resulting existence of near-static dipolar interactions predominantly affects T_2 relaxation time; nevertheless, spatial restriction of the motion of bound HDO is rather small [40]. Such interpretation probably holds also for the bound EtOH. Moreover, as discussed in the paragraph 3.2, a contribution from the chemical exchange to the total spin-spin relaxation rate can be also important.

^{13}C NMR spectra of the PVME/D_2O/EtOH solution with the highest polymer concentration (c = 20 wt%) and EtOH fraction in the mixed solvent c_{EtOH} = 10 vol%, again measured at 37 °C and 52 °C, are shown in Figure 14. The most significant new feature in the spectrum measured at temperature above the phase transition (52 °C) is the existence of two additional peaks that appear in the vicinity of the original EtOH resonances. In accord with ^1H NMR spectra discussed above (cf. Figure 11) these new signals obviously belong to CH_2 and CH_3 carbons of EtOH molecules bound (probably forming hydrogen bonds with oxygen atoms of PVME units) in PVME globular-like structures. Contrary to the system with polymer concentration c = 6 wt% where the exchange between bound and free ethanol molecules was fast on the NMR time-scale, for 20 wt% solution the existence of separate resonances for bound and free EtOH molecules shows a slow exchange between both states; the lifetime of the bound EtOH molecules has to be much larger than 10 ms (the difference between chemical shifts of bound and free ethanol molecules is approx. 100 Hz on the frequency scale), again in accord with ^1H NMR results. From

integrated intensities of the lines of bound and free EtOH in ^{13}C NMR spectra we obtained that the ratio of ethanol molecules in the bound and free states is 0.06:0.94, i.e., the relative amount of bound EtOH as obtained from ^{13}C NMR spectra is in rather good agreement with the respective value obtained from ^{1}H NMR spectra (cf. Table 2). It is interesting that while CH_3 line of bound EtOH is shifted 1.2 ppm downfield from the CH_3 line of the free EtOH, the CH_2 line of bound EtOH is shifted 0.8 ppm upfield from the respective line of free EtOH, i.e., CH_2 carbons in bound EtOH are more shielded in comparison with free EtOH. In accord with results obtained from ^{1}H NMR spectra, higher shielding of CH_2 carbons in bound EtOH can be probably attributed to a weakening of the hydrogen bonding in comparison with free EtOH, similarly as decribed for carboxylic acid derivatives (anhydrides, esters, amides etc) [52].

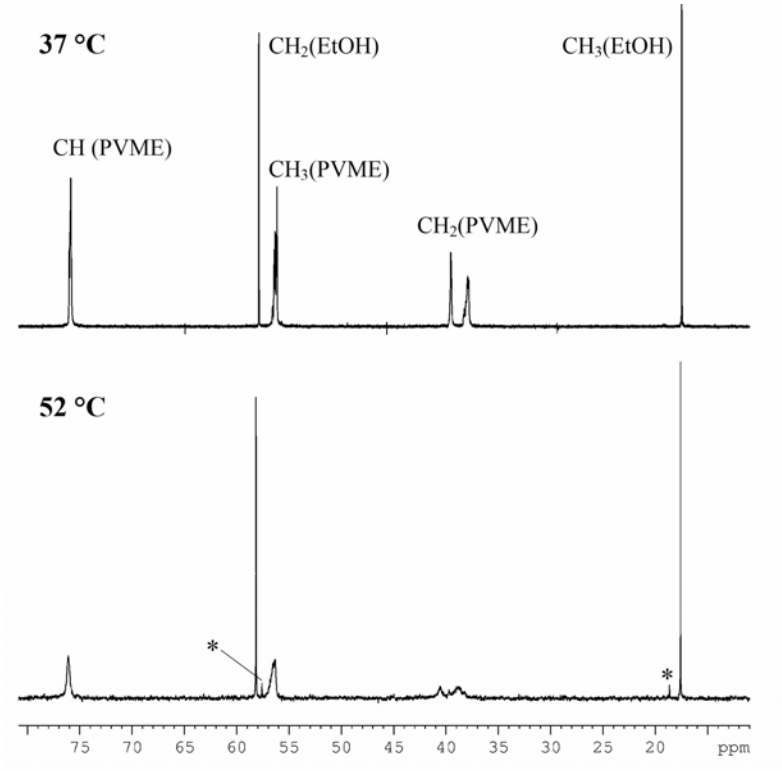

Figure 14. ^{13}C NMR spectra of PVME/D_2O/EtOH solution (c = 20 wt%, c_{EtOH} = 5 vol%) measured at 37 °C and 52 °C. Lines of the bound EtOH CH_2 and CH_3 carbons are marked by asterisks.

For PVME/D_2O/EtOH solution (c = 20 wt%) the study of dynamics of the ethanol molecules in bound and free states was performed using measurements of

^{13}C spin-spin and spin-lattice relaxation times T_2 and T_1, respectively. The values of the relaxation times as obtained for ethanol carbons in PVME/D_2O/EtOH solutions with c = 20 wt% and various ethanol fraction in D_2O/EtOH mixture are shown in Tables 5 and 6.

Table 5. ^{13}C spin-spin relaxation times T_2 of EtOH in PVME/D_2O/EtOH solutions with c = 20 wt%.

EtOH content in D_2O/EtOH mixture c_{EtOH} [vol%]	T_2 [s]			
	CH_2		CH_3	
	37 °C	52 °C	37 °C	52 °C
5	8.7	12.9[a], 2.4[b]	6.3	8.8[a], 3.5[b]
10	7.1	11.6[a], 1.1[b]	5.7	8.1[a], 3.0[b]
20	7.2	11.7[a], 5.1[b]	6.1	8.4[a], 4.7[b]

[a] From the signal of free EtOH, cf. text.
[b] From the signal of bound EtOH, cf. text.

From Table 5 it follows that at temperature above the transition, EtOH bound in globules is characterized by the T_2 values significantly shorter than those corresponding to free ethanol, though the observed differences are smaller than those obtained from ^1H T_2 measurements (cf. Table 1, c = 20 wt%). Simultaneously, the values obtained at temperature below the transition are located between the T_2 relaxation times of the free and bound ethanol as found for the systems above the transition. This is in accord with an idea of solvent (in our case ethanol) molecules which are initially (at temperatures below the transition) in contact with polymer chains, probably through hydrogen bonding, and their motion is consequently slightly restricted. However, as the solution passes the LCST transition, ethanol occurs either in free state, without any restriction in its mobility, or in bound state, where it is bound in relatively immobilized PVME globular-like structures. As seen from Table 6, for solution with c = 20 wt%, in contrast to c = 6 wt%, T_1 values are also significantly shorter for bound EtOH as compared with free EtOH indicating that in this case the rates of the motion of bound and free EtOH are somewhat different. At the same time, T_1 values at the temperatures below the transition are in between T_1 values of free and bound EtOH in the phase-separated system.

Table 6. ^{13}C spin-lattice relaxation times T_1 and correlation times τ_c (values in brackets) of EtOH in PVME/D_2O/EtOH solutions with c = 20 wt%.

EtOH content in D_2O/EtOH mixture c_{EtOH} [vol%]	T_1 [s] (τ_c [ps])					
	CH_2			CH_3		
	37 °C	52 °C		37 °C	52 °C	
		free[a]	bound[b]		free[a]	bound[b]
5	11.9 (2.0)	17.6 (1.4)	3.4 (7.2)	8.5 (1.9)	12.4 (1.3)	5.8 (2.8)
10	9.8 (2.5)	17.1 (1.4)	8.0 (3.0)	7.5 (2.2)	12.1 (1.3)	8.0 (2.1)
20	9.6 (2.5)	17.3 (1.4)	6.7 (3.7)	7.6 (2.1)	12.1 (1.3)	6.9 (2.4)

[a] Determined from the respective signal of free EtOH.
[b] Determined from the respective signal of bound EtOH.

Taking into account the fact that the spatial anisotropy of the bound motion of EtOH is similar to previously found one for the bound HDO, i.e. rather small in both cases [40], then assuming a model of rigid sphere isotropic rotation and the relaxation predominantly due to the dipolar interactions of carbons with directly attached protons, we calculated the values of the correlation times τ_c using the following expressions [53]

$$(T_1)^{-1} = \frac{1}{10} n \left(\frac{\mu_0}{4\pi} \frac{\gamma_C \gamma_H \hbar}{r^3} \right)^2 \left(J(\omega_H - \omega_C) + 3J(\omega_C) + 6J(\omega_H + \omega_C) \right), \quad (8)$$

$$J(\omega) = \frac{\tau_c}{1 + \omega^2 \tau_c^2}, \quad (9)$$

where n is the number of attached protons; μ_0 is vacuum permeability; γ_C, γ_H and r are gyromagnetic ratios of corresponding spins and spin-spin distance, respectively; $\hbar$ is reduced Planck constant; ω_H and ω_C are resonance frequencies of protons and carbons, respectively; and $J(\omega)$ is spectral density at ω frequency. Equation (9) is an expression for spectral density of rigid sphere isotropic rotation. The obtained values of the correlation times are given in Table 6 in brackets. From Table 6 it follows that for the bound EtOH, τ_c values are 2-3 times longer in average as compared to free EtOH, indicating that the motion of EtOH bound in globules formed in 20 wt% PVME/D_2O/EtOH solutions is slowed down. For PVME/D_2O/EtOH solutions at 52 °C, the τ_c values of free EtOH are virtually the same as we have found at the same

temperature for EtOH in neat D_2O/EtOH mixtures (without PVME) of the same composition (τ_c = 1.3 ps both for CH_2 and CH_3 carbons), so that supporting the idea that at 52 °C, molecules of free EtOH do not interact with PVME chains. Similarly as T_1 and T_2 values, correlation times of EtOH at 37 °C are in between the τ_c values as obtained for free and bound EtOH at 52 °C.

3.4 DSC measurement

In following part of this thesis we will concentrate on special features of the coil-globule transition during heating and cooling. For purposes of discussion, the terms 'demixing' (undergoing transition upon heating) and 'remixing' (undergoing transition upon cooling) are introduced.

3.4.1 Narrow temperature range DSC measurement

Cooling and heating DSC scans were performed on solutions with PVME concentrations c = 6 and 20 wt% and EtOH concentration c_{EtOH} = 1 and 10 vol% (four samples in total). Measurement procedure consisted of several (from three to five) heating-cooling cycles starting from 0 °C with heating to 55 °C then cooling to 0 °C.

For a homogeneous PVME/D_2O/EtOH solution, demixing was observed upon heating with an endothermic phase transition, whereas for an already phase separated solution remixing occurred upon cooling with an exothermic transition.

In order to investigate in detail the dynamic reversibility of the phase separation of PVME, all heating and cooling thermograms corresponding to particular sample were sorted and are plotted in Figure 15. Comparing the samples of low EtOH concentration c_{EtOH} = 1 vol% (Figure 15a,b) to those samples of high EtOH concentration c_{EtOH} = 10 vol% (Figure 15c,d), several differences are apparent but which in fact originate from the same phenomenon. It is clear that for samples at high EtOH concentration the thermograms contain nearly symmetric peaks due to the phase transitions during heating and cooling only, whereas at low EtOH concentration the thermal response has an unsymmetrical appearance. In the case of

low EtOH concentration solutions, the enthalpy increments per unit mass of PVME ΔH are slightly larger than those of high EtOH concentration as presented in Table 7.

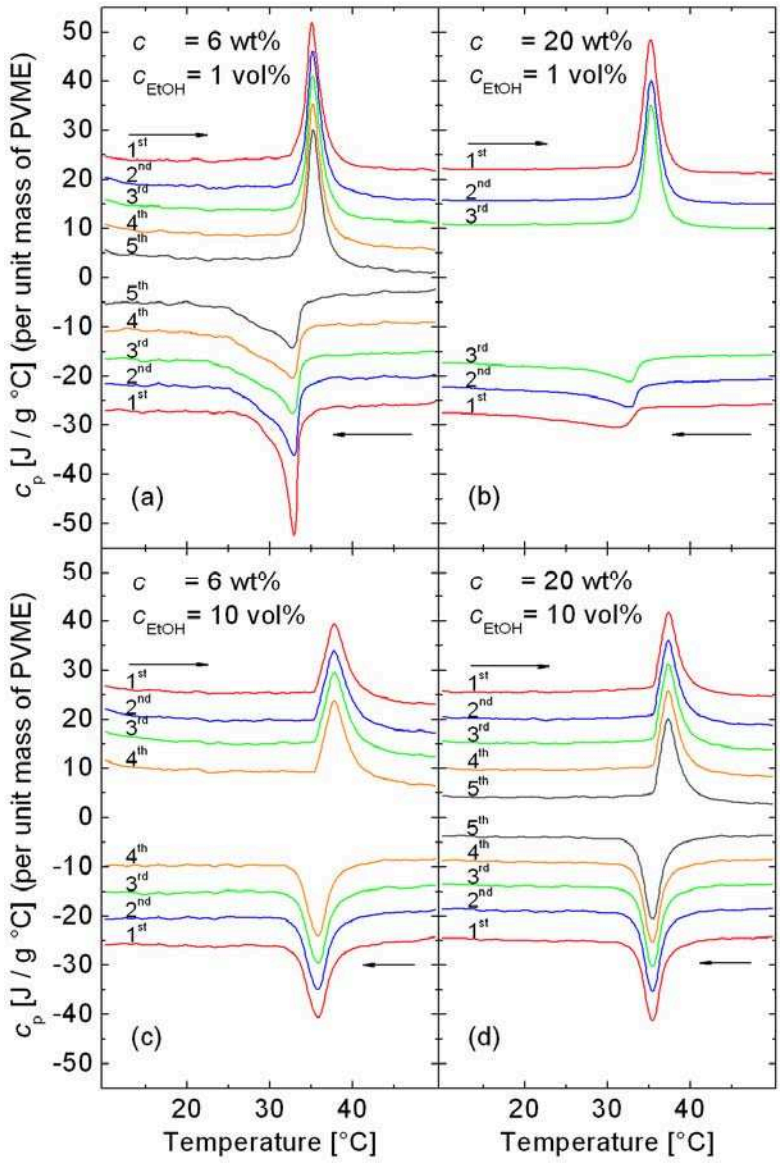

Figure 15. DSC scans of PVME/D_2O/EtOH solutions obtained on heating (→) and cooling (←). PVME concentration c and EtOH concentration c_{EtOH} are specified for each set of thermograms. Curves are shifted vertically for clarity.

In Table 7, columns (a) and (b) show larger values of enthalpy increments for each run than columns (c) and (d). For the lower EtOH concentration, the onset temperature of phase separation during heating and cooling is lower (around 33.7 °C) than that for higher EtOH concentration (around 36.0 °C). Moreover, a hysteresis

(around 2.3 °C) in onset temperature between heating and cooling can be observed at higher EtOH concentration.

Table 7. Enthalpy increment per unit mass of PVME ΔH and onset temperature T_{on} of PVME peak in PVME/D_2O/EtOH solutions as determined for n-th heating or cooling (run). (Double columns are marked from (a) to (d) as in corresponding thermograms in Figure 15).

	c_{EtOH} = 1 vol%				c_{EtOH} = 10 vol%			
	c = 6 wt% (a)		c = 20 wt% (b)		c = 6 wt% (c)		c = 20 wt% (d)	
Run	ΔH [J/g]	T_{on} [°C]	ΔH [J/g]	T_{on} [°C]	ΔH [J/g]	T_{on} [°C]	ΔH [J/g]	T_{on} [°C]
1st heating	58.9	33.7	57.5	33.5	53.1	35.3	52.4	35.4
2nd heating	60.8	33.8	55.8	33.7	54.1	35.3	51.4	35.4
3rd heating	56.7	33.7	53.2	33.7	56.9	35.3	52.4	35.4
4th heating	57.0	33.7	----	----	54.6	35.4	52.7	35.4
5th heating	54.6	33.7	----	----	----	----	52.9	37.3
5th cooling	58.2	33.9	----	----	----	----	50.0	37.3
4th cooling	58.4	33.9	----	----	51.4	38.0	50.0	37.3
3rd cooling	55.4	33.8	47.9	34.1	51.7	38.0	50.6	37.3
2nd cooling	59.5	33.7	47.1	34.1	52.6	38.1	49.8	37.3
1st cooling	57.5	33.6	46.4	34.0	52.1	38.1	50.5	37.4

Experimental error of ΔH was estimated to be ± 6 % and ± 3 % for all samples with PVME concentrations c = 6 wt% and c = 20 wt%, respectively.

These experimentally observed features can be explained by the positive role of EtOH in stabilization of polymer-solvent interactions [27,35]. The EtOH molecules eventually prevent the hydrophobic polymer-polymer interaction so that the onset temperature of demixing and remixing is shifted towards higher temperatures for higher EtOH concentrations. Lower values of enthalpy increments at higher EtOH concentration could be due to existence of some non-separated polymer chains that do not contribute to the enthalpy of transition. High-temperature shift of the LCST and decrease of transition enthalpy with higher EtOH content agree well with results obtained by NMR spectroscopy in subsection 3.1. Broad unsymmetrical peaks in cooling thermograms of samples with lower EtOH concentration imply that

processes of demixing and remixing occur by different mechanisms. During demixing, the solution undergoes a transition from a homogenous solution to a locally heterogenous state. On the molecular level almost all hydrogen bonds in the sample are disrupted uniformly with subsequent formation of globules. In the case of remixing, a transition from locally heterogenous to homogenous state takes place. Here, the compact globules with low or almost no solvent content are available for hydrogen bonding but the solvent molecules must penetrate and permeate the globules' interior through their surfaces (a feature which will be shown and discussed in greater detail in the OM study below). This effect is also driven by diffusion of solvent into the globules which can be more time consuming. Since the EtOH molecules support hydrophilic polymer-solvent interactions [27], the penetration of EtOH-rich solvent mixtures is facilitated. As seen in thermograms of cooling in Figures 15a and 15b, the slope and width of thermograms can vary significantly and depend on the ratio of PVME and EtOH concentration. As shown in Figure 15b, the cooling thermograms are so broad that the enthalpy increments calculated in Table 7 were affected becoming smaller. Therefore, enthalpy increments were recalculated from thermograms measured over a wider temperature range (see subsection 3.4.2, Table 9). Regarding the hysteresis at higher EtOH concentration, the onset temperature of heating and cooling are shifted slightly (Table 7, columns c,d) indicating that PVME chains are maintained in solution up to higher temperatures upon demixing while, on the other hand, the globules are more easily penetrated by solvent upon remixing.

Another considerable effect can also be seen in Figure 15. The slope and width of cooling thermograms change with respect to the order of runs. This change in shape is observed only for lower EtOH concentration samples. After one or two heating-cooling cycles, the system reaches a stable state and subsequent thermograms are static in terms of profile. The value of enthalpy increment upon cooling does not change significantly and therefore, it can be concluded that the same number of PVME chains undergo remixing. The gradual change of shape of cooling thermograms indicates that globules formed over several heating-cooling cycles are difficult to dissolve and, therefore, are more compact.

3.4.2 Wide temperature range DSC measurement

Cooling and heating DSC scans were performed on solutions with PVME concentrations c = 0, 0.1, 6 and 20 wt% and EtOH concentration c_{EtOH} = 1 and 10 vol% (eight samples in total). Data were collected during second cooling-heating cycles on cooling from 55 °C to -100 °C and then reheating to 55 °C.

The wide temperature range allowed us to consider in detail the solvent behavior with respect to PVME concentration and to investigate PVME in solutions that had undergone freezing and melting. The thermograms plotted in Figure 16 contain (cooling-heating order of measurement) PVME remixing peak, D_2O/EtOH freezing peak, D_2O/EtOH melting peak, and PVME demixing peak.

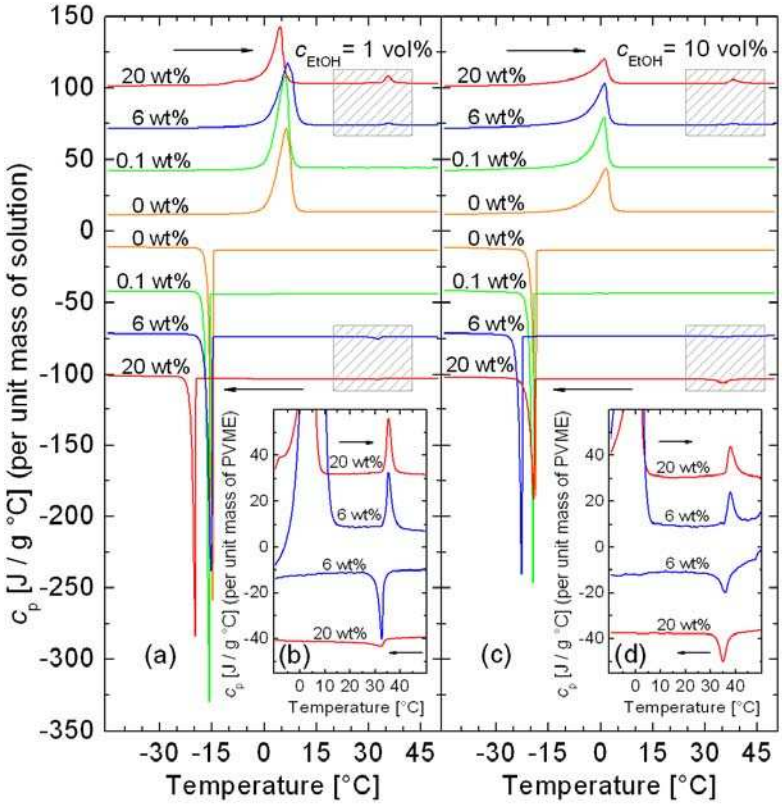

Figure 16. DSC scans of PVME/D_2O/EtOH solutions obtained during second cooling (←) and second heating (→) in a wide temperature range. PVME concentration c is specified at each thermogram and two EtOH concentrations c_{EtOH} are presented for (a), (b) and (c), (d). The shaded parts are enlarged within the insets. In (a) and (c) the specific heat capacity c_p is calculated per unit mass of solution while in (b) and (d) it is calculated per unit mass of PVME. Curves are shifted vertically for clarity.

The PVME remixing and demixing peaks are enlarged in the insets in Figure 16. Only two PVME concentrations are shown in the insets since the peaks were intense enough for further processing. PVME peaks in samples with PVME concentration c = 0.1 wt% were weak and are hence subject to large error.

The onset temperatures T_{on} of the D_2O/EtOH melting and freezing peaks are listed in Table 8. As shown in Table 8, all T_{on} temperatures for c_{EtOH} = 1 and 10 vol% do not vary significantly and do not show any regular occurrence depending on PVME concentration. In the work by Meeussen et al. [54], a decrease in the melting temperature of water with increasing PVME concentration was found for PVME/H_2O systems. According to measurements in Ref. [54], the drop in melting temperature between PVME concentrations c = 6 wt% and c = 20 wt% should be about 2 °C. If this latter fact is taken into account, a slight decrease in the melting point with increasing PVME concentration is apparent (see Table 8). Regarding the freezing peak, the onset temperature is not reliably reproducible because of the supercooling needed to overcome the surface Gibbs barrier for formation of the crystalline phase. The changes in T_{on} between samples with EtOH concentration c_{EtOH} = 1 vol% and 10 vol% are driven only by EtOH which shifts the T_{on} towards lower values.

Table 8. Onset temperature T_{on} of D_2O/EtOH peak in PVME/D_2O/EtOH solutions determined from wide temperature range scans during the second cooling-heating cycle.

		T_{on} [°C]	
Run	c [wt%]	c_{EtOH} = 1 vol%	c_{EtOH} = 10 vol%
heating	20	0.4	-6.7
	6	0.7	-5.3
	0.1	1	-4.5
	0	0.9	-5.1
cooling	0	-14.4	-18.4
	0.1	-15.5	-19.2
	6	-14.9	-22.4
	20	-19.6	-18.9

The PVME demixing and remixing peaks for PVME concentration over a wide temperature range are shown in Figure 16b and 16d. The enthalpy increment and onset temperatures are presented in Table 9. These values are in good agreement with those obtained during measurement over a narrower temperature range (cf. Table 7), i.e. when the sample was not cooled below the freezing point. Moreover, it was possible to determine the correct enthalpy increment value for the broad PVME remixing peak for the sample with PVME concentration c = 20 wt% and EtOH concentration c_{EtOH} = 1 vol% (Table 9).

Table 9. Enthalpy increment per unit mass of PVME ΔH and onset temperature T_{on} of PVME peak in PVME/D_2O/EtOH solutions determined from wide temperature range and second cooling-heating cycle.

Run	c [wt%]	c_{EtOH} = 1 vol%		c_{EtOH} = 10 vol%	
		ΔH [J/g]	T_{on} [°C]	ΔH [J/g]	T_{on} [°C]
heating	20	58.2	33.9	53.2	35.8
	6	58.5	33.7	51.9	35.7
cooling	6	58.2	33.5	50.5	38.6
	20	57.5	34.4	52.4	37.5

Experimental error of ΔH was estimated to be ± 6 % and ± 3 % for all samples with PVME concentrations c = 6 wt% and c = 20 wt%, respectively.

3.5 Optical microscopy measurement

In order to understand what occurs in these systems at the mesoscale, the optical microscopy was used. Images of PVME/D_2O/EtOH solutions at certain temperatures during heating-cooling were taken. Since almost no difference in the images of samples with EtOH concentration c_{EtOH} = 1 vol% and 10 vol% could be observed, the samples with c_{EtOH} = 10 vol% were chosen for investigation. Thus, imaging of two PVME/D_2O/EtOH samples with PVME concentration c = 6 wt% and 20 wt% and EtOH concentration c_{EtOH} = 10 vol% is presented.

The measurement procedure for study of demixing and remixing phenomena was as follows. The initial temperature was set at 30 °C followed by heating up to ~50 °C at a rate of 0.1 °C/min. In the critical temperature region (36 °C - 40 °C)

when phase transition in the samples commences, heating was discontinued after each 0.1 °C gain and the temperature allowed to stabilize for about 3 minutes. A similar procedure was followed on cooling. Images were taken at intervals of 0.5 °C except during the critical temperature range, where images were taken at intervals of 0.1 °C. Thus, the images obtained show the stable states at the indicated temperatures.

Figure 17 and 18 show transitions though demixing and remixing at two different scales for the same sample of concentrations c = 20 wt% and c_{EtOH} = 10 vol%. When phase separation occurs, the PVME-rich phase is present in images with a darker colour tone while the solvent-rich phase is displayed in lighter tones. At a lower magnification (Figure 17), a satisfactory overview is seen, at higher magnification (Figure 18), the structure is revealed in greater detail. In these figures, the initial state of phase separation (demixing) has a sponge-like structure with an increasing particle size as the temperature is increased with a subsequent formation of mostly ellipsoidal cell-like structures containing a complex internal substructure together with many small spherical globules. During remixing small globules redissolve relatively quickly while the cell-like structures dissolve gradually starting at their surface. Processes of demixing and remixing are clearly not equivalent from this point of view. Moreover, at a temperature below the LCST (first and last image layers in each of Figures 17 and 18) some small undissolved globules remain. Since it is unclear how long it might take for the entangled globule to transform back into a swollen coil by thermal motion [8], it is possible that some of these globules remain in a particular semi-stable globular state below the LCST. Complete dissolution of such globules might be prevented by existing entanglements and also by solution conditions in the vicinity of the LCST, i.e. when the character of solvent is on the limit between that of a thermodynamically good and bad solvent. In all the imaged samples, these globules were observed below the LCST after the first demixing. The number of such globules decreased significantly for the samples which were kept at room temperature for 24 hours and observed again below the LCST. Apparently, time periods of tens of hours are required for complete redissolution to occur. This behavior might also affect DSC measurements but could not be detected here probably because of the low content of these slowly remixing globules.

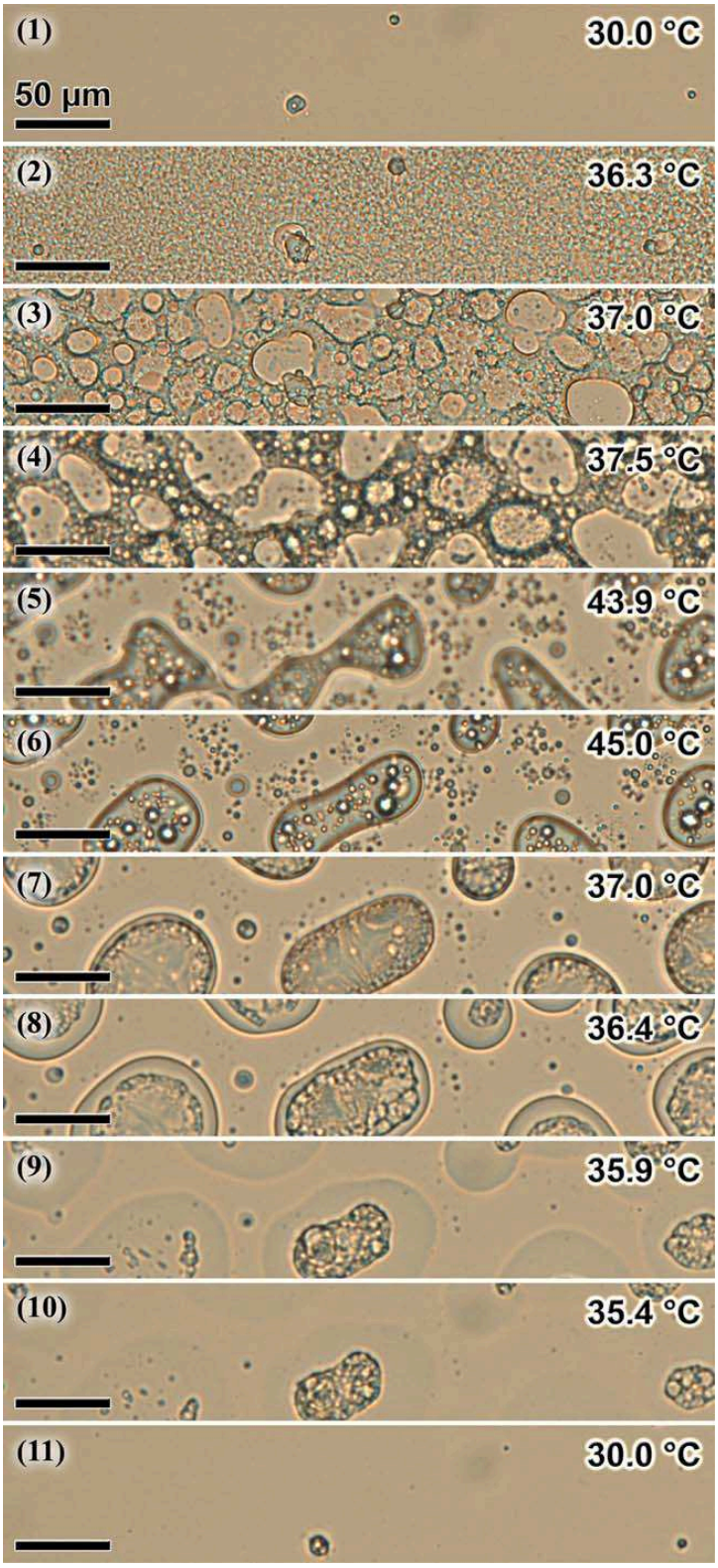

Figure 17. OM images captured with a 20x objective magnification. Temperature stack taken during one heating (from 30 °C to 45 °C, layers 1-6) and cooling (from 45 °C to 30 °C, layers 6-11) of PVME/D_2O/EtOH sample with PVME concentration c = 20 wt% and EtOH concentration c_{EtOH} = 10 vol%. Scale bar and temperature are presented in each layer.

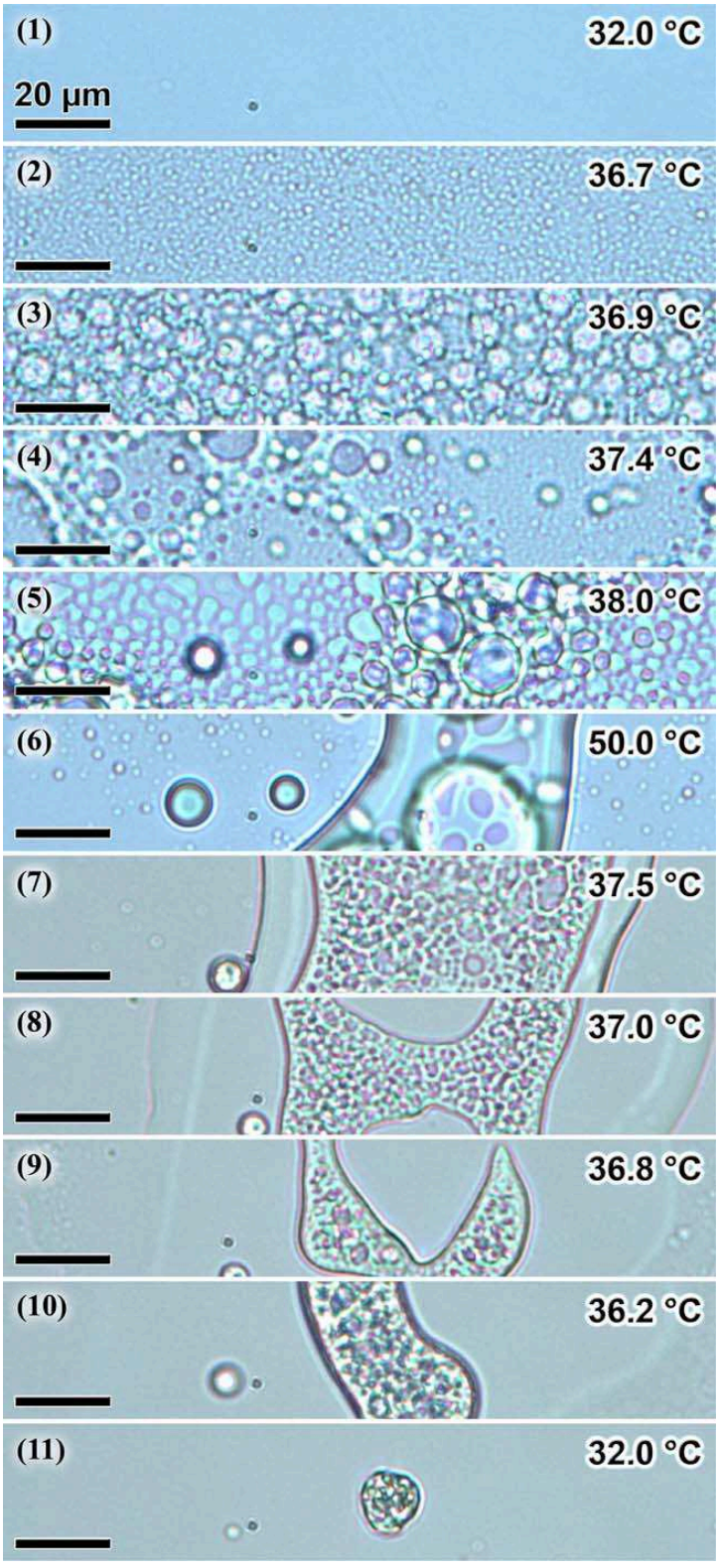

Figure 18. OM images captured with a 50x objective magnification. Temperature stack taken during one heating (from 32 °C to 50 °C, layers 1-6) and cooling (from 50 °C to 32 °C, layers 6-11) of PVME/D_2O/EtOH sample with PVME concentration c = 20 wt% and EtOH concentration c_{EtOH} = 10 vol%. Scale bar and temperature are presented in each layer.

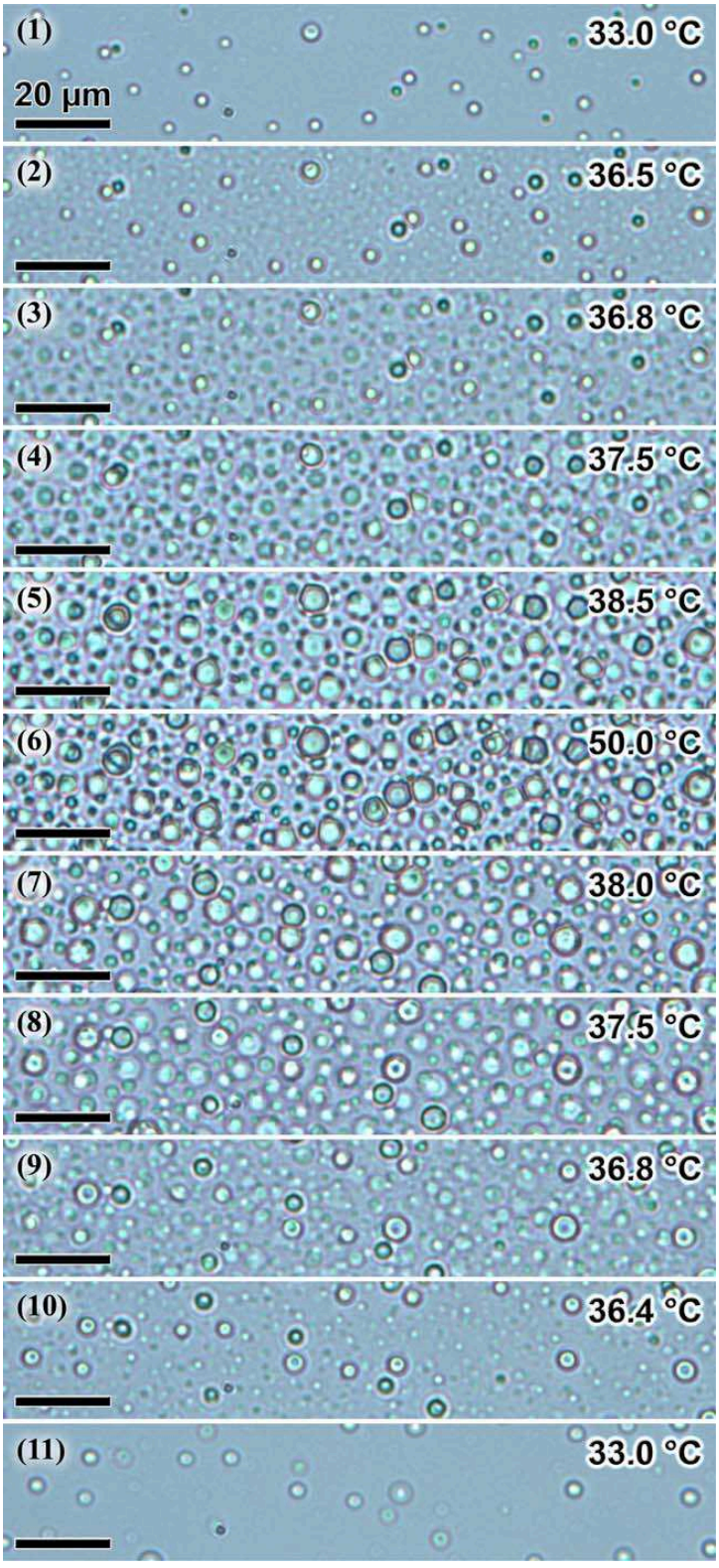

Figure 19. OM images captured with a 50x objective magnification. Temperature stack taken during one heating (from 33 °C to 50 °C, layers 1-6) and cooling (from 50 °C to 33 °C, layers 6-11) of PVME/D_2O/EtOH sample with PVME concentration c = 6 wt% and EtOH concentration c_{EtOH} = 10 vol%. Scale bar and temperature are presented in each layer.

A significant difference in morphology pattern was found for the samples with PVME concentrations c = 20 wt% (Figure 18) and c = 6 wt% (Figure 19). Although the initial stages of phase separation in these two samples appear similar, further temperature increase results in formation of spherical globules in sample with concentration c = 6 wt%. Globules in Figure 19 reach a certain size above the LCST and do not form the ellipsoidal cell-like structures, only the number of globules increases. At this PVME concentration, c = 6 wt%, PVME chains are not so strongly linked and so can demix more finely into relatively small spherical objects thus forming a droplet pattern.

Phase separation in polymer systems can exhibit a phase inversion [55-57]. The phase inversion occurs when the PVME-rich sponge-like structure is broken and the PVME-rich phase changes from being continuous (Figure 17, layer 4) to being discontinuous (layer 6). This effect was clearly observed for the sample with high PVME concentration c = 20 wt% (Figure 17 or 18) while for the sample with PVME concentration c = 6 wt% it was not so well pronounced (Figure 19). Zhou et al. [57] presented continuum models of phase separation derived from a two-fluid model of viscoelastic phase separation from nonequilibrium thermodynamics. In their work, the pattern evolution over time was calculated after the system passed its critical temperature. The results obtained in Ref. [57], including the phase inversion mentioned there, are in good agreement with the observations presented here for the sample with high PVME concentration c = 20 wt%.

Further investigations were concerned with morphology changes in the initial state below the LCST (at 30 °C) and in the final state above the LCST (at 45 °C) as shown in Figures 20 and 21. These figures contain several cycles consisting of heating from 30 °C to 45 °C at a rate of 1 °C/min followed by holding the sample at this temperature for 10 minutes. The sample was subsequently cooling to 30 °C at the same rate and held at that temperature for 10 minutes. After the first demixing (Figure 20, layer 2), a different pattern containing larger cell-like structures as compared to subsquent cycles after demixing (layers 4 and 6) was found. This observation suggests that after the first heating above the LCST the sample reaches some semi-stable state which is accompanied by creation of a larger amount of non-remixible globules as seen in odd layers in Figure 20. When the sample is kept for a

day at room temperature, a similar observation can be made. States above the LCST, in even layers of Figure 21, appear similar. Since in this case the pattern consists of many spherical globules, the difference between the first and other states after demixing is not clear.

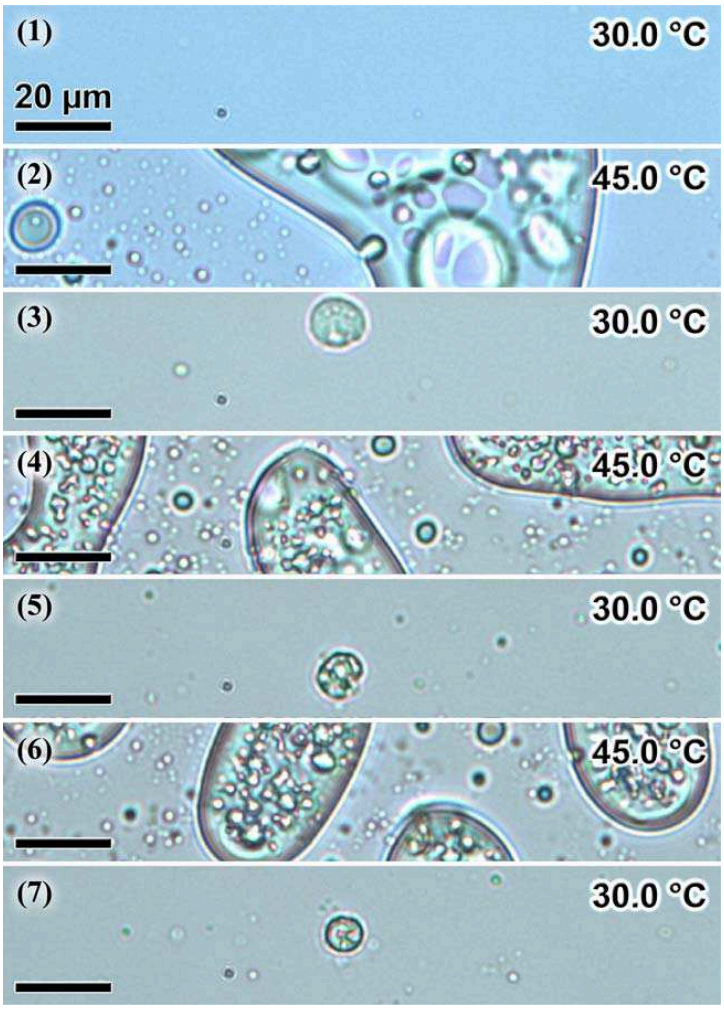

Figure 20. OM images captured with a 50x objective magnification. PVME/D_2O/EtOH sample with PVME concentration c = 20 wt% and EtOH concentration c_{EtOH} = 10 vol%. The states below (at 30 °C) and above (at 45 °C) the phase separation are presented. The stack starts from the top at 30 °C. Heating and cooling between the states was provided at a rate of 1 °C/min. Scale bar and temperature are presented in each layer.

Distinct similarities are also exhibited between all the low temperature images (odd layers) and suggest that undissolved globules are immobile. This reduced mobility could be caused by adherence to the glass slide. Another remarkable feature which can be seen in Figure 21 is that the number of non-remixible globules below the

LCST is greater but their size is smaller than for those observed in Figure 20. In odd layers (except layer 1) of Figure 20, much bigger non-remixible globules are observed. Only a single globule is seen within the visual field, however, the rest of them are uniformly distributed in the sample with an average inter-globule distance of about 200 μm. This effect can be explained as follows. After remixing, one or none undissolved residue remains from each globule. Therefore Figure 20 and 21 (odd layers) have different number of non-remixible globules below the LCST.

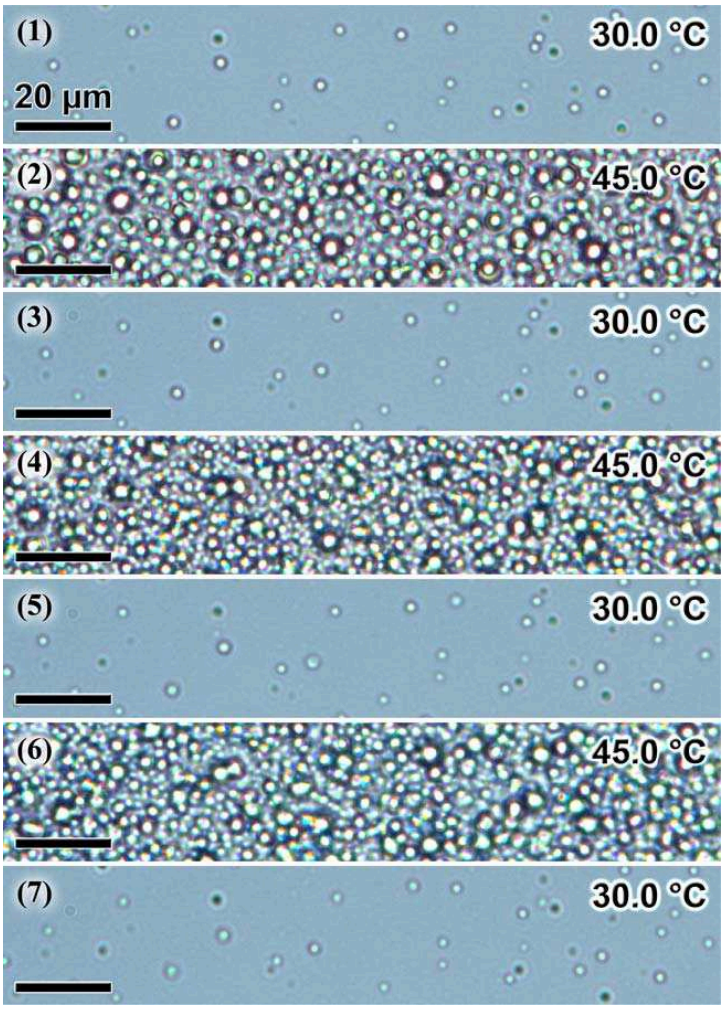

Figure 21. OM images captured with a 50x objective magnification. PVME/D_2O/EtOH sample with PVME concentration c = 6 wt% and EtOH concentration c_{EtOH} = 10 vol%. The states below (at 30 °C) and above (at 45 °C) the phase separation are presented. The stack starts from the top at 30 °C. Heating and cooling between the states was provided at a rate of 1 °C/min. Scale bar and temperature are presented in each layer.

3.6 Digital image processing - size distribution of globules

Since the pattern evolution of the sample with PVME concentration c = 6 wt% and EtOH concentration c_{EtOH} = 10 vol% is characterized by formation of spherical globules, the size distribution of globules within the visual field of OM was defined at several temperatures during demixing as seen in Figure 22.

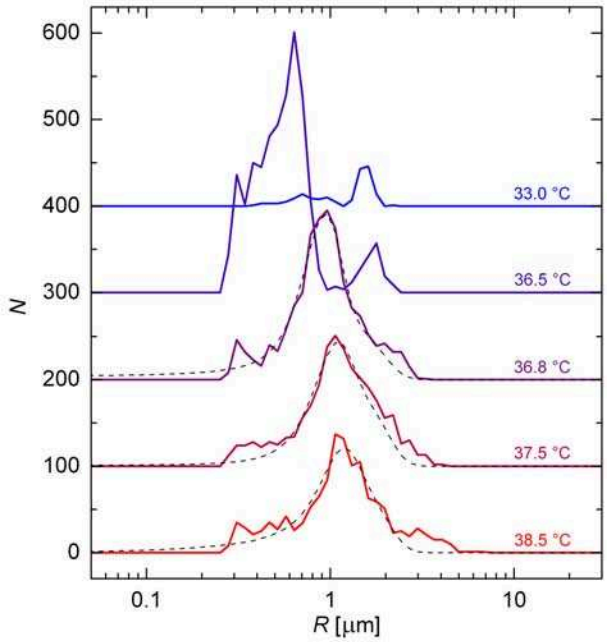

Figure 22. Globule size distribution (number of globules within the visual field N vs. radius R) obtained by digital image processing (solid lines) for sample with PVME concentration c = 6 wt% and EtOH concentration c_{EtOH} = 10 vol%. Smoothing of distributions above the LCST is presented as dashed lines. Curves are shifted vertically for clarity and temperatures are shown.

In this figure, the evolution of size distribution during demixing indicates that after heating above then cooling below the LCST to 30 °C, non-remixible globules are presented in the system and they compose about 13 % of all globules above the LCST (at 37.5 or 38.5 °C). By using formula (12) derived in subsection 3.7 (see below), we have recalculated that this 13 % proportion of globules represents only 7 % in globule mass. As it is clearly seen in Figure 19, these globules remain during the whole demixing process and then contribute to the distribution build up. At the initial stages of phase separation (at 36.5 °C), a large number of small globules was

detected as seen in Figure 22. These globules quickly coagulate into larger ones and supposedly contain some solvent since the sample did not undergo complete phase separation. Above the LCST, notably from 36.8 °C, the profile of the size distribution does not vary considerably. Only the peak maximum shifts slightly towards the larger values of radii, and the total number of globules decreases slightly as the temperature increases, which indicates further globule coagulation.

For a further comparison of OM and DLS results, the size distributions above the LCST were smoothed (dashed lines in Figure 22). The smoothing was done with respect to accuracy of image processing affected by overlapping of globules. The accuracy will be discussed in detail in subsection 3.8.

3.7 DLS measurement - size distribution of globules

DLS is a widely used method for determination of particle sizes in solutions. In this work, it was used as a second independent method for analysis of globule size. The remixing process of one sample with PVME concentration c = 0.6 wt% and EtOH concentration c_{EtOH} = 1 vol% was investigated. Relative mass m_r and relative number n_r of globules versus the hydrodynamic radius R_H, as obtained by DLS, are plotted in Figure 23 and 24, respectively. In both figures the absorbance (R.H.S.) was used as a normalizing factor. The first distribution from top in both figures is normalized to unity. Thus, the decrease in relative mass and relative number of globules can be observed during remixing.

The relative mass representation (Figure 23) is more sensitive for detection of larger particles than the relative number representation (Figure 24), and the opposite is true for smaller particles. During remixing, larger globules are dissolved more slowly than small ones and so persist for longer periods, as seen in Figure 23. In Figure 24, during the critical part of demixing (at absorbance 0.014), the number of small globules dramatically decreased while some larger globules temporarily appeared (distribution is shifted towards the higher radii). These globules became partly solvated and increased in volume. This can be seen in the OM measurement in Figure 17 (layers 7 and 8) and we speculate that the same effect also occurs for a much lower PVME concentration. Non-remixible globules were not detected in the

DLS measurements. The likely reason for this is that stirring of the sample in the DLS cell helps to redissolve them.

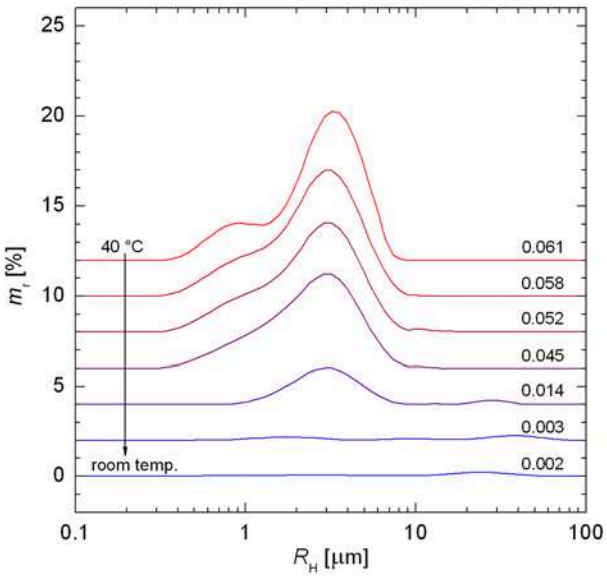

Figure 23. Globule size distribution (relative mass of globules m_r vs. hydrodynamic radius R_H) obtained by DLS measurement for sample with PVME concentration c = 0.6 wt% and EtOH concentration c_{EtOH} = 1 vol%. Curves are shifted vertically for clarity. Initial temperature (on the left side) and absorbance (on the right side) are shown.

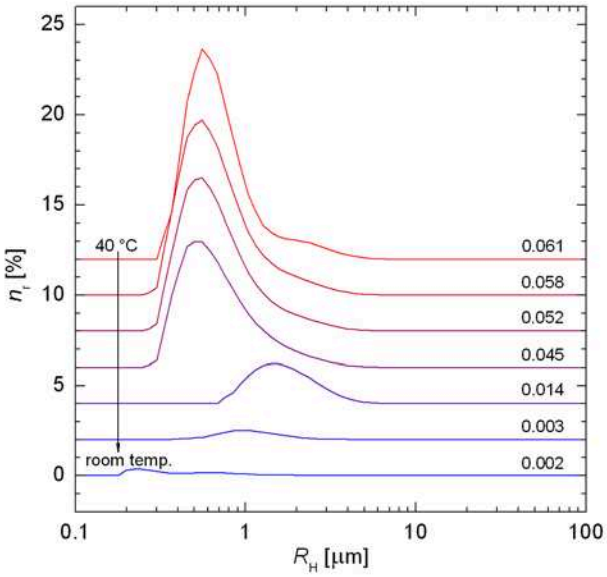

Figure 24. Globule size distribution (relative number of globules n_r vs. hydrodynamic radius R_H) obtained by DLS measurement for sample with PVME concentration c = 0.6 wt% and EtOH concentration c_{EtOH} = 1 vol%. Curves are shifted vertically for clarity. Initial temperature (on the left side) and absorbance (on the right side) are shown.

3.8 Comparison of OM and DLS globule size distributions

In this subsection the OM and DLS measurements are compared. In order to connect the two types of data obtained, which is represented in Figures 22-24, some basic assumptions and background should be first introduced. Let us suppose that globules are of spherical shape in dilute solutions with concentrations c = 0.6 wt%, c_{EtOH} = 1 vol% and c = 6 wt%, c_{EtOH} = 10 vol% for DLS and OM data, respectively. The size distribution obtained at 38.5 °C using OM and the size distribution measured at 40 °C using DLS were chosen for comparison since they are above the LCST and the respective temperatures are similar.

The following procedure was used to superimpose DLS and OM data. It is necessary to derive the relation between the relative number n_r and relative mass m_r of globules and number N and mass M of globules within the visual field. The relationship between the relative mass and mass of globules within the visual field can be expressed by equation $M_i = M_{PVME}\, m_{ri}$, where M_i is the mass of globules in the visual field corresponding to i-th radius R_i, M_{PVME} is a mass of PVME within the OM visual field volume and m_{ri} is the relative mass corresponding to i-th radius R_i. Since we are working with distributions the index i is used as an independent variable. Value N (or M) with and without index i represents i-th element of distribution and a whole distribution, respectively. At this step we suppose that the densities of solvent (D_2O/EtOH) and PVME are the same since the values at 40 °C are ρ_{D2O} = 1.100 g/cm^3 [58], ρ_{EtOH} = 0.772 g/cm^3 [59] and ρ_{PVME} = 1.044 g/cm^3 [60]. Moreover, no solvent is present within globules at 40 °C above the LCST. Based on these conditions, M_{PVME} can be easily expressed, and the mass within the visual field M_i takes the following form:

$$M_i = c\rho_{PVME}V_{visual}m_{ri}\,, \tag{10}$$

where c is concentration of PVME (in this case c = 6 wt%) and V_{visual} is the volume of the OM visual field. The latter is the same volume from which the OM distributions were determined using image processing. A crucial part of the volume evaluation was a layer thickness measurement. Weigh of cover glasses with and without the sample and the sample area were measured several times. After that, the thickness was calculated using known sample density. The visual field dimensions

are x = 175(±2) μm, y = 130(±2) μm and z = 10.1(±1.6) μm. The number of globules within the visual field N_i can be derived from formula (10) and expression $N_i = M_i/M_{0i}$, where M_{0i} is a mass of globule with radius R_i and equals to $M_{0i} = \rho_{\mathrm{PVME}}\, 4/3\, \pi\, R_i^3$. Thus, the formula for N_i is written as

$$N_i = \frac{c V_{\mathrm{visual}} m_{ri}}{\frac{4}{3}\pi R_i^3}, \tag{11}$$

Distribution obtained by OM (Figure 22) gives only the number of globules within the visual field N but in order to be compared with DLS results, the mass of globules within the visual field M is required. Thus, M was derived from the relation $M_i^{\mathrm{OM}} = N_i^{\mathrm{OM}} M_{0i}$ as

$$M_i^{\mathrm{OM}} = \frac{4}{3}\pi R_i^3 N_i^{\mathrm{OM}} \rho_{\mathrm{PVME}}, \tag{12}$$

where M_i^{OM} is the mass of globules within the visual field corresponding to OM measurement and N_i^{OM} is number of globules in the visual field as obtained by OM (these values are plotted in Figure 22).

The number of globules N for OM and DLS measurement is shown in Figure 25 while the mass of globules M is shown in Figure 26. Basically, the DLS data were extrapolated into the range of higher PVME concentration and sample volume in order to be compared with those obtained by OM. If one takes into account absence of fitting parameters, the proximity of peaks maxima and coincidence of distributions are relatively good in both cases (cf. Figure 25 and 26). However, the data obtained by the DLS method provide a distribution of mass or number of globules versus the hydrodynamic radius while OM gives a common geometrical radius. Nevertheless, these two radii are similar and can be compared. The error in extrapolation of DLS data is caused mainly by determination of the visual field volume. The error in image processing of OM measurement arises from our not being able to identify overlapped or very small globules. Thus, the size distribution obtained by OM is systematically slightly lowered, especially for the region of very small globules. Stirring of the sample was employed during the DLS measurement. This process changes the sample conditions as well as influencing the distribution. Consequently, non-remixible globules are dissolved. Errors caused by the extrapolation and image processing imperfections are shown in the inset of Figures 25 and 26 (error for

extrapolation process appears mainly in y-axis while the error in image processing is mainly in x-axis).

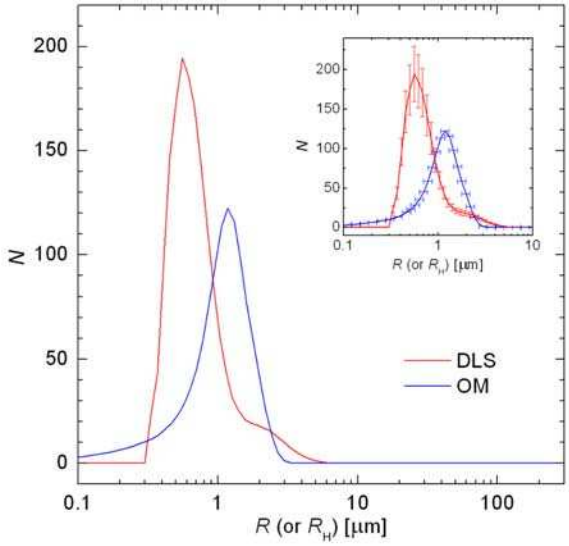

Figure 25. Comparison of globule size distributions obtained by DLS (red lines, extrapolated sample with concentration c = 0.6 wt%, c_{EtOH} = 1 vol%) and OM (blue lines, sample with concentration c = 6 wt%, c_{EtOH} = 10 vol%) measurement above the LCST. Number of globules within the visual field N plotted versus radius R (or hydrodynamic radius R_H). DLS data were calculated using formula (11). The inset shows the error bars.

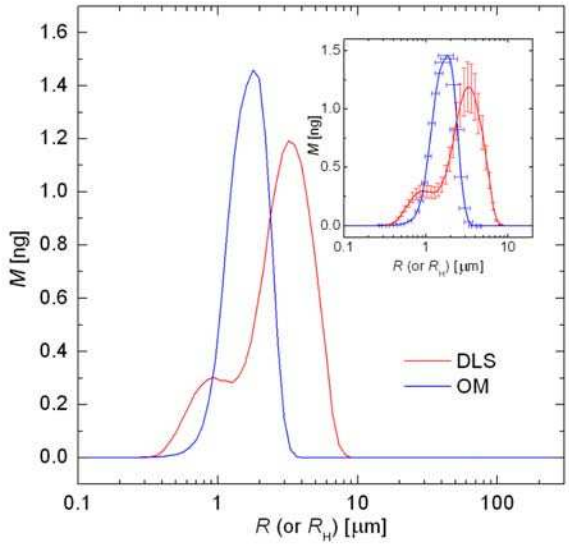

Figure 26. Comparison of globule size distributions obtained by DLS (red lines, extrapolated sample with concentration c = 0.6 wt%, c_{EtOH} = 1 vol%) and OM (blue lines, sample with concentration c = 6 wt%, c_{EtOH} = 10 vol%) measurement above the LCST. Calculated mass of globules within the visual field M plotted versus radius R (or hydrodynamic radius R_H). DLS data were calculated using formula (10) and OM data using formula (12). The inset shows the error bars.

In the number distribution representation (Figure 25), a greater proportion of small globules obtained by DLS in comparison with OM observation is seen. The DLS method is more sensitive for detection of small globules while OM is limited in this respect. In Figure 26, the ratio between the areas under distributions obtained by OM and DLS is about 0.8/1 which suggests that OM measurement can be used to identify about 80 % of PVME in samples as globular structures. Taking into account the results obtained from both methods, radius distribution of globules can be approximately determined as 0.2-8 μm.

4 Conclusions I

In this work the temperature-induced phase separation in PVME/D_2O/EtOH solutions was investigated by NMR spectroscopy, DSC, OM and DLS methods. The NMR measurement of the temperature dependences of PVME integrated intensities permitted to determine the influence of polymer concentration and ethanol content in D_2O/EtOH mixture on the phase transition. It was found that the transition region was shifted to lower temperatures with increasing polymer concentration, probably due to the preferred polymer-polymer contacts in more concentrated solutions. For lower polymer concentrations (c = 0.1 and 1 wt%), the broadening of the transition temperature region was observed and at the same time the fraction of PVME units involved in globular-like structures was only 0.5. The effect of the stabilization of hydrogen bonding in presence of ethanol in solution was manifested by marked shift of the transition region to higher temperatures and by decrease of the phase-separated fraction p with increasing ethanol content in D_2O/EtOH mixture.

Measurements of the temperature dependencies of PVME integrated intensities were improved using a spin-echo pulse sequence, which gives a higher accuracy for the phase-separated fraction p in PVME solutions. The half-width of peaks, which corresponds to phase-separated fraction of PVME, was determined at various temperatures above the LCST and therefore dynamical behaviour of collapsed polymer chains at particular temperatures was approximately determined.

^1H and ^{13}C NMR relaxation behaviour of EtOH molecules above the phase transition showed a distinct dependence on the polymer concentration. EtOH molecules in the most dilute solution (c = 0.1 wt%) were probably all expelled from polymer structures at elevated temperatures, whereas a certain portion of ethanol

molecules remained bound in PVME globules in the solution with c = 6 wt%, as revealed from ^{1}H and ^{13}C spin-spin relaxation times T_2 of EtOH. While there is fast exchange between bound and free sites in solutions with $c \leq 10$ wt%, slow exchange regime follows from the existence of separate signals of bound and free EtOH as found for PVME/D_2O/EtOH solutions with c = 20 wt% in ^{1}H NMR spectra (resonance of OH protons) and especially in ^{13}C NMR spectra (resonances of CH_2 and CH_3 carbons). The lifetime of the bound EtOH molecules is much larger than 10 ms (the difference between ^{13}C chemical shifts of bound and free EtOH is approx. 100 Hz on the frequency scale). From the chemical shifts of OH protons it follows that the hydrogen bonding is for bound EtOH somewhat smaller in comparison with that existing in neat D_2O/EtOH mixtures. While for solutions with c = 6 wt%, the ^{13}C spin-lattice relaxation times T_1 of bound EtOH were virtually the same as for free EtOH indicating that the rate of the motion of bound ethanol molecules is not changed, for solutions with c = 20 wt% ^{13}C T_1 values of bound EtOH were significantly shorter in comparison with free EtOH. For the latter case, the correlation times of the bound EtOH were 2-3 times longer in comparison with free EtOH, indicating that the motion of EtOH bound in globular-like structures is slowed-down. Much larger differences between bound and free EtOH molecules were found from T_2 measurements (both ^{1}H and ^{13}C), where T_2 values were for bound EtOH up to 2 orders of magnitude shorter in comparison with free EtOH molecules. The main sources of these large differences are evidently that the motion of bound EtOH is spatially restricted and anisotropic (molecules cannot reach all orientations) and for the solutions with $c \leq 10$ wt%, where a fast exchange regime exists, also a contribution from the chemical exchange. With time the originally bound EtOH is very slowly released from phase-separated globules. A similar behaviour as described above for EtOH molecules from ^{1}H and ^{13}C NMR spectra and ^{1}H and ^{13}C relaxation measurements was previously found for water (HDO) molecules in PVME/D_2O solutions [38-40] so indicating that the decisive factor in this behaviour is in both cases a polar character of these molecules (dipole moments of water and EtOH are very similar) and hydrogen bonding.

DSC, OM and DLS methods were chosen in order to obtain information regarding reversibility, microscopic morphology and the size of globules during

phase separation events. It was found using DSC that a higher content of EtOH in solution shifts the LCST towards higher temperatures and that thermograms are almost symmetric for heating and cooling. Moreover, higher EtOH content decreases the enthalpy increment of separation and a hysteresis (around 2.3 °C) in onset temperature between heating and cooling can be observed. At low EtOH content, the thermograms were found to be quite unsymmetrical during remixing. These broad unsymmetrical peaks in cooling thermograms imply that processes of demixing and remixing occur by different mechanisms. During demixing, the solution undergoes a transition from a homogenous solution to a locally heterogenous state. On the molecular level almost all hydrogen bonds in the sample are disrupted uniformly with subsequent formation of globules. In the case of remixing, a transition from locally heterogenous to homogenous state takes place. Here, the compact globules with low or almost no solvent content are available for hydrogen bonding but the solvent molecules must penetrate and permeate the globules' interior through their surfaces. It was possible to prove this fact using OM study.

OM measurement also revealed two different pattern evolutions for samples with lower (c = 6 wt%) and higher (c = 20 wt%) PVME concentrations. For the higher PVME concentration, the initial state of phase separation (demixing) has a sponge-like structure with an increasing particle size as the temperature is increased with a subsequent formation of mostly ellipsoidal cell-like structures containing a complex internal substructure together with many small spherical globules. Although the initial stages of phase separation in these two samples appear similar, further temperature increase results in formation of spherical globules in sample with concentration c = 6 wt%. PVME chains are not so strongly linked and so can demix more finely into relatively small spherical objects thus forming a droplet pattern. In both samples non-remixible globules were found.

The size distribution of globules at various temperatures for PVME/D_2O/EtOH sample with concentrations c = 6 wt% and c_{EtOH} = 10 vol% was determined using a digital image analysis. Relative mass and relative number distributions were measured by DLS for the sample with concentration c = 0.6 wt%, c_{EtOH} = 1 vol%. These distributions were extrapolated in PVME concentration and volume to those observed by OM and a satisfactory match was found. Using the OM

technique, it was possible to identify about 80 % of PVME in sample forming globules above the LCST. The range of the globule radii was estimated by OM and DLS measurements as 0.2-8 μm.

5 Introduction II

5.1 Introduction to porphyrins

Porphine and its derivatives (i.e. the porphyrins, see Figure 27) are widely studied functional pigments that can complex a great variety of metal cations at their tetrapyrrole macrocyclic core [61-63]. In biological systems, porphyrins play essential roles as photosynthetic antenna and reaction centre components, in the heme proteins, and as coenzyme B_{12}, [64,65]. Porphyrins can coordinate cationic species, especially transition metal cations, and these complexes exhibit unique functions depending on the metallating species. Furthermore, the coordinated metal cation can accommodate a variety of ligands resulting in, for instance, sophisticated catalytic activity. The large extinction coefficients of porphyrin chromophores imply use as photo-electronic components while their well-defined redox potentials suggest many electrochemical applications based on this feature. Consequently, porphyrins remain the most widely studied of all macrocyclic systems.

In addition, synthetic procedures to porphyrins are amenable to various modifications permitting a continuous expansion of the family of porphyrin compounds, which may now be more accurately referred to as the cyclic oligopyrroles. New aspects of porphyrinoid chemistry, such as the expanded, contracted, and isomeric analogs, are continuously being developed. Figure 27 illustrates some unusual core structures of porphyrins [66-68]. Corrole is the macrocyclic porphyrin analogue contained in vitamin B_{12}. The absence of one *meso*-carbon permits corroles to retain the aromaticity characteristic of porphyrins, but

induces tribasicity of the ligand over the usual dibasicity of porphine. In a similar way, introduction or removal of macrocyclic carbon atoms to or from porphyrin results in structures such as porphycene, corrphycene, hemiporphycene, and isoporphycene (see Figure 27). The variation in the electronic and physical structure of these porphyrins caused by skeletal transformations is likely to lead to the manifestation of unique electronic or catalytic properties.

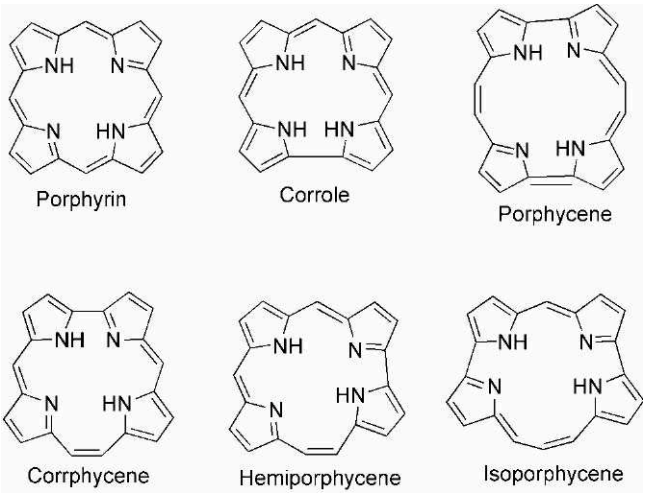

Figure 27. Porphyrins with unusual core structures.

The porphyrin core usually consists of four pyrrole rings linked through *meso*-carbon atoms. However, porphyrins containing larger numbers of pyrrole groups have been developed, some of which are summarized in Figure 28. These "expanded porphyrin" derivatives [69-72] have extended π-electron conjugation, which results in novel photonic, electronic and magnetic properties. The expanded polypyrrolic macrocycles contain a greater number of coordinating heteroatoms and a larger central binding cavity exhibiting unique molecular recognition functions, including anion sensing.

Porphyrin isomers may exist where a pyrrole ring is inverted such that its amine function is positioned at the periphery of the porphyrin while a carbon atom appears at the interior of the macrocycle. These pyrrole ring inversion isomers are referred to as N-confused porphyrins (NCPs) (see Figure 29 for NCP families) [73,74]. One result of this inversion is that the carbon atom at the macrocyclic

interior is now available for formation of metal-carbon bonds where the coordinated metal ion is suitable for such organometallic interaction.

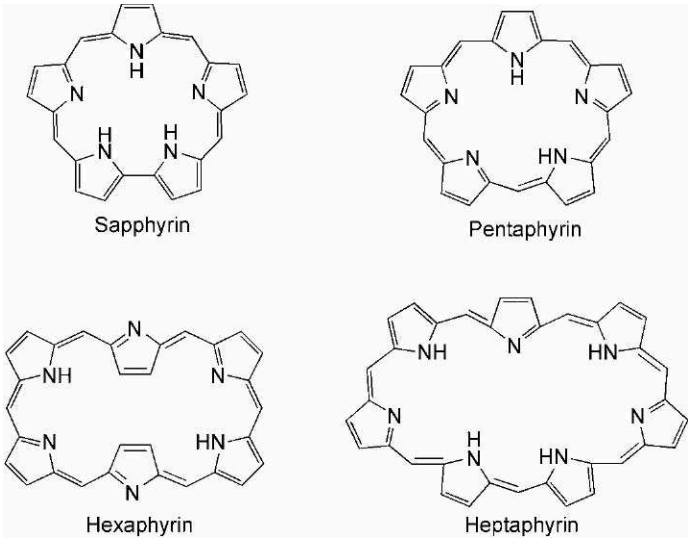

Figure 28. Expanded porphyrins.

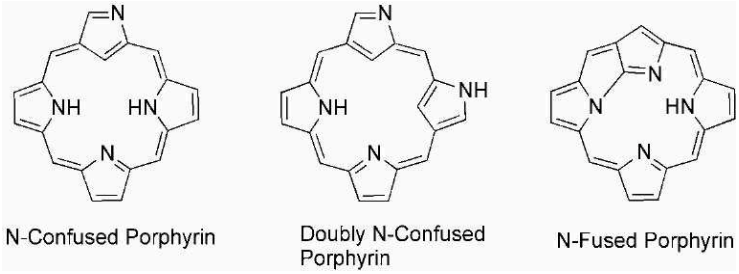

Figure 29. N-Confused porphyrins

Synthetic modification at the porphyrin macrocyclic nitrogen atoms has also been investigated [75]. *N*-alkylation of *meso-tetrakis*-3,5-di-*tert*-butyl-4-oxo-2,5-cyclohexadienylideneporphyrinogen (Figure 30) was shown to be a useful way of stabilizing the structure of the compounds against protic tautomerism. As it was reported in [76] the redox and spectral properties of the latter compound are tunable through an increase in multiplicity of N-substituents.

As summarized above, the porphyrin structure permits a variety of synthetic procedures, resulting in a multitude of functional molecules. However, more elaborate functional systems can be constructed by array formation or assembly of such functional porphyrin molecules.

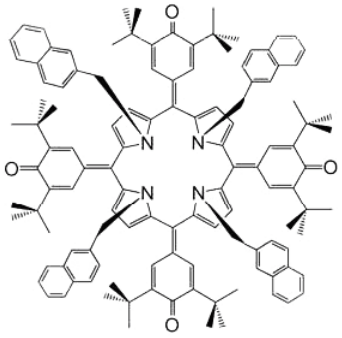

Figure 30. An N-substituted (naphthalene substitution) porphyrin.

An example can be observed in photosynthetic systems. The photosynthetic systems consist of a sophisticated supramolecular arrangement of proteins and dyes, and efficiently convert incident light energy into chemical energy (adenosine triphosphate - ATP). The entire process is initiated by adsorption of a photon by a light-harvesting (LH) antenna system, where arrays of various porphyrin derivatives (i.e. chlorophylls, bacteriochlorophylls, etc.) play the important role of rapid and efficient energy transfer to the photosynthetic reaction center. This function cannot be performed by individual porphyrin molecules but rather requires the large absorption cross-section and supramolecular arrangement provided by the entire light-harvesting system.

5.2 Anion binding

Complexation of anionic species by molecules containing an appropriate binding site is an area of recent substantial interest in supramolecular chemistry [77-83] Additionally, binding of a particular anion is involved in the activity or inhibition of activity of some proteins [84]. The specificity of this interaction is a desirable characteristic for synthetic derivatives, and many small molecules have been investigated in relation to this. Second, the ability to complex and report the presence of several environmentally deleterious or toxic anions would be a valuable means for determination of those anions. Certain types of molecules are suitable for anion complexation applications, notable examples being polyamide macrocycles [85], calixarenes [86] and the calix[4]pyrroles [87-89]. Certain of these have been found to

bind specific anions with great selectivity permitting speculation on their applications [90].

The calix[4]pyrroles (see Figure 31) have been investigated intensively from the point of view of anion binding [87-89,91-94]. They are ideal for this purpose since they are available in high yield from a relatively simple synthesis. Their appeal is furthered by availability of various post-macrocyclization modifications [95] and because unsymmetrical derivatives can be prepared facilitating, for instance, the introduction of a fluorophoric reporting group [96,97]. Anion binding properties of the calix[4]pyrroles depend on hydrogen bonding interactions between the pyrrole NH groups and the analyte anion with the inherent flexibility of their porphyrinogen skeleton allowing the calix[4]pyrroles to exist in conformations somewhat analogous with the calixarenes.

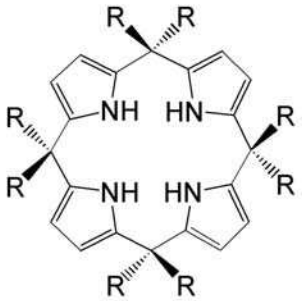

Figure 31. Structure of calix[4]pyrrole.

5.3 Objectives of the doctoral thesis (supramolecular part)

A species related to the calix[4]pyrroles is the 5,10,15,20-*tetrakis*-3,5-di-*tert*-butyl-4-oxocyclohexadienylidene porphyrinogen, **1**, and its di-N-benzylated derivative, **1a**, (see Figure 32 in subsection 6.1), which although bearing essential similarities in its structure with the calix[4]pyrroles, can be distinguished from them by an increased macrocyclic rigidity as a result of its conjugated electronic system. Another novel feature of the extended π-electronic system is an intense color in all of its derivatives. After adventitiously observing an effect (red shift) related to the presence of an anionic species in the electronic absorption spectra of the cyclohexadienylidene-substituted porphyrinogens during spectroelectrochemical analyses [76] we were

encouraged to investigate their behavior in the presence of a wider range of substrate anions. Since these compounds possess intense electronic absorptions, we hoped to obtain an anion-dependent chormogenic response. Further to this, these molecules bear a moderate solvatochromism, which we believed could improve anion differentiation.

Therefore, the aims of this study can be summarize as:

1) Synthesis of compounds **1** and **1a**.
2) Solvatochromic response of **1** and **1a** in various solvents (with different polarities) studied using UV/Vis spectrophotometry methods.
3) UV/Vis spectrophotometry nvestigation of anion binding (using wide range of anions) for **1** and **1a**. Determination of binding constant between anion and host molecule (**1** or **1a**).
4) Study of influence of anion binding to ^{1}H NMR spectra of host molecules **1** and **1a**.
5) Investigation of colorimetric response to anion selectivity by a combination of anion binding and solvatochromic effects.

6 Experimental II

6.1 Samples

The compounds 5,10,15,20-*tetrakis*-3,5-di-*tert*-butyl-4-oxocyclohexadienylidene porphyrinogen, (OxP) **1**, and $N_{21}N_{23}$-dibenzyl-5,10,15,20-*tetrakis*-3,5-di-*tert*-butyl-4-oxocyclohexadienylidene porphyrinogen, ($OxP(Bz)_2$) **1a** (see Figure 32, and Figure 33 for numbering), used in this study were prepared as described in subsection 6.3. Solvents, spectroscopic solvents, reagents and tetra-*n*-butylammonium salts (Figure 34) for anion binding studies were obtained from Aldrich Chemical Co., Wako Chemical Co., Tokyo Kasei Chemical Co. or Kanto Chemical Co.

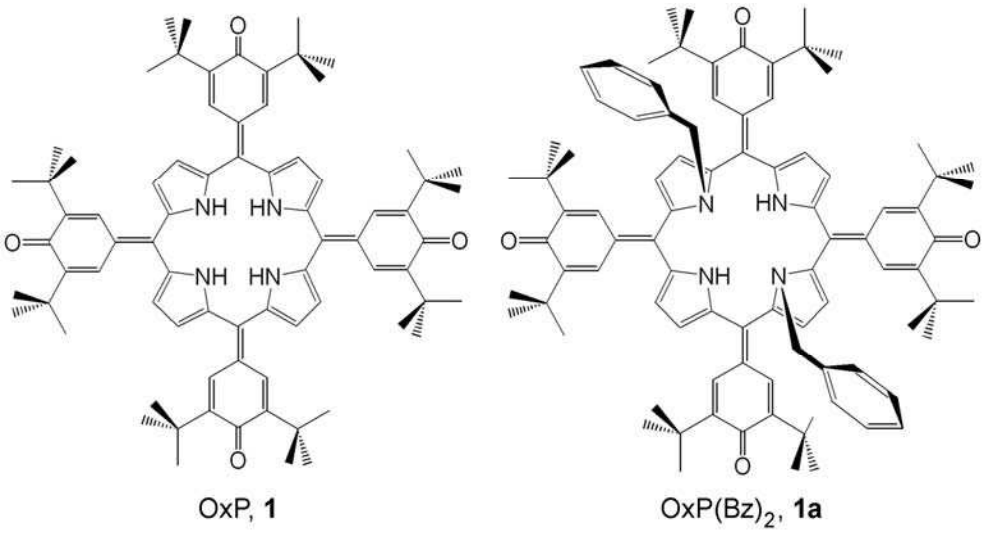

Figure 32. Structure of 5,10,15,20-*tetrakis*-3,5-di-*tert*-butyl-4-oxocyclohexadien ylidene porphyrinogen, (OxP), **1;** and $N_{21}N_{23}$-dibenzyl-5,10,15,20-*tetrakis*-3,5-di-*tert*-butyl-4-oxocyclohexadienylidene porphyrinogen, ($OxP(Bz)_2$), **1a**.

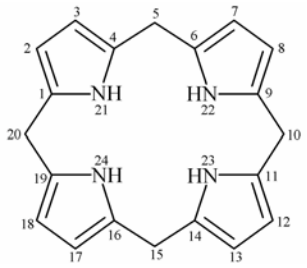

Figure 33. Numbering of porphyrinogen ring.

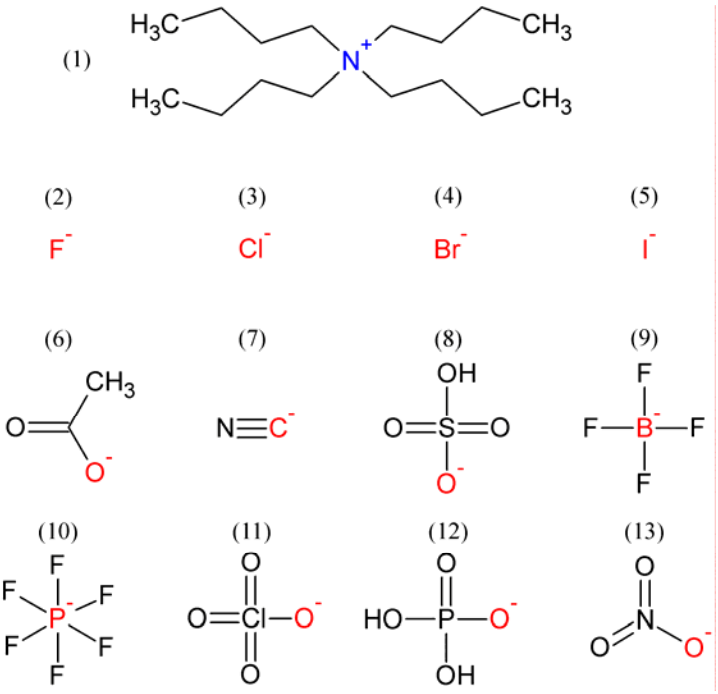

Figure 34. Tetra-*n*-butylammonium (1) salts: fluoride F^- (2), chloride Cl^- (3), bromide Br^- (4), iodide I^- (5), acetate $CH_3CO_2^-$ (6), cyanide CN^- (7), hydrogen sulfate HSO_4^- (8), tetrafluoroborate BF_4^- (9), hexafluorophosphate PF_6^- (10), perchlorate ClO_4^- (11), dihydrogen phosphate $H_2PO_4^-$ (12), and nitrate NO_3^- (13).

6.2 Characterization

6.2.1 Used spectrophotometers and spectrometers

Electronic absorption spectra were measured using JASCO V-570 UV/Vis/NIR spectrophotometer, Princeton Applied Research (PAR) diode array rapid scanning spectrometer or a Shimadzu UV/Visible spectrophotometer. ^{1}H-NMR spectra were obtained using JEOL AL300BX (operating at 300.4 MHz) or Bruker AM400

(operating at 400.1 MHz) spectrometers. Variable temperature measurements were performed using either instrument equipped with the appropriate liquid nitrogen cooling apparatus.

6.2.2 X-ray crystallography

Crystals of the acetone solvate of compound **1a** were grown by refrigeration (T = –20 °C) of a solution of **1a** in anhydrous acetone. Very thin purple plates, which had appeared after two-three weeks, were subjected to X-ray crystallographic analysis using a rotating anode Mo K_α source. A suitable crystal was selected and mounted on a glass fibre using perfluoropolyether oil. This was placed in the cold stream of the diffractometer (Bruker-Nonius Kappa CCD) at 120K prior to data collection. The X-ray crystallography data collection and refinement were done by EPSRC UK National Crystallography Service.

Crystal data for **1a·acetone** (see the structure in Figure 35c): $C_{93}H_{110}N_4O_5$, M = 1363.85, triclinic, centrosymmetric point group $P\bar{1}$, a = 12.1693(11) Å, b = 17.5849(13) Å, c = 21.0965(17) Å, α = 69.870(4) °, β = 78.140(4) °, γ = 82.865(5) °, V = 4141.3(6) Å^3, Z = 2, D_c = 1.094 g cm^{-3}, μ(Mo K_α) = 0.067 mm^{-1}, crystal size 0.12 × 0.10 × 0.02 mm^3, structure solved by direct methods, F^2 refinement, 946 parameters.

6.3 Synthesis

5,10,15,20-*Tetrakis*-3,5-di-*tert*-butyl-4-oxocyclohexadienylidene porphyrinogen, (OxP) **1**, was prepared by modifications of procedure previously published by Milgrom [98]. The synthesis of **1** was performed in propionic acid (250 mL) with addition of 3,5-di-*tert*-butyl-4-hydroxybenzaldehyde (11.74 g, 0.05 mol) refluxing at 140 °C. The reaction mixture was stirred during the addition of pyrrol (3.35 g, 0.05 mol). After 3 hours the mixture was cooled to 70 °C and 150 mL of propionic acid was removed by evaporation under reduced pressure (280 hPa, 80 °C). Then the mixture was kept in refrigerator at -10 °C for 24 hours. The solid compound aggregated on the sides of flask. After filtration the sample was dissolved in

dichloromethane (200 mL) and during stirring the triethylamin (~ 10 mL) was gradually added to deprotonize the product. After addition of methanol (200 mL) the product was filtered and we obtained 5,10,15,20-*tetrakis*-3,5-di-*tert*-butyl-4-hydroxyphenylporphyrinogen, (P), **0**, (2.7 g, yield 19.2 %) as a purple blue solid.

To obtain its two-electron oxidized product, **1**, the **0** (1 g) was dissolved in dichloromethane (500 mL) at room temperature. The mixture of potassium hydroxide (100 mg) with methanol (5 mL) was prepared in separate veil and gradually injected into the stirring dichloromethane with **0** until the solution changed the colour to green. After 16 hours of stirring at room temperature the distilled water (300 mL) was added. The dichloromethane was removed from solution by evaporation under reduced pressure (270 hPa, 40 °C). The remaining mixture is filtered through paper filter using vacuum pump. The obtained product is a green solid OxP, **1** (0.98 g, yield 98 %).

N-alkylation of the OxP, **1**, was performed in refluxing anhydrous ethanol/potassium carbonate with 5 equiv of benzyl bromide. **1** (200 mg, 1.8×10^{-4} mol) was dissolved in dry ethanol (20 mL), and anhydrous potassium carbonate (0.25 g) was added. The reaction mixture was stirred during the addition of benzyl bromide (150 mg, 8.8×10^{-4} mol, ~5 equiv) followed by warming to reflux. Typically, the reaction was allowed to proceed until none of the parent compound **0** remained (thin layer chromatography (tlc) monitoring). Following completion of the reaction, the solvent was removed by evaporation under reduced pressure, and the resulting solid was partitioned between dichloromethane and water. Evaporation of the highly coloured dichloromethane fraction yielded a green solid that was dissolved in minimum of dichloromethane and chromatographed on silica gel eluting with *n*-hexane/dichloromethane, 1:1. The major products are consistently the di- and tetra-substituted products when benzyl bromide is used in the N-alkylation. The two main products are separated easily, but care must be taken to avoid contamination by small amounts of tri-substituted derivative that are present in the mixture. Relative yield depends on reaction time, but the tetra-substituted product could be obtained in >80 % yield if the reaction was allowed to proceed until virtually no di-substituted material remained. After the silica gel chromatography, the di-substituted product **1a** (75 mg, yield 38 %) used in this study, was obtained.

7 Results and discussion II

7.1 Solvatochromism

Solvatochromism is the term for changes in electronic spectra of compounds when dissolved in different media and is related to changes in the electronic structure in the subject molecules caused by variation of solvent polarity or other interactions, especially hydrogen bonding [99-103]. For compounds **1** and **1a**, absorption maxima in different solvents appear in the range 400-900 nm and this is illustrated by the spectra shown in Figure 35 while the positions of the absorption maxima in different solvents are summarized in Table 10. Low solubility of **1** in several of the solvents used here did not prevent us from observing the trends in its electronic absorption spectrum. However, **1a** proved soluble in a greater variety of solvents. Hexane is the least polar of the solvents employed and gives λ_{max} for **1a** at 486 nm. Increasing the polarity of the solvent results in a red shift so that λ_{max} for 1,4-dioxane occurs at 504 nm. Other non-hydrogen bonding solvents with comparable polarities, such as chloroform and dichloromethane, have λ_{max} of similar value. When solvents capable of H-bonding are used new absorption bands appear at 600 and 750 nm, the relative intensity of which varies with the solvent polarity and may be a measure of how strongly the hydrogen bonding interaction occurs with the oxoporphyrinogens, **1** and **1a**. The original 'Soret'-type band (a very strong absorption band in the blue region of the optical absorption spectrum of a porphyrin) at 500 nm reduces in intensity with increasing solvent polarity.

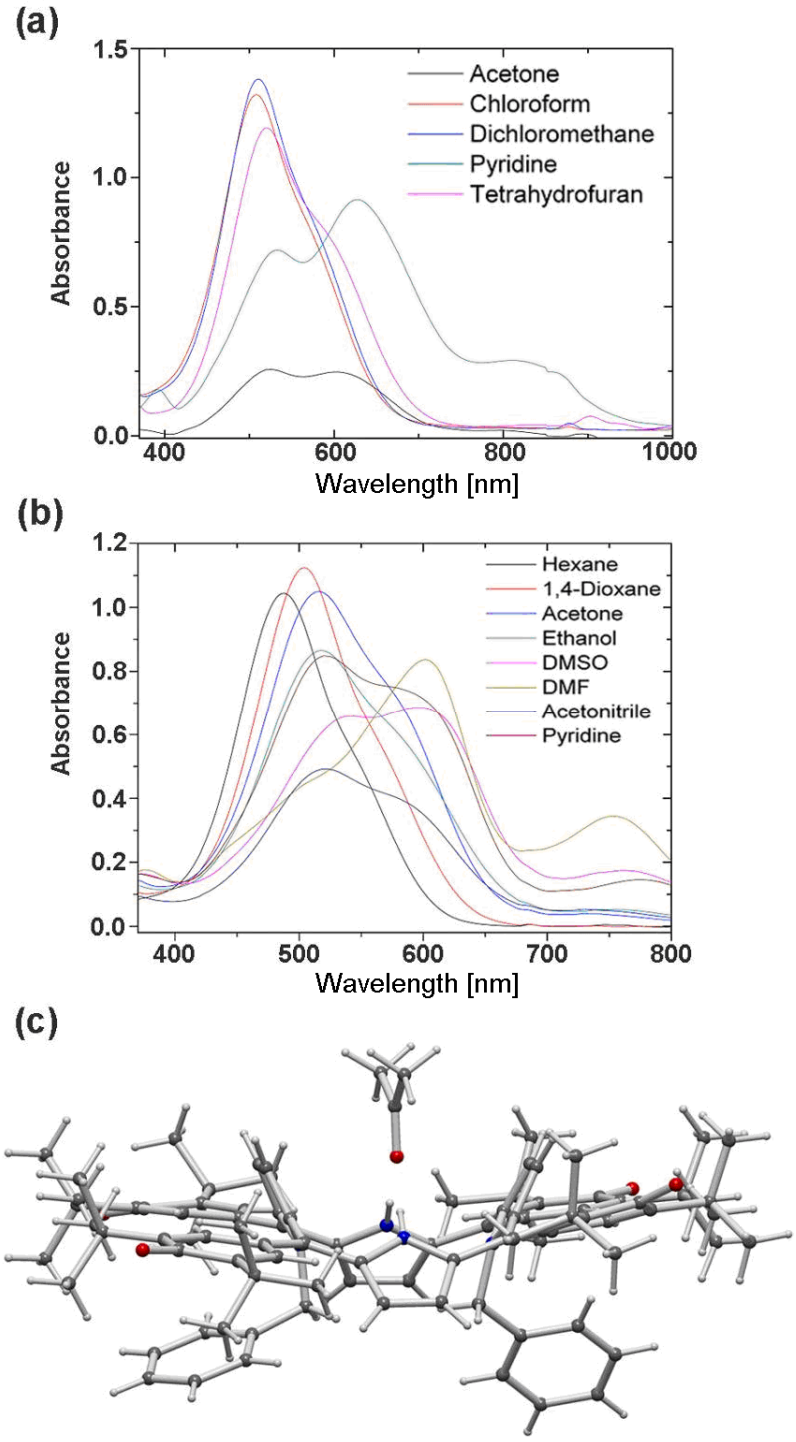

Figure 35. Solvatochromism in **1** and **1a**: (a) and (b) electronic absorption spectra of **1** and **1a**, respectively, in solvents of various polarities, and (c) molecular structure of the acetone solvate of **1a** as obtained using X-ray crystallography. (For the molecular structure of the water solvate see Ref. [104]). **1a·acetone** hydrogen bond N–O distance: 2.904 Å.

Table 10. Donor numbers and β values of the employed solvents, and optical absorption spectral data for the investigated porphyrinogens in different solvents.

Solvent	Donor number[a] [kJ/mol]	β[b]	OxP, **1** [nm]	$OxP(Bz)_2$, **1a** [nm]
Hexane	0.0	0.00	330, 364, 538(sh), 660	322, 486, 552(sh)
Benzene	0.1	0.10	343, 514, 583(sh)	329, 503, 569(sh),
Nitrobenzene	4.4	0.30	530, 592(sh)	521, 585(sh)
Benzonitrile	11.9	0.41	342, 531, 594(sh)	339, 522, 589(sh)
Acetonitrile	14.1	0.31	367, 543, 682	344, 519, 586
Dioxane	14.8	0.37	350, 512.5, 584(sh)	338, 504, 574(sh)
Acetone	17.0	0.48	360, 524, 590(sh)	352, 516, 580(sh)
Ethyl acetate	17.1	0.45	356, 521, 602(sh)	348, 510, 583(sh)
Ethanol	19.2	0.77	360, 535, 604(sh)	353, 517, 588(sh)
Diethyl ether	19.2	0.47	343, 500, 577(sh)	344, 497
Tetrahydrofuran	20.0	0.55	356, 521, 598(sh)	349, 507, 575(sh)
Dimethylformamide	26.6	0.69	372, 535, 637	360, 534, 586, 757
Dimethylsulphoxide	29.8	0.76	371, 544, 625	365, 536, 606(sh)
Pyridine	33.1	0.64	389, 537, 631	374, 532(sh), 601, 679

[a] Taken from Ref. [105].
[b] Taken from Ref. [106].

Variation of solvent polarity could also be accomplished using a binary mixture. Spectra were measured in dichloromethane-dimethylformamide (CH_2Cl_2-DMF) mixtures of various ratios. Even at high CH_2Cl_2-DMF ratios there is a notable color change from pink to violet with a gradual attainment of the blue color (Figure 36).

To emphasize the possibility of hydrogen bonding involving the pyrrolic NH groups and solvent molecules the crystal structure of the acetone solvate of **1a** was determined using X-ray crystallography. Figure 35c shows the inclusion of acetone at the binding site of **1a** in the compound **1a·acetone**. Notably, crystals of **1a·acetone** are purple, which represents a departure from the usual green/red dichroism in crystals of these compounds. However, the purple color of the crystals is consistent with the observed solvatochromism of **1a**. When compared with the known structures of di-N-alkylated **1** [76,104], the most obvious difference is the displacement of the water molecule from the binding site between the pyrrolic NH

groups. The N_{22}-$O_{acetone}$ distance (cf. Figure 35c) in **1a·acetone** is 2.90 Å compared to 3.02 Å for the case where water is hydrogen bonded [104]. This is one of the factors affecting the dihedral angles subtended between the pyrrole groups and the macrocyclic least squares plane so that while the angle between benzyl-substituted pyrroles is similar in both water and acetone solvates, the angle subtended by the pyrroles involved in the H-bonding interaction is lower in the acetone solvate (41° and 43° against 47° and 52.4° for the water solvate [104]).

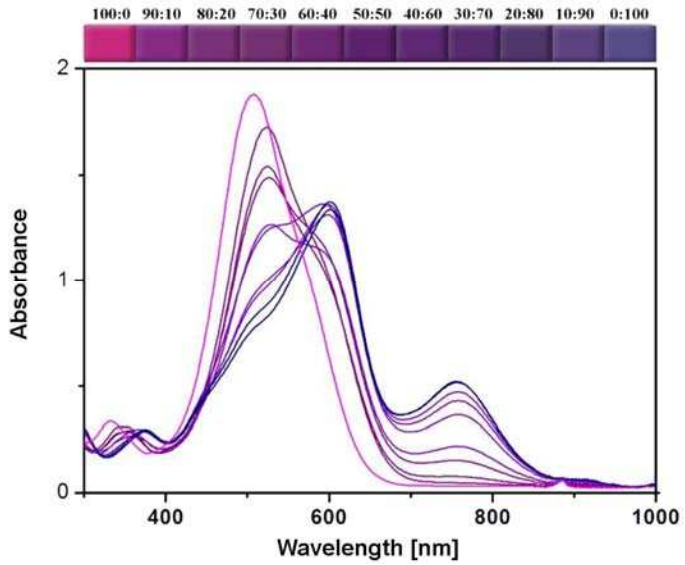

Figure 36. Spectral and color variation accompanying changes in the ratio of dichloromethane:dimethylformamide solutions of **1a**.

Qualitatively, the solvatochromism of **1** and **1a** results in a color change from red/pink in non-polar solvents through violet to blue for the most polar solvents used here (N,N-dimethylformamide, dimethylsulfoxide). For the fully N-substituted derivatives of **1** there is predictably no substantial change in the electronic spectrum upon variation of solvent polarity since the possibilities for hydrogen bonding and protic tautomerism have been effectively negated by complete N-alkylation.

Several models have been developed in the literature to visualize the linear solvation energy relationships [99-103,105]. A comprehensive collection of solvatochromic parameters and methods for simplifying the generalized solvatochromic equations has been reported by Kamlet et al [106]. In the present study, we utilized solvent donor number (quantitative measurement of Lewis

basicity) and the β scale of hydrogen-bond acceptor (HBA) basicities to seek linear solvation energy relationships. The β scale provides a measure of the solvent's ability to accept a proton (donate an electron pair) in a solute-to-solvent hydrogen bond. Figure 37 illustrates the relationships between the solvent donor number, the β values, and the spectral shifts of compounds **1** and **1a**. The correlation coefficients for these plots were found to be 0.85, 0.97, 0.73, 0.90, respectively, for plots (a)-(d). The linear trend in the plots suggests that solute-solvent hydrogen bonding is primarily responsible for the observed solvatochromic effect of porphyrinogens.

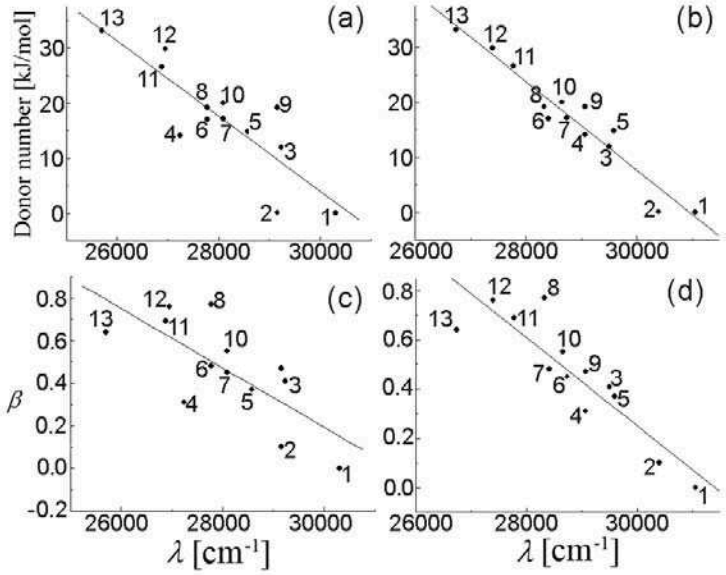

Figure 37. Plots of donor number versus absorption peak maxima (a and b), and β versus absorption peak maxima (c and d) for **1** (plots a and c) and **1a** (plots b and d). Solvents: 1 (hexane); 2 (benzene); 3 (benzonitrile); 4 (acetonitrile); 5 (1,4-dioxane); 6 (acetone); 7 (ethyl acetate); 8 (ethanol); 9 (diethyl ether); 10 (tetrahydrofuran); 11 (dimethylformamide); 12 (dimethyl sulfoxide); 13 (pyridine).

7.2 UV/Vis Spectrophotometry of anion binding

The potential of polytopic hydrogen bonding sites can be exploited by assessing their anion binding properties. Therefore, electronic absorption spectroscopy was used to quantify the binding of halides and several other anions.

Figure 38 illustrates the spectral changes observed during the titration of tetrabutylammonium fluoride against a solution of **1a** in dichloromethane. During the

titration absorption bands located at 333 and 509 nm underwent a red shift to 374 and 604 nm, respectively. In addition, a new intense band was observed at 753 nm. An isosbestic point was observed at 420 nm suggesting the presence of one equilibrium process in solution. Similar spectral changes were observed for all of the anions investigated.

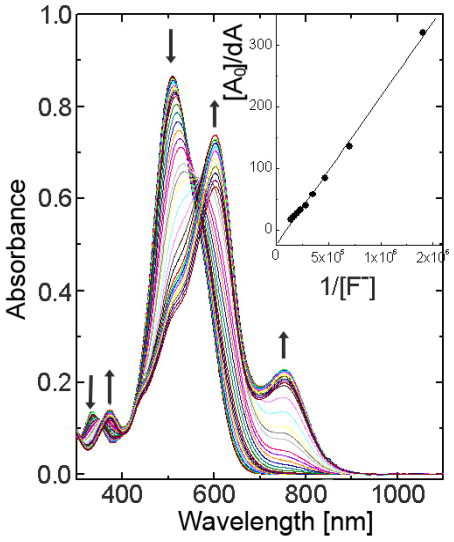

Figure 38. Spectral changes observed during titration of **1a** with tetrabutylammonium fluoride in dichloromethane. The figure inset shows the Benesi-Hildebrand plot constructed for determination of the binding constants.

Job's method (also called as a method of continuous variation) is effective approach to the determination of stoichiometry for the porphyrinogen·anion complexes. When we assume reaction aA + dD <==> cC, where A is host (electron acceptor, porphyrinogen), D is guest (electron donor, anion), C is complex (porphyrinogen·anion), and a, d, c are number of moles of host, guest, complex, respectively. The latter equation can be rewritten in the form A + kD <==> mC (by dividing all coefficients by a), where $k = d/a$ and $m = c/a$. Job's method is based on the following: if a series of solution is prepared, each containing the same total number of moles of A and D, but a different ratio, R, of moles D to moles A, the maximum amount of product (complex), C, is obtained in the solution in which $R = k$ (the stoichiometric ratio). In order to obtain preliminary information regarding stoichiometric ratio, the method was slightly modified. The absorbance of the strongest band was plotted against the molar ratio of F^- anion and **1** (or **1a**). The

changes in the trend of this plot suggested that the **1**·anion complexes hold stoichiometry 1:2 while **1a**·anion complexes hold 1:1. An example of modified Job's plot for **1**·F^- complex is seen in Figure 39. In this figure the trend is changed twice, at the ratio 1 and 2.

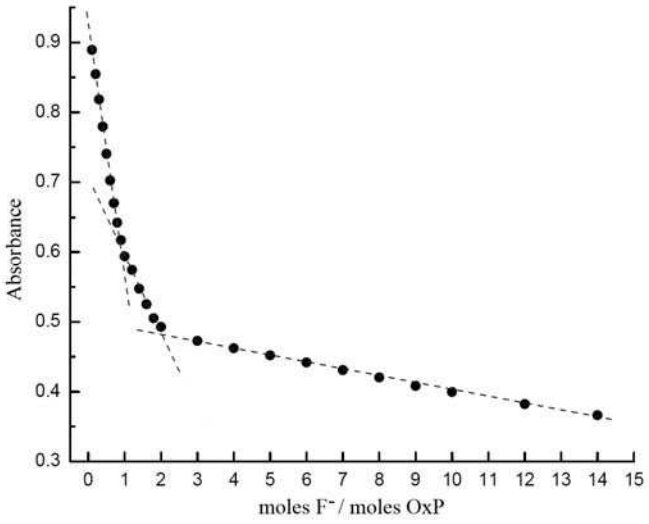

Figure 39. Job's plot for binding of fluoride ions by compound **1** indicating a 2:1 stoichiometry.

The anion binding constants were evaluated using the spectral data by construction of Benesi-Hildebrand plots [107]. This method is a widely used approach for determination the stoichiometry and equilibrium binding constants of nonbonded interactions, particularly 1:1 and 1:2 interactions. The method is based on equation

$$\frac{[A_0]}{dA} = \frac{1}{l\,\Delta\varepsilon\,K\,[D_0]} + \frac{1}{l\,\Delta\varepsilon}, \qquad (13)$$

where $[A_0]$ and $[D_0]$ are initial molar concentrations of host and guest, respectively; dA is change in absorbance and satisfies $dA = A_0 - A$, where A_0 is the initial absorbance before the interaction of A and D, and A is the absorbance taken at any point of titration; K is binding constant; $\Delta\varepsilon$ is a difference between molar extinction coefficient of complex and guest, and l is distance the light travels through the material (i.e. the path length). The slope of dependence of $[A_0]/dA$ vs. $1/[D_0]$ is closely related to the value of binding constant.

The compound **1a** has only one binding site and therefore only one set of spectral changes was observed (see Figure 38). The inset in the latter figure shows

Benesi-Hildebrand plot constructed for determination of the binding constant. The compound **1** has two binding sites which was supported (besides the Job's plot) by observation of two sets of spectral changes in Figure 40a and 40b. Two binding constants were determined for F^- anion using Benesi-Hildebrand plot (see insets in Figure 40). Linear plots were observed for all of the studied anions and the binding constants thus calculated are summarized in Table 11.

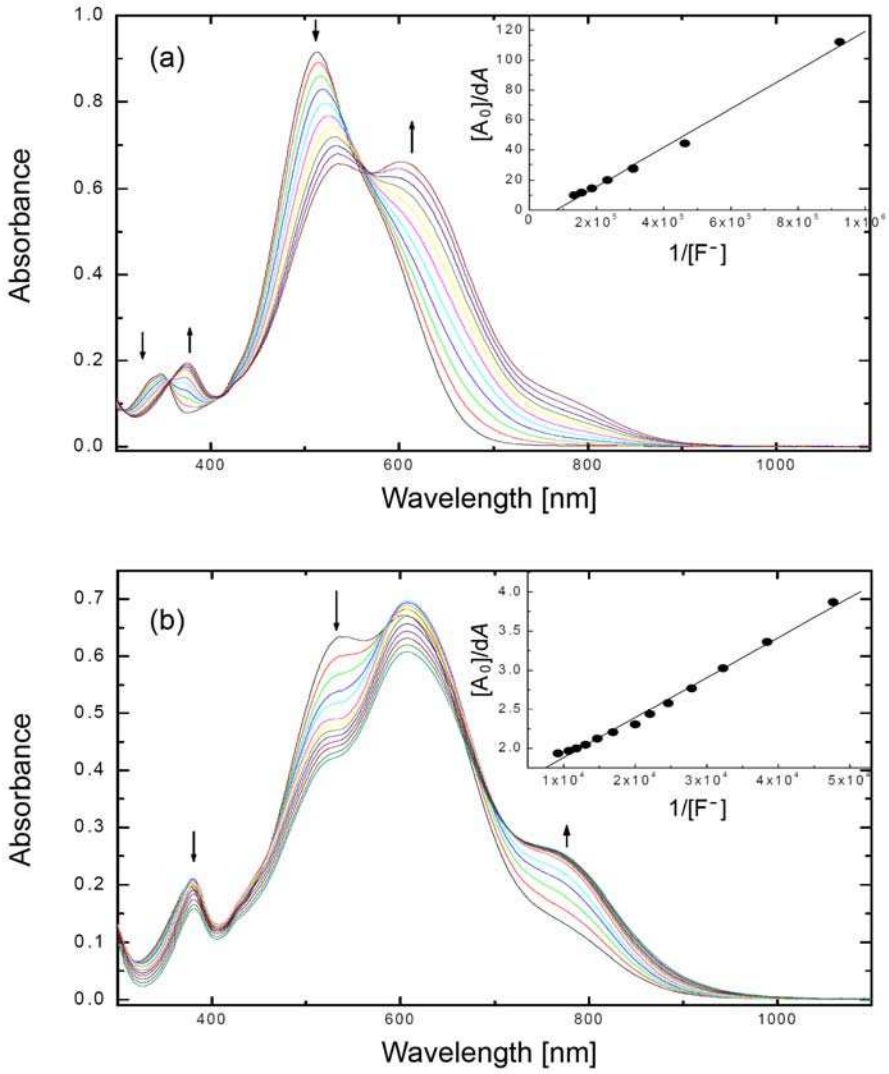

Figure 40. Spectral changes observed during the titration of **1** with tetrabutylammonium fluoride in dichloromethane**.** (a) The first set of spectral changes and (b) second set of spectral changes. The insets show the respective Benesi-Hildebrand plots constructed for evaluation of binding constants.

Table 11. Spectral shifts of the UV band and anion[a] binding constants for OxP, **1**, and $OxP(Bz)_2$, **1a**, receptors determined from absorption titration method in dichloromethane at room temperature.

anion	OxP, **1**			$OxP(Bz)_2$, **1a**	
	$\Delta\lambda$, cm^{-1}, [b]	K_1 [L mol^{-1}]	K_2 [L mol^{-1}]	$\Delta\lambda$, cm^{-1}	K [L mol^{-1}]
F^-	821	1.0×10^5	2.7×10^4	854	1.2×10^5
Cl^-	647	8.3×10^4	3.2×10^4	521	5.1×10^4
Br^-	534	8.2×10^4	2.4×10^4	247	1.9×10^4
I^-	83	4.8×10^4	1.6×10^3	58	3.5×10^3
PF_6^-	15	1.2×10^4	1.5×10^3	8	3.2×10^3
ClO_4^-	19	1.4×10^4	2.1×10^3	62	7.9×10^3
NO_3^-	383	9.7×10^4	2.7×10^4	548	8.2×10^4
$CH_3CO_2^-$	554	6.6×10^4	3.3×10^4	526	6.1×10^4
$H_2PO_4^-$	520	3.3×10^4	2.3×10^4	570	6.1×10^4

[a] Tetrabutylammonium salts were utilized.
[b] For the first set of spectral changes.

The magnitudes of K values suggest stable anion binding by both porphyrinogens, which for halides follows the trend: $I^- < Br^- < Cl^- < F^-$. However, for polyatomic anions, no clear tread could be observed perhaps due to different modes of binding of these anions to the porphyrinogen pyrrolic NH groups. In general, porphyrinogen **1** shows higher K values compared to **1a** for a given anion (K_1 was chosen for comparison). The spectral shifts of the UV band were correlated with the K values as shown in Figure 41. Good trends were observed for both of the investigated porphyrinogen derivatives. Based on the results of solvatochromic studies in Figure 37 and the results of Figure 41 one can conclude that hydrogen bonding interactions are primarily responsible for these observations. Further ^1H NMR studies were performed to confirm the hydrogen bonding interactions for solvent and anions by the investigated porphyrinogens.

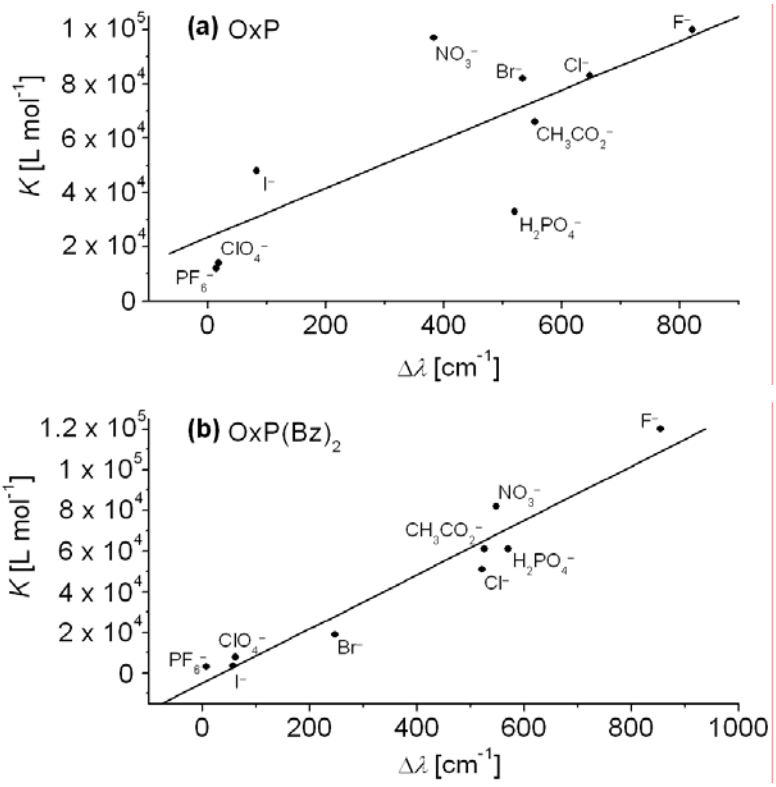

Figure 41. Plots of binding constant of different anions versus spectral shift for (a) **1** and (b) **1a**.

7.3 ^{1}H NMR spectroscopy

In general, it is possible to detect hydrogen bonding interactions during binding of an anion by a small molecule using proton NMR spectroscopy. Observation of the interaction is preferred in a solvent, such as dimethylsulfoxide or acetonitrile, where formation of an ion pair by the anion salt (e.g. tetra-*n*-butylammonium fluoride) is not favored. For derivatives of **1**, which are poorly soluble in these solvents, this presented a problem. However, in the presence of excesses of the analyte anion the compounds are somewhat solubilized permitting measurement of their NMR spectra. This solubilization is evidently caused by anion complexation.

Proton NMR spectra of **1** in the absence and presence of chloride ions in chloroform ($CDCl_3$) are shown in Figure 42. We interpret the spectra with reference to the known protic tautomerization of **1** [108]. The tautomerism is illustrated together with the ^{1}H NMR spectrum of a $CDCl_3$ solution of the tautomers in admixture. The aromatic and OH peaks assigned to the porphyrinogen (Figure 42b)

and porphodimethene (Figure 42c) forms, respectively, are present. In the aromatic region, the peak due to residual chloroform obscures one of the peaks. It is notable that increasing the temperature of measurement shifts the tautomeric equilibrium to the porphyrinogen form. Stabilization of the porphyrinogen form can also be accomplished by introduction of a hydrogen bonded guest species such as a halide or other anion. In the presence of anions the peaks due to the porphodimethene form are diminished as illustrated in Figure 42b.

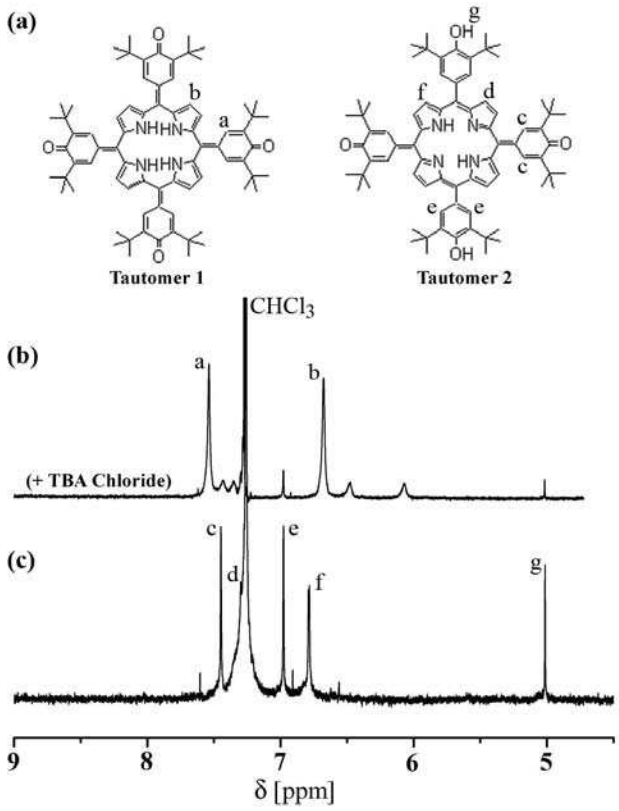

Figure 42. ^{1}H NMR spectra of aromatic region of **1** in $CDCl_3$ in the absence and presence of excess tetra-*n*-butylammonium chloride at room temperature. (a) Structures of the two tautomers of **1** (Tautomer 1: porphyrinogen form, Tautomer 2: porphodimethene form). (b) ^{1}H NMR spectrum of **1** in the presence of excess tetra-*n*-butylammonium chloride revealing binding of chloride by the porphyrinogen form ("a": meso-substituent alkene-H; "b": pyrrolic β-H). (c) ^{1}H NMR spectrum of **1** in the absence of excess tetra-*n*-butylammonium chloride indicating its existence as the porphodimethene form ("c" and "e": meso-substituent alkene-H; "d" and "f": pyrrolic β-H; "g": meso-substituent hydroxyl-H).

In the case of **1a** in $CDCl_3$ (Figure 43), the complexation of an anion is again obviated not only by a downfield shift of the pyrrolic NH protons (assigned as "a" in

Figure 43) but by variations in the chemical shifts of the pyrrolic β-proton resonances (assigned as "d" in Figure 43). ^{1}H NMR titration spectra of **1a** against amount of Cl^- anion are presented Figure 43b and 43c. The downfield shift of the NH proton peak is a result of hydrogen bonding with the substrate anion.

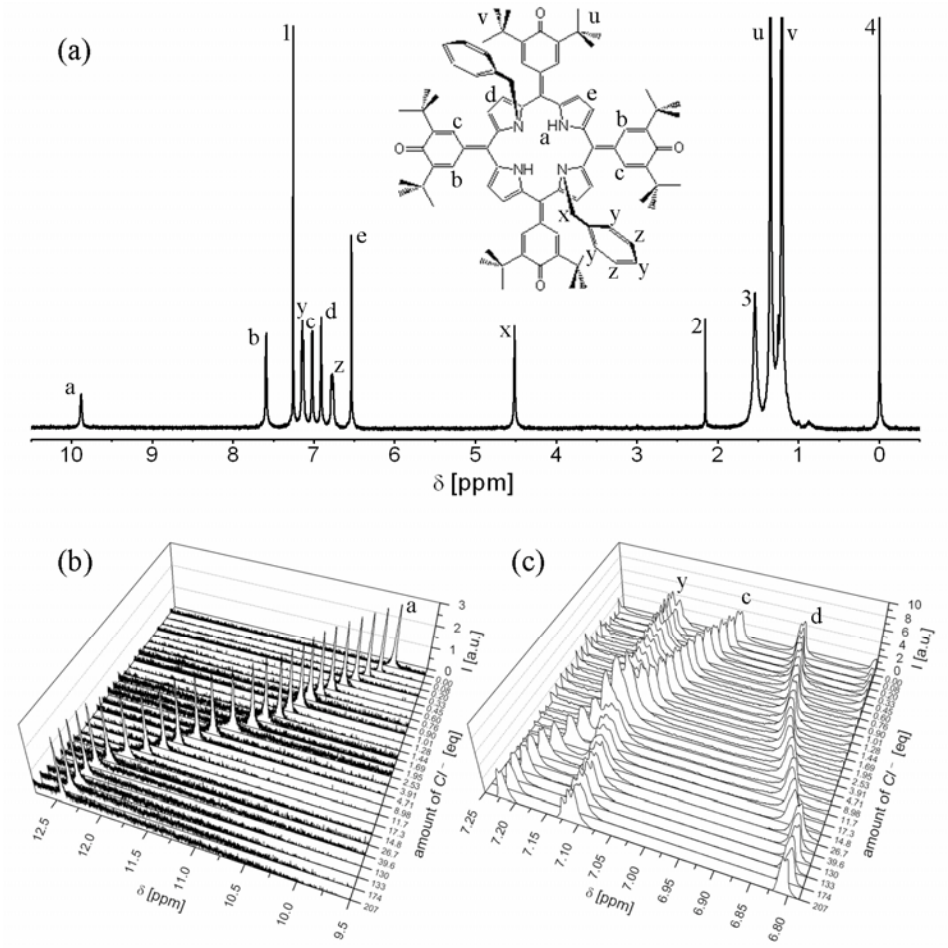

Figure 43. ^{1}H NMR spectra of **1a** in $CDCl_3$ at room temperature. (a) ^{1}H NMR spectrum of **1a** in the absence of any tetra-*n*-butylammonium salt. The peaks are assigned as they correspond to the structure: "a": pyrrolic NH protons; "b" and "c": meso-substituent alkene-H; "d" and "e": pyrrolic β-H; "u" and "v": *tert*-butyl-H; "x": benzyl CH_2; "y": benzyl ortho-, para-H; "z": benzyl meta-H; "1": residual $CHCl_3$; "2" and "3": impurities (acetone and water, respectively) from synthesis; "4": tetramethylsilane (TMS) standard. (b) and (c) ^{1}H NMR spectra of titration of **1a** against tetra-*n*-butylammonium chloride. Pyrrolic NH proton (b) and part of aromatic region (c) are shown in detail.

For the more strongly interacting fluoride, cyanide and acetate anions, the resonance due to the NH protons gradually broadens with a slight downfield shift. Shifts in the positions of the β-proton resonances are also more pronounced than for

the other anions studied because of larger macrocyclic perturbations. For instance, complexation by the smaller fluoride ion must cause more serious macrocyclic deformations and this is born out by the substantial red shift in the electronic spectrum. The potential coupling between proton and fluorine nuclei could not be initially observed in **1a** although NMR spectra at depressed temperatures (Figure 44) indicate the presence of more than one species in solution assigned to complexed and non-complexed **1a**. (Measurement of NMR spectra at lower temperature permits to detect NH peaks due to slowing down of chemical exchange.) A third peak observed during the low temperature measurements (at about 0.2 equivalent) could be due to complexation of one fluoride ion by two molecules of **1a**.

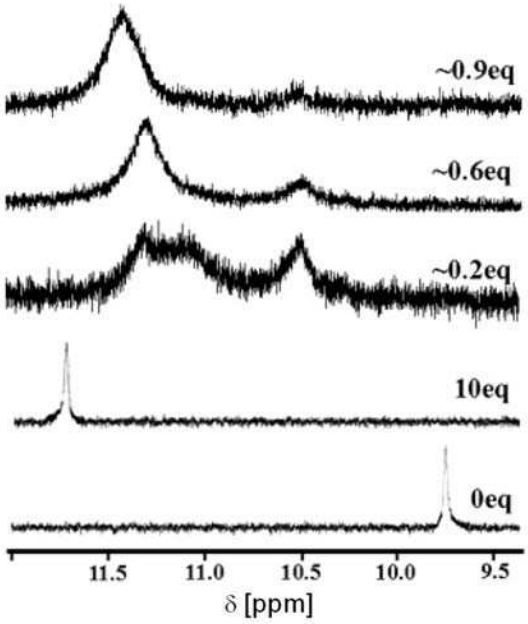

Figure 44. Low temperature ^{1}H NMR data for **1a** in $CDCl_3$ solution at −70 °C and in the presence of increasing proportion (as indicated) of tetra-*n*-butylammonium fluoride. The N-H resonance for complexed (on the left) and non-complexed (on the right) **1a** is seen.

When dichloromethane was used as solvent the complexation by fluoride ion can be more easily observed and a titration of **1a** against fluoride ions in d_2-dichloromethane (CD_2Cl_2) is shown in Figure 45. During the titration and for low proportions of fluoride ion, there appear two distinct NH resonances. As fluoride ion concentration is increased the NH peak at lower field (assigned to the **1a**·F^- complex) increases then diminishes until at proportions above 1 equivalent it disappears from the

spectrum altogether, presumably because of anionic exchange. In the initial stages of the titration involving very low concentrations of fluoride ion the NH resonance becomes significantly broadened although the NH peak(s) reappear at higher fluoride concentrations. The peak at higher field is due to the anion-free **1a**.

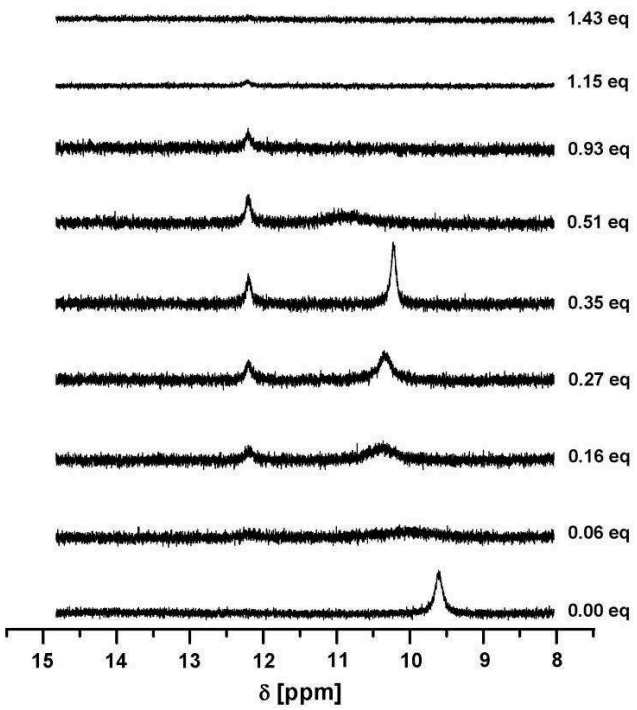

Figure 45. ^{1}H NMR spectra of titration of **1a** against fluoride ions perfomed in d_2-dichloromethane solution at room temperature. The N-H resonance for complexed (on the left) and non-complexed (on the right) **1a** is seen.

7.4 Anion selectivity by a combination of anion binding and solvatochromic effects

The effect of the solvatochromism of **1** and its di-N-benzylated derivative **1a** on their electronic spectra in the presence of complexing anions was observed. This is intended as a qualitative assessment of the colorimetric responses of **1** and **1a** to anions in various solvents. For **1**, accessible solvents for this study were dichloromethane, chloroform, tetrahydrofuran and pyridine. For several other solvents **1** was virtually insoluble except in the presence of excesses of the more strongly interacting anions. Electronic absorption spectra indicate the effect of anion

binding and solvent identity on the color of the solutions. The most attractive example of this for **1** is in dichloromethane solution where changing the identity of the anions gives relatively well defined changes in the UV/Vis spectrum. Tetrafluoroborate anions interact weakly and do not perturb the spectrum of the parent significantly. Binding of the halides gradually increases the intensity of a new band at 665 nm passing from iodide to chloride (Figure 46b). However, when fluoride is present, the absorption spectrum departs much more significantly from that of the parent. A broad band appears at 758 nm as was noted previously. This band is significant in that it would allow monitoring for the presence of fluoride at around 860 nm without interference from the other anions studied. In acetone the response of **1** to different anions is similar to that in dichloromethane. The effect of the presence of particular anions on the color of solutions of **1** is summarized in Figure 46. It is interesting to note in Figure 46b that an apparent isosbestic point appears in the spectra containing non-identical anions. This is because the mode of binding of the anion is similar for those participating in this phenomenon.

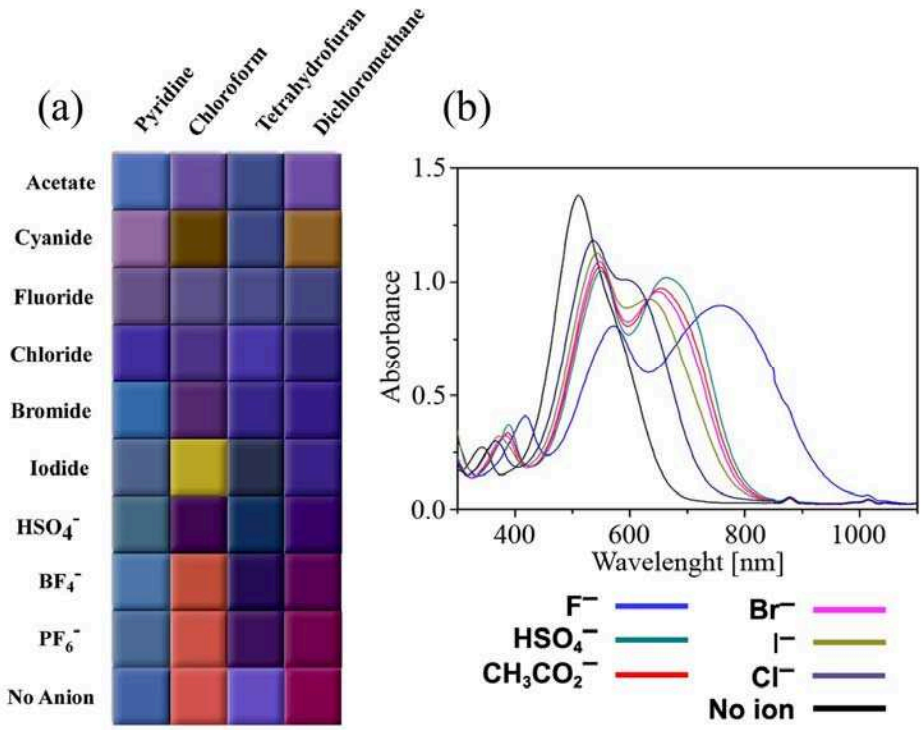

Figure 46. (a) Colors of solutions of **1** in the presence of various anions and solvents (see Figure 49 for the photograph from which the tile pattern was generated). (b) The electronic spectra of **1** in dichloromethane and in the presence of the indicated anions are shown as an example.

Electronic absorption spectra of solutions containing individual anions, **1a** and in selected solvents are shown in Figure 47. For **1a**, fluoride ions could be easily distinguished from the other halides in most solvents while they could also be distinguished from acetate and cyanide by variation of the solvent. In solvents of higher polarity, differentiation of fluoride became increasingly unlikely because the characteristic color for fluoride ions coincides increasingly with the native color of **1a** in those solvents. This is shown in fluoride electronic spectra in Figure 47, where the dichloromethane represents less polar solvent than the ethanol. Generally, the ions acetate, cyanide and fluoride can be differentiated from the other ions by the blue color of their solutions. The presence of other anions tends to result in violet solutions. The most notable separation of anion response comes in dichloromethane where fluoride can be distinguished from all the other ions studied by virtue of the absorption band at 750 nm. When ethanol is used as a solvent, cyanide ions may be distinguished from the other studied anions. In that case it is the lack of response from other anions which enables almost unobstructed observation of an absorption band at 756 nm.

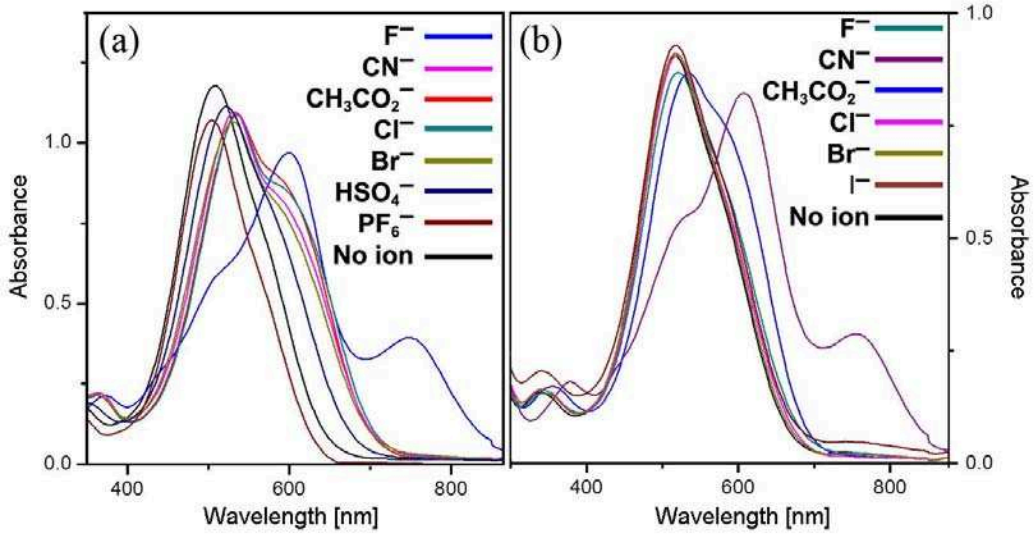

Figure 47. Electronic spectra of **1a** in dichloromethane (a) or ethanol (b) and in the presence of the indicated anions.

Further, iodide ions give a variety of responses depending on solvent (Figure 48). Often a new absorption band(s) is observed in the UV around 380 nm. When

propionic acid is the solvent iodide is the only analyte to induce a distinct response from **1a**. In the UV/Vis spectrum, this manifests itself as intense new absorption bands at 350, 440 nm with a less intense band at 785 nm which does not overlap with the absorption bands in the spectra of solutions containing other anions. The tiling representation in Figure 48 illustrates the colors of dilute solutions (~10^{-6} M) of **1a** in various solvents and in the presence of excesses of the respective anions. The solvents are arranged in order of their polarities while the anions are arranged approximately by the apparent strengths of interaction with the anion complexing agent **1a** according to the color changes.

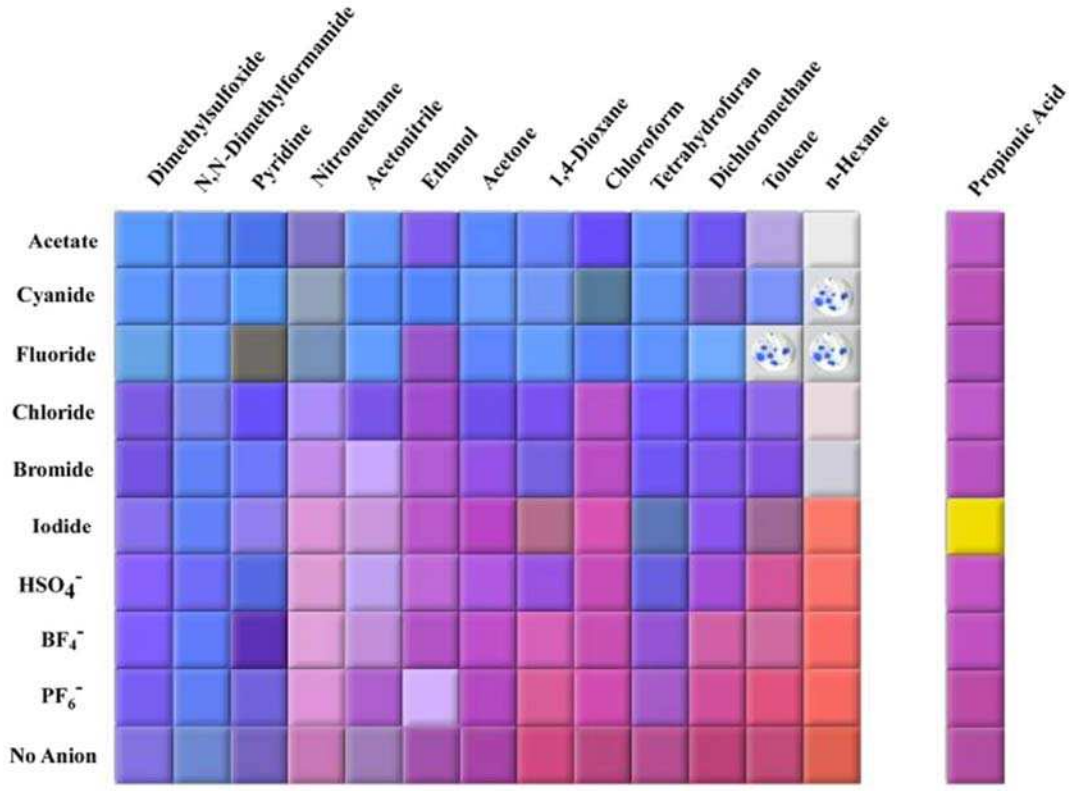

Figure 48. Tiling representation of the colors of dilute (~ 10^{-6} M) solutions of **1a** in several solvents and in the presence of the anions studied (see Figure 50 for the photograph from which the tile pattern was generated).

Finally, anomalous effects are obtained when solvents containing peroxides are employed. In the absence of **1**, traces (~10ppm) of peroxides cause a yellow color in solutions of iodide ions in tetrahydrofuran, propionic acid or 1,4-dioxane. The yellow colour is an accepted indicator for the presence of peroxides, which are in this

case present because of the use of stabilizer-free solvents. Discoloration of the solutions generally occurs on a timescale of minutes. In propionic acid no chromogenic response can be observed except in the case of iodide ions. The intense yellow color replaces the dark pink of non-complexed **1**. However, although the effect is intense, no change is observed in the electronic absorption band of **1**. The lack of response by the other anions simply serves to emphasize a chromogenic response in propionic acid.

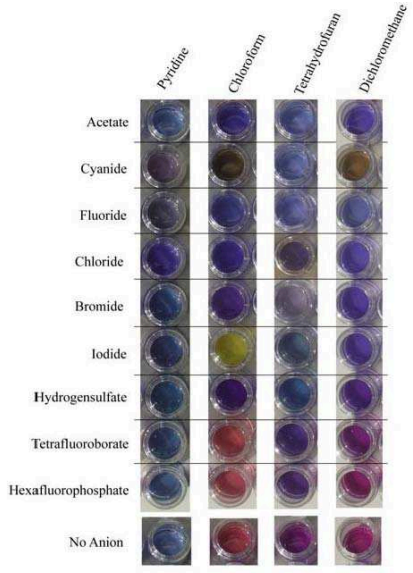

Figure 49. Original photographs of solutions of **1** in the stated solvents in the presence of excesses of the respective anions as their tetra-*n*-butylammonium salts.

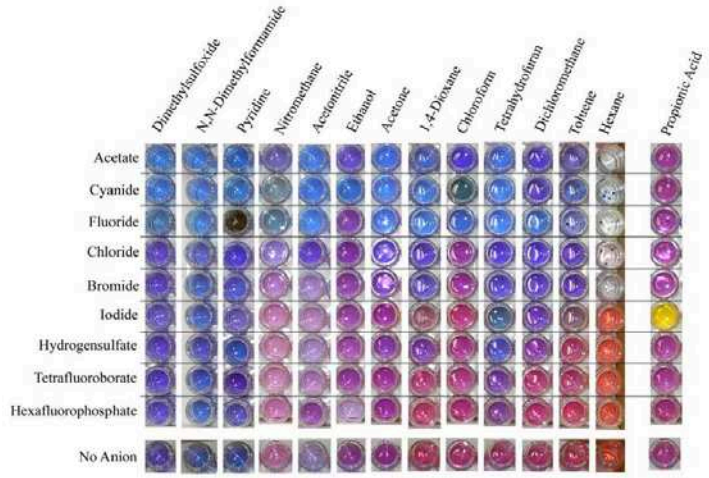

Figure 50. Original photographs of solutions of **1a** in the stated solvents in the presence of excesses of the respective anions as their tetra-*n*-butylammonium salts.

The anion binding by **1** and its N-substituted derivatives is not only of interest from the point of view of determination of ions but also has connotations for the actual N-alkylation reaction leading to those derivatives. In our case, we routinely use solvent ethanol with anhydrous potassium carbonate as the base during these preparations. The **1** is poorly soluble in ethanol (and other polar solvents) which affects the reactions with this compound. However, in the presence of carbonate anions **1** is sufficiently solubilized in ethanol, although at elevated temperature, presumably by binding of the carbonate anion and the consequent higher polarity of the anion complex, that the N-alkylation reaction is promoted. In this way, the use of 18-crown-6 as a promoter is not required since **1** itself acts as a phase transfer catalyst by binding of carbonate. Phase transfer catalyst facilitates the migration of a reactant in a heterogeneous system from one phase into another phase where the reaction can take place. It is also now likely that anion binding of carbonate influences the distribution of the N-alkylates obtained from the reaction between **1** and alkyl bromides. Hence, N-benzylation of **1** should displace a bound carbonate anion resulting in N_{21}-benzyl-**1**. Carbonate ions interact weakly with the single NH group at N_{23} increasing the rate of reaction between this pyrrole group and a subsequent alkylating species. Thus, N_{21},N_{23}-dibenzyl-**1** is obtained as one major product. A similar situation occurs for N_{21},N_{23}-dibenzyl-**1** at its unalkylated face where displacement of the carbonate by N_{22}-alkylation enhances reactivity at N_{24}. We also considered that the carbonate anion binding may effectively prevent formation of the other isomers of multiple substitution products by fixing the macrocyclic conformation. In addition, use of other bases apparently does not affect the identity of the resulting N-alkylates although variation of base and solvent can lead to changes in the distribution of products obtained from the alkylation reaction [109].

8 Conclusions II

In conclusion, the solvatochromic effect of 5,10,15,20-*Tetrakis*-3,5-di-*tert*-butyl-4-oxocyclohexadienylidene porphyrinogen **1** and its di-N-benzylated derivative **1a** in various solvents was investigated using UV/Vis spectrophotometry. It was illustrated that relationship between solvent's β value (scale of hydrogen-bond acceptor) or solvent's donor number versus spectral shift of **1** and **1a** is linear which suggests that solute-solvent hydrogen bonding is primarily responsible for the observed solvatochromic effect of porphyrinogens. It was also found that **1** and **1a** are capable of binding anionic species such as the halides and other more complex anions. The measure of strength of anion binding, the binding constants, were determined using Benesi-Hildebrand plots. It was shown that binding constant between halides and both porphyrinogens follows the trend $I^- < Br^- < Cl^- < F^-$. Moreover, the spectral shifts of the UV band were higher for anions with larger value of binding constant. This is manifested by shift in solution colour towards blue for more strongly bounded anions. Further, there is some specificity in the chromogenic response of **1** and its di-N-benzylated derivative **1a** when in the presence of certain anions. Thus, fluoride ions can be distinguished from the other halides by the more substantial change in color that occurs upon fluoride ion binding. This difference is even more substantial in spectrophotometric terms with fluoride ion binding resulting in a strong absorption band at longer wavelength. In addition, derivatives of **1** exhibit solvatochromism allowing some chromogenic distinction between other ions, such as acetate or cyanide, and fluoride. Both solvatochromic and anion binding effects are influenced by the hydrogen bonding ability of the pyrrolic NH groups so that increased H-bonding between **1**, **1a** and the solvent obscures the effect of anion binding.

Hydrogen bonding by **1a** to solvent acetone molecules was observed in the crystal structure of that solvate. Furthermore, **1** tends to undergo a tautomerism which can be weighted in favor of the porphyrinogen form by complexation with appropriate anions which was proved by ^{1}H NMR spectroscopy. It was found using ^{1}H NMR titration spectra of **1a** that complexation of an anion is obviated not only by a downfield shift of the pyrrolic NH protons but also by variations in the chemical shifts of the pyrrolic β-proton resonances. The titrations suggest that complexation by the smaller fluoride ion must cause more serious macrocyclic deformations and this is born out by the substantial red shift in the electronic spectrum as well.

The tile patterns containing colours of dilute solutions of **1** or **1a** in different solvents and in presence of excesses of the respective anions were constructed. The colorometric response of **1** and **1a** was illustrated directly in these patterns as well as possibility of specific anion selection.

Finally, some connotation of anion binding for N-alkylation reaction leading to **1a** was described. The influence of binding of the carbonate anion and the consequent higher polarity of the **1a**·anion complex was suggested in the terms of distribution of products from the alkylation reaction towards predominantly di- and tetra-N-substituted **1**.

9 References

[1] *Responsive Gels: Volume Transition I, II* (Ed. Dušek K.), Springer-Verlag, Berlin (1993), (*Adv. Polym. Sci.*, 109, 110 (1993))

[2] Tanaka T., *Phys. Rev. Lett.* 40, 820 (1978)

[3] Ilavský M., *Adv. Polym. Sci.* 109, 1 (1993)

[4] Hirotsu S., *Adv. Polym. Sci.* 110, 1 (1993)

[5] Schild H.G., *Prog. Polym. Sci.* 17, 163 (1992)

[6] Aseyev V.O., Tenhu H., Winnik F.M., *Adv. Polym. Sci.* 196, 1 (2006)

[7] Stockmayer W.H., *Rev. Mod. Phys.* 31, 103 (1959)

[8] Grosberg A.Y., Khokhlov A.R., *Giant Molecules: Here and There and Everywhere...*, Academic Press, New York (1997)

[9] Wichterle O., in *Encyclopedia of Polymer Science and Technology*, Vol. 15, Wiley, New York (1971), pp. 273

[10] *Hydrogels in Medicine and Pharmacy* (Ed. Peppas N.), CRC Press, Boca Raton, Florida (1985)

[11] Chytrý V., Netopilík M., Bohdanecký M., Ulbrich K., *J. Biomater. Sci. Polym. Ed.* 8, 817 (1997)

[12] Chung J.E., Yokoyama M., Yamato M., Aoyagi T., Sakurai Y., Okano T., *J. Control. Release* 62, 115 (1999)

[13] Matsumoto A., Ikeda S., Harada A., Kataoka K., *Biomacromolecules* 4, 1410 (2003)

[14] Atkins P., *Physical Chemistry*, Oxford University Press (2001)

[15] McQuarrie D.A., Simon J.D., *Physical Chemistry*, University Science Books, Sausalito, California (1997)

[16] Dušek K., Patterson D.J., *J. Polym. Sci.* 6, 1209 (1968)

[17] Dušek K., Prins W., *Adv. Polym. Sci.* 6, 1 (1969)

[18] Khokhlov A., *Polymer* 21, 376 (1980)

[19] Tanaka T., *Polymer* 20, 1404 (1979)

[20] Stejskal J., Gordon M., Torkington J.A., *Polym. Bull.* 3, 621 (1980)

[21] Cuniberti C., Bianchi U., *Polymer* 15, 346 (1974)

[22] Flory P.J., *Principles of Polymer Chemistry*, Cornell Univ. Press (1954)

[23] Graziano G., *Int. J. Biol. Macromol.* 27, 89 (2000)

[24] Ptitsyn O.V., Kron A.K., Eizner Y.Y., *J. Polym. Sci. Part C* 16, 3509 (1968)

[25] Lifshitz I.M., Grosberg A.Y., Khokhlov A.R., *Rev. Mod. Phys.* 50, 683 (1978)

[26] Molyneux P., *Water-soluble synthetic polymers: Properties and Behavior*, Vol. I. CRC Press, Boca Raton, Florida (1983), pp. 58-61

[27] Horne R.A., Almeida J.P., Day A.F., Yu N.T., *J. Colloid. Interfac.e Sci.* 35, 77 (1971)

[28] Schäfer-Soenen H., Moerkerke R., Berghmans H., Koningsveld R., Dušek K., Šolc K., *Macromolecules* 30, 410 (1997)

[29] Maeda H., *J. Polym. Sci. Part B Polym. Phys.* 32, 91 (1994)

[30] Maeda Y., *Langmuir* 17, 1737 (2001)

[31] Aseyev V., Hietala S., Laukkanen A., Nuopponen M., Confortini O., Du Prez F.E., Tenhu H., *Polymer* 46, 7118 (2005)

[32] Swier S., Van Durme K., Van Mele B., *J. Polym. Sci. Part B Polym. Phys.* 41, 1824 (2003)

[33] Van Durme K., Loozen E., Nies E., Van Mele B., *Macromolecules* 38, 10234 (2005)

[34] Zhang J., Teng H., Zhou X., Shen D., *Polymer bulletin* 48, 277 (2002)

[35] Maeda Y., Yamamoto H., Ikeda I., *Langmuir* 20, 7339 (2004)

[36] Hanyková L., Spěváček J., Ilavský M., *Polymer* 42, 8607 (2001)

[37] Spěváček J., Hanyková L., Ilavský M., *Macromol. Symp.* 166, 231 (2001)

[38] Spěváček J., Hanyková L., *Macromol. Symp.* 203, 229 (2003)

[39] Spěváček J., Hanyková L., Starovoytova L., *Macromolecules* 37, 7710 (2004)

[40] Spěváček J., Hanyková L., *Macromolecules* 38, 9187 (2005)

[41] Farrar T.C., Becker E.D., *Pulse and Fourier Transform NMR*, Academic Press, New York (1971), pp. 27

[42] Kay L.E., Nicholson L.K., Delaglio F., Bax A., Torchia D.A., *J. Magn. Reson.* 97, 359 (1992)

[43] Spěváček J., *Macromol. Symp.* 222, 1 (2005)

[44] Spěváček J., Hanyková L., Ilavský M., *Macromol. Chem. Phys.* 202, 1122 (2001)

[45] Spěváček J., Schneider B., *Adv. Colloid. Interface Sci.* 27, 81 (1987)

[46] Starovoytova L., Spěváček J., Hanyková L., Ilavský M., *Macromol. Symp.* 203, 239 (2003)

[47] Coccia A., Indovina P.L., Podo F., Viti V., *Chem. Phys.* 7, 30 (1975)

[48] Luz Z., Meiboom S., *J. Chem. Phys.* 39, 366 (1963)

[49] Korzhnev D.M., Billeter M., Arseniev A.S., Orekhov V.Y., *Prog. Nucl. Magn. Reson. Spectrosc.* 38, 197 (2001)

[50] Mirau P.A., *A Practical Guide to Understanding the NMR of Polymers*, Wiley, Hoboken, New York (2004), pp. 24 and 27

[51] Vinogradov S.N., Linnell R.H., *Hydrogen bonding*, Van Nostrand Reinhold Co., New York (1971), chapters 3 and 4

[52] Kalinowski H.O., Berger S., Braun S., *Carbon-13 NMR spectroscopy*, Wiley, Chichester (1988), pp. 214

[53] Bovey F.A., Mirau P.A., *NMR of polymers*, Academic Press, San Diego (1996), pp. 16 and 354-356

[54] Meeussen F., Bauwens Y., Moerkerke R., Nies E., Berghmans H., *Polymer* 41, 3737 (2000)

[55] Tanaka H., *Phys. Rev. Lett.* 71, 3158 (1993)

[56] Tanaka H., *Phys. Rev. Lett.* 76, 787 (1996)

[57] Zhou D., Zhang P., E W., *Phys. Rev. E* 73, 061801 (2006)

[58] Hill P.G., MacMillan R.D.C., Lee V., *J. Phys. Chem. Ref. Data* 11, 1 (1982)

[59] Dean J.A., *Lange's Handbook of Chemistry*, 15th ed., McGraw-Hill Inc., New York (1999)

[60] Orwoll R.A., *Physical Properties of Polymers Handbook*, AIP Press, Woodbury, New York (1996), chapter 7

[61] Imahori H., Tamaki K., Guldi D. M., Luo C., Fujitsuka M., Ito O., Sakata Y., Fukuzumi S., *J. Am. Chem. Soc.* 123, 2607 (2001)

[62] Choi M. S., Yamazaki T., Yamazaki I., Aida T., *Angew. Chem. Int. Ed.* 43, 150 (2004)

[63] de la Torre G., Vázquez P., Agulló-López F., Torres T., *Chem. Rev.* 104, 3732 (2004)

[64] Lu Y., Berry S. M., Pfister T. D., *Chem. Rev.* 101, 3047 (2001)

[65] Denisov J. G., Makris T. M., Sliger S. G., Schlichting I., *Chem. Rev.* 105, 2253 (2005)

[66] Vogel E., Kocher M., Schmickler H., Lex J., *Angew. Chem., Int. Ed. Engl.* 25, 257 (1986)

[67] Gross Z., Galili N., Saltsman I., *Angew. Chem. Int. Ed.* 38, 1427 (1999)

[68] Hayashi T., Dejima H., Matsuo T., Sato H., Murata D., Hisaeda Y., *J. Am. Chem. Soc.* 124, 11226 (2002)

[69] Broadhurst M. J., Grigg R., Johnson A. W., *Chem. Commun.* 23 (1969)

[70] Sessler J. L., Cyr M. J., Lynch V., McGhee E., Ibers J. A., *J. Am. Chem. Soc.* 112, 2810 (1990)

[71] Král V., Davis J., Andreivsky A., Kralová J., Synytsya A., Poucková P., Sessler J. L., *J. Med. Chem.* 45, 1073 (2002)

[72] Sessler J. L., Camiolo S., Gale P. A., *Coord. Chem. Rev.* 240, 17 (2003)

[73] Furuta H., Asano T., Ogawa T., *J. Am. Chem. Soc.* 116, 767 (1994)

[74] Maeda H., Furuta H., *Pure Appl. Chem.* 78, 29 (2006)

[75] Krattinger B., Callot H. J., *Eur. J. Org. Chem.* 1857 (1999)

[76] Hill J. P., Schmitt W., McCarty A. L., Ariga K., D'Souza F., *Eur. J. Org. Chem.* 2893 (2005)

[77] Gale P. A., *Coord. Chem. Rev.* 199, 181 (2000)

[78] *Supramolecular Chemistry of Anions* (Eds: Bianchi A., Bowman-James K., Garcia-Espana E.), VCH, Weinheim (1997)

[79] Choi K., Hamilton A. D., *Coord. Chem. Re*v. 240, 101 (2003)

[80] Bowman-James K., *Acc. Chem. Res*. 38, 671 (2005)

[81] Koskela S. J. M., Fyles T. M., James T. D., *Chem. Commun*. 945 (2004)

[82] Arimori S., Davidson M. G., Fyles T. M., Hibbert T. G., James T. D., Kociok-Koehn G. I., *Chem. Commun*. 1640 (2004)

[83] Choi K., Hamilton A. D., *J. Am. Chem. Soc.* 123, 2456 (2001)

[84] Doyle D. A., Cabral J. M., Pfuetzner R. A., Kuo A., Gulbis J. M., Cohen S. L., Chait B. T., MacKinnon R., *Science* 280, 69 (1998)

[85] Choi K., Hamilton A. D., *J. Am. Chem. Soc.* 125, 10241 (2003)

[86] Blazejczyk A., Szczupak M., Wieczorek W., Cmoch P., Appetecchi G. B., Scrosati B., Kovarsky R., Golodnitsky D., Peled E., *Chem. Mater.* 17, 1535 (2005)

[87] Sessler J. L., Gale P. A. in *The Porphyrin Handbook*, Vol. 6, (Eds. Kadish K. M., Smith K. M., Guilard R.), Academic Press, San Diego, CA and Burlington, MA (2000), pp. 257-278

[88] Camiolo S., Gale P. A., *Chem. Commun.* 1129 (2000)

[89] Gale P. A., Sessler J. L., Král V., Lynch V., *J. Am. Chem. Soc.* 118, 5140 (1996)

[90] Sessler J. L., Gale P. A., Genge J. W., *Chem. Eur. J.* 4, 1095 (1998)

[91] Sessler J. L., Cho W. S., Gross D. E., Shriver J. A., Lynch V. M., Marquez M., *J. Org. Chem.* 70, 5982 (2005)

[92] Sessler J. L., An D., Cho W. S., Lynch V., Yoon D. W., Hong S. J., Lee C. H., *J. Org. Chem.* 70, 1511 (2005)

[93] Gale P. A., Anzenbacher P., Sessler J. L., *Coord. Chem. Rev.* 222, 57 (2001)

[94] Schmidtchen F. P., *Org. Lett.* 4, 431 (2002)

[95] Woods C. J., Camiolo S., Light M. E., Coles S. J., Hursthouse M. B., King M. A., Gale P. A., Essex J. W., *J. Am. Chem. Soc.* 124, 8644 (2002)

[96] Miyaji H., Kim H. K., Sim E. K., Lee C. K., Cho W. S., Sessler J. L., Lee C. H., *J. Am. Chem. Soc.* 127, 12510 (2005)

[97] Nishiyabu R., Anzenbacher P., *J. Am. Chem. Soc.* 127, 8270 (2005)

[98] Milgrom L. R., *Tetrahedron* 39, 3895 (1983)

[99] Dodsworth E. S., Hasegawa M., Bridge M., Linert W., *Comprehensive Coord. Chem. II* 2, 351 (2004)

[100] Karelson M. in *Handbook of Solvents*, (Ed. Wypych G.), ChemTec Publishing, Toronto, Canada (2001), pp. 639-679

[101] Nigam S., Rutan S., *Applied Spectroscopy* 55, 361A (2001)

[102] Carr P. W., *Microchem. J.* 48, 4 (1993)

[103] Sone K., Fukuda Y., *Reviews Inorg. Chem.* 11, 123 (1990)

[104] Hill J. P., Hewitt I. J., Anson C. E., Powell A. K., McCarty A. L., Karr P. A., Zandler M. E., D'Souza F., *J. Org. Chem*. 69, 5861 (2004)

[105] Gutman V., *Coord. Chem. Rev*. 18, 225 (1976)

[106] Kamlet M. J., Abboud J. L. M., Abraham M. H., Taft R. W., *J. Org. Chem*. 48, 2877 (1983)

[107] Benesi H. A., Hildebrand J. H., *J. Am. Chem. Soc*. 71, 2703 (1949)

[108] Milgrom L. R., Hill J. P., Yahioglu J., *Heterocyclic Chem.* 32, 97 (1995)

[109] Dolušić E., Toppet S., Smeets S., Meervelt L. V., Tinant B., Dehaen W., *Tetrahedron* 59, 395 (2003)

10 List of publications

Publications in journals

1) Labuta J., Hill J. P., Hanyková L., Ariga K.: Morphology Study of Coil-Globule Transition in Poly(vinyl methyl ether)/D_2O/Ethanol Solutions, *submitted to Polymer* (July 2008)
2) Xie Y., Hill J. P., Schumacher A.L., Sandanayaka A. S., Araki Y., Karr P. A., Labuta J., D'Souza F., Ito O., Anson C. E., Powell A. K., Ariga K.: Twisted, Two-Faced Porphyrins as Hosts for Bispyridyl Fullerenes: Construction and Photophysical Properties, *J. Phys. Chem. C* 112, 10559-10572 (2008)
3) Hill J. P., Schumacher A.L., D'Souza F., Labuta J., Redshaw C., Elsegood M. R. J., Aoyagi M., Nakanishi T., Ariga K.: Chromogenic Indicator for Anion Reporting Based on an N-substituted Oxoporphyrinogen, *Inorganic Chemistry* 45, 8288-8296 (2006)
4) Hanyková L., Labuta J., Spěváček J.: NMR Study of Temperature-induced Phase Separation and Polymer-Solvent Interactions in Poly(vinyl methyl ether)/D_2O/Ethanol Solutions, *Polymer* 47, 6107-6116 (2006)

Publications in monographs

5) Ariga K., Hill J. P., Labuta J.: Bottom-Up Nanofabrication through Self-Assembly of Lipids, Peptides, and Related Molecules for Preparation of Nano- and Micro-Objects, (chapter in) *BOTTOM-UP NANOFABRICATION: Supramolecules, Self-Assemblies, and Organized Films*, Editors: K. Ariga and H. S. Nalwa, Publisher: American Scientific Publishers, Los Angeles (2007), ISBN: 1-58883-079-9

6) Hill J. P., Labuta J., Ariga K.: Supramolecular Porphyrin Arrays in Solution, at Liquid Interfaces, and at Solid Surfaces, (chapter in) *BOTTOM-UP NANOFABRICATION: Supramolecules, Self-Assemblies, and Organized Films*, Editors: K. Ariga and H. S. Nalwa, Publisher: American Scientific Publishers, Los Angeles (2007), ISBN: 1-58883-079-9

Publications in proceedings

7) Labuta J., Hill J. P., Hanyková L.: New NMR Approaches to the Study of Phase Separation in Polymer Solutions, *WDS'07 Proceedings of Contributed Papers, Part III – Physics*, Editors: J. Šafránková and J. Pavlů, Publisher: Matfyzpress, Prague, pp. 112-117 (2007)

Other publications

8) Hill J. P., Labuta J.: Self-Assembly and Anion Sensing by Nanosized Molecules, *NIMS NOW International*, Vol. 4 No. 6 (2006)
9) Hill J. P., Labuta J.: ナノサイズの分子による自己組織化とアニオンセンシング, *NIMS NOW*, Vol. 6 No. 6 (2006)

Conference contributions

10) Labuta J., Hanyková L.: New NMR Approaches for Study of a Phase Separation in Polymer Solutions (poster), *16th Annual Student Conference WDS'07*, Prague, Czech Republic (2007)
11) Labuta J., Hanyková L., Lang J., Spěváček J., Hill J. P., Ariga K.: NMR Study of the Coil-Globule Transition in Poly(vinyl methyl ether)/Water/Ethanol Solutions (poster), *5th Workshop on Interfacial Nano-Architectonics (Nano-Architectonics and Their Function Beyond Organic-Inorganic Boundary)*, Tsukuba, Japan (2006)
12) Hill J. P., McCarty A. L., D'Souza F., Labuta J., Wakayama Y., Aoyagi M., Nakanishi T., Ariga K.: Self-Assembly and Chromogenic Properties of a Conjugated Porphyrinogen (poster), *5th Workshop on Interfacial Nano-Architectonics (Nano-Architectonics and Their Function Beyond Organic-Inorganic Boundary)*, Tsukuba, Japan (2006)

13) Labuta J., Hanyková L.: Phase Separation in Polymer Solutions (oral presentation), *14th Annual Student Conference WDS'05*, Prague, Czech Republic (2005)
14) Hanyková L., Labuta J., Spěváček J., Lang J., Ilavský M.: Temperature Induced Phase Separation in Poly(vinyl methyl ether)/Water/Ethanol Solutions Studied by NMR Spectroscopy (poster), *46th ENC - Experimental Nuclear Magnetic Resonance Conference*, Providence, USA (2005)
15) Labuta J., Hanyková L., Lang J., Spěváček J.: Relaxation Behaviour of Solvent Molecules During the Phase Separation in Poly(vinyl methyl ether)/Water/Ethanol Solutions (oral presentation), *Central European NMR Discussion Groups: 20th NMR Valtice*, Valtice, Czech Republic (2005)
16) Hanyková L., Labuta J., Spěváček J., Lang J., Ilavský M.: Coil-globule Transition in Poly(vinyl methyl ether)/Water/Ethanol Solutions Studied by NMR Spectroscopy (poster), *The 44th Microsymposium of P.M.M.: Polymer Gels and Networks*, Prague, Czech Republic (2005)